TOWARDS RELATIVISTIC HEAVY ION COLLISIONS
"BY SMALL STEPS TOWARDS THE STARS"

David K. Scott

Nuclear Science Division
Lawrence Berkeley Laboratory
Berkeley, California 97420

INTRODUCTION

The study of relativistic heavy ion collisions began in the Heavens and that may well be where it will end. Almost thirty years ago the foundation of current approaches to high energy interactions between nuclei were laid, when in the primary cosmic radiation components with $Z > 2$ were discovered (Freier, 1948). At roughly the same time theorists were led by the properties of the nucleon-nucleon tensor force to speculate that the familiar saturation of nuclear density might be overcome and that tightly bound collapsed nuclei might occur in nature (Feenberg, 1946). Today there are many more speculations on the possible phases of nuclear matter under extreme conditions of temperature and pressure, and these speculations are being sharpened by the study of relativistic heavy ion collisions with accelerators at energies up to a few GeV/nucleon (for recent reviews of the field, see Goldhaber, 1978; Nix, 1978; Webb, 1978; Bock, 1978). Nevertheless, for a long time to come, the interactions generated by ultra relativistic cosmic rays in the atmosphere will constitute our only source of information on hadronic matter at very high energies of 10^6-10^9 GeV and beyond (Gaisser, 1978). In order to portray this unity between the cosmic and man-made accelerators, I show in Fig. 1.1 the Bevalac inside the exploding matter of the Crab Nebula. This is a symbolic illustration of the universal interest throughout the whole of physics in the collision of structured objects, especially insofar as they can be explained in the context of a microscopic theory. It is likely, indeed, that the study of relativistic heavy ion collisions holds the greatest hope for ultimately reunifying elementary particle physics, nuclear physics and astrophysics.

The relevance of cosmological events to relativistic heavy ion collisions is both profound and practical. In Fig. 1.2 is shown the temperature reached in the nuclear fireball, formed when two heavy ions collide, for two assumptions about the hadronic mass spectrum (Glendenning, 1978). The curve labelled "experimental" corresponds to a mass spectrum containing the known particles whereas that labelled "Hagedorn" corresponds to the bootstrap hypothesis of an exponential growth of hadrons. In this model the temperature limits at 140 MeV which may have been observed (Laasanen, 1977), a temperature approaching the limit reached in the earliest recognizable moments of our Universe (Weinberg, 1977).

XBB 728-4273

Fig. 1.1

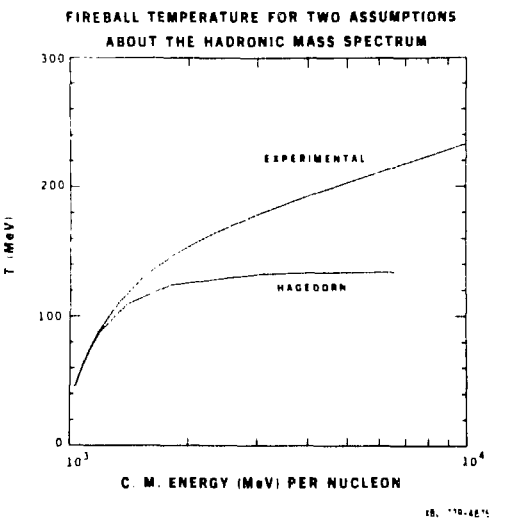

Fig. 1.2

In the case of the neutron stars (Baym, 1975) one is faced with the study of cold matter at super-nuclear densities, greater than 2.8×10^{14} gm/cm^3. In such a regime the nuclear fluid is believed likely to undergo a phase transition to a Bose condensate of charged pions (Bethe, 1978; Toki, 1978). Heavy ion reactions could also result in nuclear shock waves producing densities far in excess of those thought necessary for the appearance of pion condensates. Unlike neutron star matter, however, such shock waves (Hofmann, 1979) would be extremely hot. Anomalous pion production might be observed in such highly condensed states, but the problem of calculating an equation of state for a hot ($T \sim 10^{12}$ ^{o}K), dense ($P \sim 10^{15}$-10^{16} gm/cm^3), strongly interacting Fermi system remains a formidable task (Irvine, 1978). On the practical side it is fascinating that the experiments to determine both the size of the nuclear fireball (Fung, 1978) and the degree of coherence or chaos

in the source (Fowler, 1977), use pion interferometry, similar to the techniques devised to measure the spatial dimensions of stars and radio-sources almost thirty years ago (Hanbury-Brown, 1956) with the Hanbury-Brown and Twiss effect. Bordering on the profound is the observation of so-called Centauro events, believed to be generated by ultra high energy cosmic rays (100-1000 TeV), which generate very few π^0 particles. It is conjectured that at these energies the strong interaction may assume totally new characteristics (Gaisser, 1978).

These lectures have the goal of describing the current attempts to search for the exotic processes occurring in relativistic heavy ion collisions. But it is clear that we must proceed, "By Small Steps Toward the Stars." So we shall start with Peripheral Collisions, then Central Collisions and finally the Search for the Exotic, which exploits the tools of the trade that have been developed for the study of peripheral and central collisions.

In order to place the subject in perspective, Fig. 1.3 shows the characteristic domains of heavy ion physics and the accelerators recently completed or under construction for an attack on the new domains. The low energy region up to 10 MeV/nucleon has revealed a wealth of new aspects, some of which are discussed by others lecturers at this school. The next decade from 10-100 MeV/nucleon might be expected to hold the last contact with the traditional regime of nuclear physics. Here one might expect to see the limits of

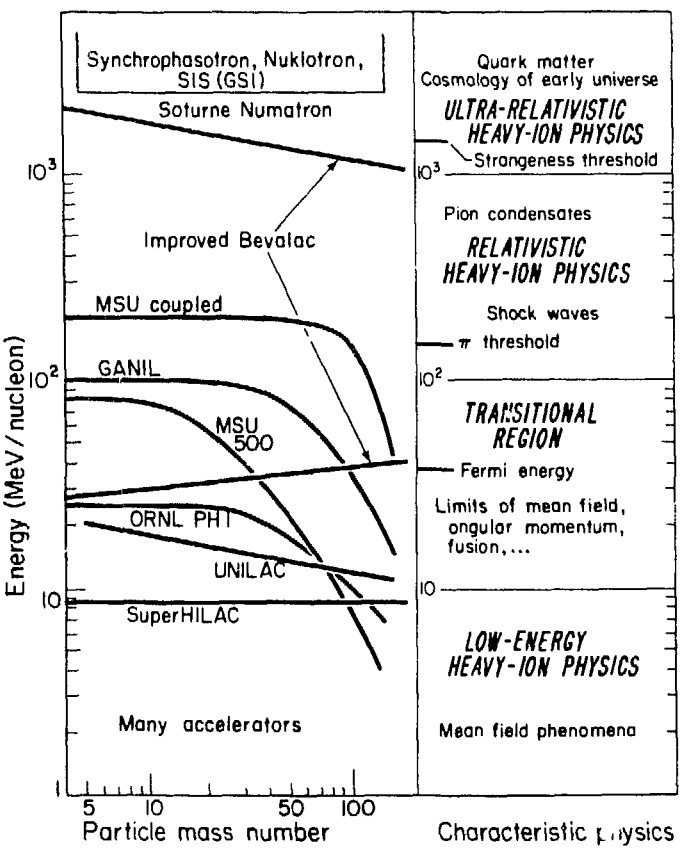

Fig. 1.3

nuclear potentials, states, fusion, angular momentum, mean field, equilibration, spatial and temporal limits and possibly the limits of nuclei, before particle physics aspects become dominant above the pion and strangeness thresholds. The fundamental reason why these limits become accessible is that the decade 10-100 MeV/nucleon contains the Fermi threshold, which defines the motion of nucleons inside the nucleus. We see that many new accelerators are emphasizing this energy domain.

In the decade from 100-1000 MeV/nucleon, the relativistic domain, we hope to uncover new limits concerning the nature of nuclear matter, of temperature and pressure. Here the accelerators available at the present time are the Berkeley Bevalac, the Dubna Synchrophasotron and Saturne at Saclay, all of which reach up to a few GeV/nucleon. A new facility (the Numatron) is under construction in Japan, in addition to the SIS Project at GSI in Germany. Finally the uppermost decade (10^3-10^4 GeV/nucleon) may be attacked by new projects in Dubna (the Nuklotron), at GSI in Germany, and by the VENUS Project under consideration at Berkeley. These experiments, far in the future, may tell us something about the phases of hadronic matter, e.g., quark matter, and who knows what else. It is clear that across the whole spectrum of heavy ion physics the emphasis of modern studies of nuclear collisions is on the relaxation of the limitations that have been imposed in the study of nuclear physics over its sixty year history—limitations such as temperatures, pressures, charge and nucleon number (Scott, 1978a).

Before embarking on our journey to Asymptotia and Wonderland it is useful to have a map to guide us over the contours (Bondorf, 1978). The one shown in Fig. 1.4 is compiled from some detailed voyages, some hearsay evidence from intrepid explorers who have ventured out into the distant continents, bringing back startling tales of strange sights—and some imagination! The plot shows the reaction cross section as a function of energy, and essentially relates impact parameter and energy.

The outer boundary is defined by $\sigma_R = \pi R^2(1 - V/E)$ where $R = R_1 + R_2$ and V is the barrier height. For large impact parameter the cross section is

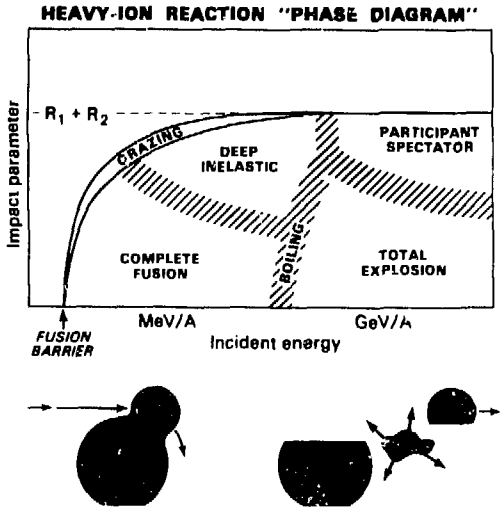

Fig. 1.4

dominated by grazing processes such as simple transfer and inelastic scattering. For closer collisions at low energies, the deeply inelastic process takes over. As illustrated schematically, a dinuclear complex may be formed, and a characteristic time can be associated with the evolution of various collective modes. Estimates of the relaxation times provide a natural hierarchy for categorizing the various degrees of freedom, such as the energy of relative motion, the n-p ratio, the rotational degrees of freedom and the mass asymmetry (for reviews, see Schröder, 1977; Volkov, 1978; Weidenmuller, 1978 and Lefort, 1978). As the energy is increased this process must merge into the still peripheral mechanism of abrasion and ablation (also illustrated schematically on the right). There may not be time for equilibration in the primary stages of the reaction at these high energies.

For close collisions, when the impact parameter is of the order 1.00 ($A_1^{1/3}$ + $A_2^{1/3}$) fm, deeply inelastic reactions merge into the complete fusion of a compound nucleus (Lefort, 1974). At relativistic energies we can speculate that the central collisions lead to a complete explosion into the constituent nucleons. The boundaries of this diagram—if they are reasonably sharply delineated--contain a great deal of interesting physics; we conjecture that the transition to the high energy processes takes place via a region of "nuclear boiling" (Bondorf, 1976). As the average excitation increases, beyond typical intrinsic particle energies (∿30 MeV), the nucleons become less degenerate, the importance of quantum mechanisms diminishes and classical methods becomes increasingly applicable. Instead of a mean field description, one may find that the mean free path becomes very short before nuclei lose cohesiveness; hydrodynamic features may come into play. From the perspective of general physics, the field of intermediate energy nucleus collisions is likely to be very interesting. One is neither in a quantal nor a classical situation, neither in the one body nor the two body extreme, neither close to the adiabatic nor the sudden regime. The explanation of the phenomena in this region may therefore require the development of entirely new theoretical approaches, which may contribute to many branches of physics.

The first lecture will be concerned with the upper sectors of the diagram, the peripheral process, the second with the bottom sectors, the central collisions, and the last will be the utilization of this framework for the study of exotic phenomena.

PERIPHERAL COLLISIONS

A semiemperical "black sphere" expression for the reaction cross section of beam and target nuclei of mass numbers A_p and A_T is (Jaros, 1978),

$$\sigma = \pi r_0^2 (A_p^{1/3} + A_T^{1/3} - \delta)^2$$

The overlap parameter δ is meant to represent the diffuseness and partial transparency of the nuclear surfaces. The fraction of this cross section defined by impact parameters up to 1.00 ($A_p^{1/3} + A_T^{1/3}$) is associated with central collisions and the remainder with peripheral collisions. Although central and peripheral processes appear (Gelbke, 1978) to exhaust roughly the same fraction of the total cross section at low and high energies, the detailed mechanisms are quite different (see Fig. 1.4).

Peripheral Collisions as a Function of Energy

We begin with a discussion of low energy processes. The relaxation of energy in a deeply-inelastic collision is shown in Fig. 1.5. If one assumes that the system rotates with angular velocity $\omega = \ell_{av}/I$ and that the centroid of the peak decays in time, one obtains the relaxation time (Moretto, 1978),

$$\tau_E = \frac{(\theta_g - \theta)}{\omega} \left[\ln \left| \frac{E(\theta_g) - E_o}{E(\theta) - E_o} \right| \right]^{-1} \tag{1.1}$$

where θ_g is the grazing angle, θ is the angle of observation and $E(\theta)$ is the centroid of the kinetic energy distribution at that angle. Typically, $E \sim 3 \times 10^{-22}$ sec, which is very fast (Weidenmuller, 1978). The two ions stick together until they snap, at the time (Bondorf, 1978),

$$t_{collision} = \int_{contact}^{snapping} dt \; \frac{2(R_1 + R_2)}{u} \tag{1.2}$$

which, at energies below 10 MeV/nucleons, is larger than τ_E. More quantitatively we can imagine two nuclei with radii R, colliding with relative velocity u. The collective energy is (Blocki, 1978)

$$E \approx \left(\frac{4}{3} \pi \rho\right) u^2 \tag{1.3}$$

(We are dropping factors of order unity.) If the nuclei are in communication through a window of area πa^2,

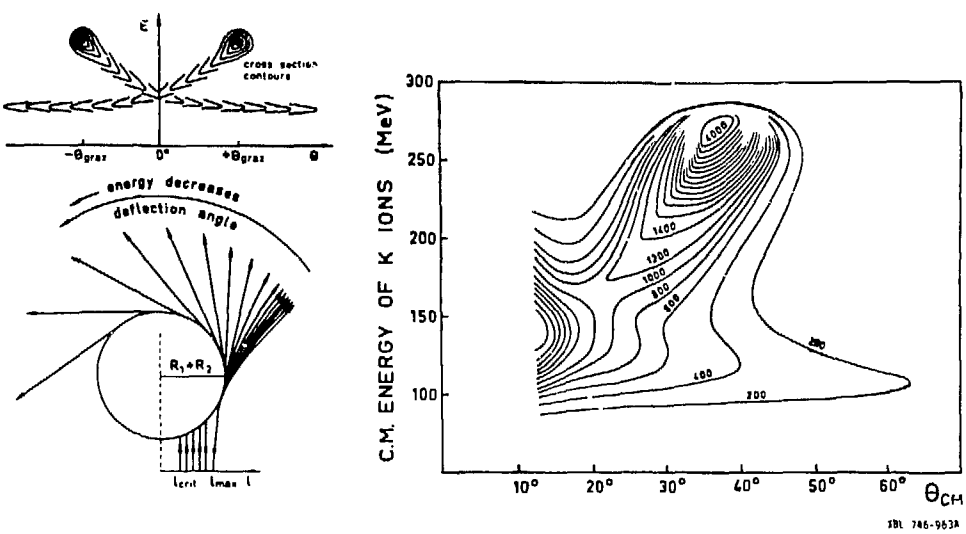

Fig. 1.5

$$\frac{dE}{dt} \approx \frac{1}{4} \rho\bar{v}(\pi a^2) u^2 \qquad (1.4)$$

where $\bar{v}$ is the average intrinsic nucleon speed. Therefore the characteristic damping or stopping time is of order,

$$t_E \approx R^3 \rho u^2/\rho v u^2 a^2 \approx (R/a)^2 (R/v) \qquad (1.5)$$

We compare this time with the collision time, $t_{coll} = R/u$ to give,

$$\frac{t_E}{t_{coll}} = \left(\frac{R}{a}\right)^2 \left(\frac{u}{\bar{v}}\right) = \left(\frac{R}{a}\right)^2 \sqrt{\frac{\text{Energy/Nucleon}}{\text{Fermi Energy}}} \qquad (1.6)$$

Therefore if "a" is not too small, complete damping plays less of a role as the incident energy approaches the Fermi energy. We must then identify the process that takes over the large deeply-inelastic cross section, i.e., at the boundary between deeply inelastic and participant-spectator processes in Fig. 1.4.

It appears that multibody fragmentation phenomena replace the essentially two-body processes of deeply-inelastic scattering. Below 10 MeV/nucleon, the collision time is longer than the transit time of a nucleon at the Fermi level; consequently the whole nucleus can respond coherently to the collision, and the dominant phenomena are characteristic of the mean field (Negele, 1978). At relativistic energies of GeV/nucleon, on the other hand, the reaction processes are dominated by independent collisions of individual nucleons. The transition region might be set by requiring the complete disjunction of the two colliding nuclei in momentum space, i.e., at a few tens of MeV/nucleon. This transition, which could be labelled "from nuclei to nucleons," has been observed in peripheral collisions (Scott, 1978).

The approach is to measure the production cross sections and energy spectra of projectile-like fragments from ^{16}O induced reactions on targets such as Pb, Au as a function of the incident energy. A characteristic feature of many peripheral heavy-ion collisions is illustrated in Fig. 1.6 (Scott, 1979) which shows energy spectra for ^{12}C fragments produced in reactions of ^{16}O on Au and Pb at incident energies of 140, 218, 250 and 315 MeV. All the spectra have a Gaussian-like shape with a maximum close to the energy, E_p, of the fragment travelling with the same velocity as the incident beam. This behavior persists at much lower energies close to the Coulomb barrier and also at relativistic energies of many GeV/nucleon (Fig. 1.7). Here the spectrum is plotted in the projectile rest frame, so that a fragment emitted with beam velocity would correspond to $P_{\parallel} = 0$, where $P_{\parallel}$ is the longitudinal momentum in the projectile frame (Greiner, 1975). At all energies the maximum of the spectrum actually appears shifted below this point, as expected from the separation energy of the projectile into the fragment (Gelbke, 1978). The uniform appearance of the energy spectra argues strongly for a uniform parameterisation. We adopt the form of a Gaussian distribution in momentum space, that has been successfully applied at relativistic energies (Goldhaber, 1974; Feshbach, 1973);

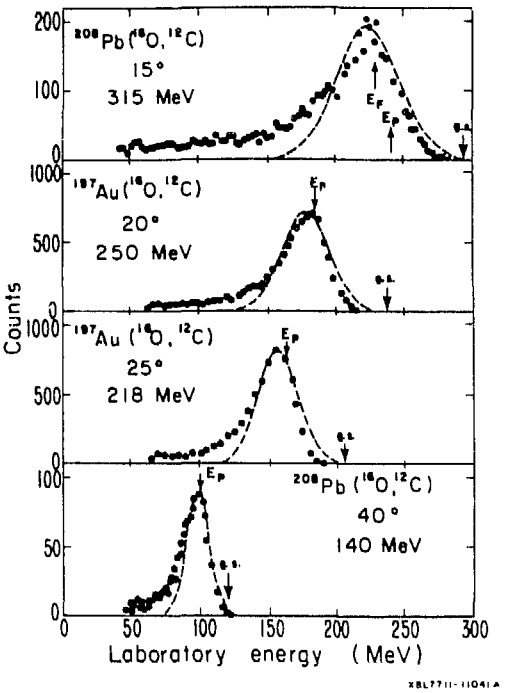
208Pb(16O,12C)
15°
315 MeV
197Au(16O,12C)
20°
250 MeV
197Au(16O,12C)
25°
218 MeV
208Pb(16O,12C)
40°
140 MeV
Counts
Laboratory energy (MeV)

Fig. 1.6

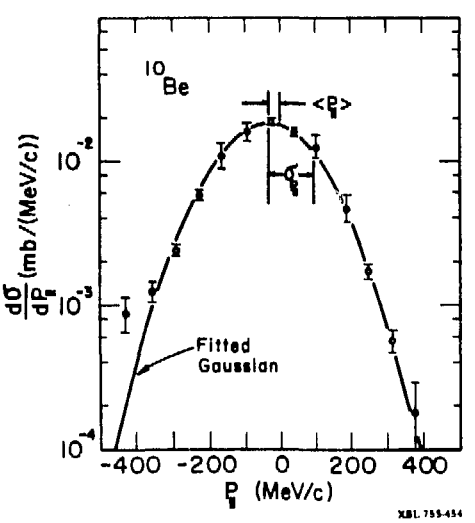
10Be
Fitted
Gaussian
dσ/dP∥ (mb/(MeV/c))
P∥ (MeV/c)

Fig. 1.7

$$\exp\left[-\frac{(p - p_o)^2}{2\sigma^2}\right] ,$$

where p_o is the momentum corresponding to the maximum of the distribution, and σ is the dispersion about the mean. An alternative parameterization of continuum spectra at low energies has recently been derived, in which it is assumed that the distribution is statistical with maximal entropy, subject to constraints imposed by the direct aspects of the reaction mechanism. It would be interesting to extend this approach of surprisal analysis over a wider region of energy (Levine, 1978; Alhassid, 1979; Nemes, 1979). The results of fitting the Gaussian form to the energy spectra are shown in Fig. 1.8. The values of σ_o are shown as a function of the energy/nucleon above the barrier by the open circles; these denote reduced values of σ defined (for reasons discussed below) as $\sigma_o = \sqrt{5/16}\,\sigma$. The values of σ_o increase rapidly between 10 and 20 MeV/nucleon, after which they approach a limiting value. Although this operational parametrization of the data already establishes a novel pattern of behavior, the underlying physics must be sought in the interpretation of the dispersion, σ.

One interpretation of the saturation region relates the value of σ_o to a Fermi momentum distribution of the fragment, which emerges by the sudden shearing of the projectile without prior excitation. Then

$$\sigma^2 = \frac{p_F^2}{5} \quad \frac{A_F(A_p - A_F)}{(A_p - 1)} \tag{1.7}$$

where A_f, A_p are the mass numbers of the fragment and projectile and p_F is the Fermi momentum. Hence

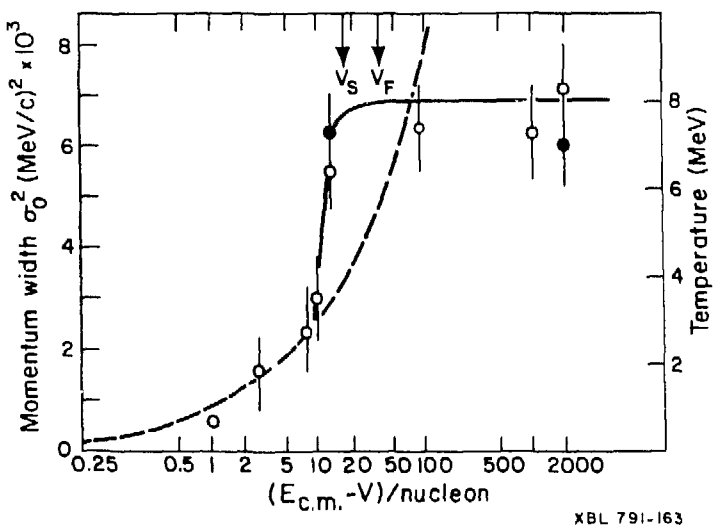

Fig. 1.8

$$\sigma^2 = \frac{16}{5}\,\frac{p_F^2}{5} = \frac{16}{5}\,\sigma_o^2$$

(hence the parameterization described above) and the constant level of σ_o, drawn at 86 MeV/c, corresponds to p_F = 192 MeV/c, which is close to the measured Fermi momentum for a projectile as light as ^{16}O. In this picture the nucleus is suddenly sheared, to give a "snapshot" of the ground state motion of the observed cluster. The process is illustrated schematually in Fig. 1.9, and is well described in the words of Dante: ". . .l'atto suo per tempo non si sporge . . . the act is done, ere time has time to flow" (Wilkinson, 1975). The trend in Fig. 1.8 implies that the onset of this fragmentation behavior is very rapid in the region of 20 MeV/nucleon. Below this energy, we conjecture that there is sufficient time for some equilibration to take place, and indeed the "temperatures" associated with the bottom of the curve (<2 MeV) are typical of the equation of state of a Fermi gas for this system (dashed line), i.e., $E^* \approx (E_c - V) = aT^2$, where $a \approx A/8$.

An alternative interpretation for the limiting value of σ_o comes from an antithetical statistical model, in which the fragments are emitted from a source at an excitation energy determined by a temperature, T (Feshbach, 1973; Goldhaber, 1974). The two models are related by conservation of energy according to the expression, $1/2\ T = 1/5\ p_F^2/2m$, which leads, for the above value of p_F, to T = 8 MeV. (The values of T associated with the scale of σ_o are shown on the right vertical axis). Additional support for the thermal interpretation of a limiting temperature comes from the observation that isotope production cross sections at 20 MeV/nucleon and at relativistic energies, are also explained by a statistical formula, exp (Q_F/T) where Q_F is the appropriate fragmentation Q-value and T is the temperature of the emitter (Lukyanov; 1975; Gelbke, 1978). These derived values of T are shown on Fig. 1.8 by the filled circles. The agreement between values of T deduced from the momentum and isotope distributions could be regarded as strong evidence in favor of the thermal interpretation. However, the apparent statistical formula, exp (Q_F/T), is also inherent in the production of

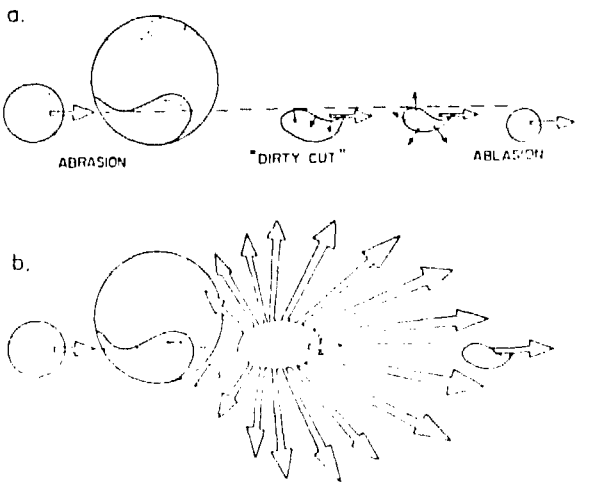

Fig. 1.9

isotopes by the rapid abrasion process, as the following argument shows (Scott, 1979).

The incident projectile in the region of overlap with the target has a part sliced out. The cross section for this process can be calculated using Glauber theory or from geometrical considerations (Hufner, 1975; Olivera, 1979). The cut is not clean but creates a hot region which causes the remaining fragments to be highly excited, so that they proceed to evaporate additional particles--the ablation stage. In the Glauber model at high energies the nucleus-nucleus cross section for an event in which n projectile nucleons are scattered out of the projectile A is given by,

$$\sigma_n = \binom{A}{n} \int d^2\underline{b}(1 - P(b))^n \, P(b)^{A-n} \tag{1.8}$$

where

$$P(b) = \int dz \, d^2s \, \rho_A(s - bz) \exp[-A_T \sigma_{NN} \int dz' \rho_T(x,z')]$$

Here $(1 - P(b))$ is the probability of finding a projectile nucleon in the overlap zone when b is the impact parameter. The above equation is then the cross section for n projectile nucleons to be in the overlap and $(A - n)$ outside. It turns out that σ_n changes very little between 20 MeV/A and 2 GeV/A in spite of a large change in σ_{NN}. However, at high energies the momentum transfer is sufficient (Abul-Magd, 1978) to knock nucleons out of the region of overlap, but at low energies they appear to stay in the prefragment and deposit their energy. The subsequent fate of the projectile fragment (the ablation stage) is therefore rather different in the two cases. This model appears to account both for the isotope differences and the element similarities observed in ^{16}O induced reactions at 20 MeV/A and 2.1 GeV/A (Hufner, 1978).

These formulae lead to the observed approximately Gaussian distribution of isotopes, based on the combinational selection of different numbers of neutrons and protons (Oliveira, 1979). In the absence of correlations in the ground state motion of neutrons and protons, the resultant distribution in isospin could be very broad, since there is a significent probability of removing only neutrons or only protrons. At the other extreme (Bondorf, 1978a, 1978b) in a completely correlated motion, every time we dip in our "sampling ladle"--the abrasion cut--we should get an identical sample of fluid and the distribution would be very narrow (see Fig. 1.10). The actual distribution of observed isotopes will be determined by the degree of correlations present in the ground state. (Recall, however, that an interpretation based on thermal equilibration is also possible.)

For the primary distribution of fragments, our earlier equations lead to a distribution in mass and isospin,

$$\exp - \left[\frac{(a - a_o)^2}{2\sigma_a^2} - \frac{(t_3 - t_{3o})^2}{2\sigma_{t_3}^2} \right] \tag{1.9}$$

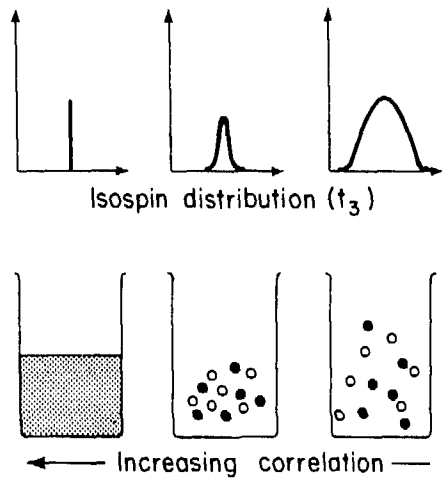

Fig. 1.10

where a = N + Z, the number of nucleons abraded, $t_3 = (N - Z)/2$ and σ_a, σ_{t_3} are the dispersions around the mean values a_o, t_{3_o}. Transforming to the variables N,Z yields the distribution of isotopes about the mean,

$$\sigma \propto \exp\left[-(N - N_o)^2\left(\frac{1}{2\sigma_a^2} + \frac{1}{8\sigma t_3^2}\right)\right] = \exp\left[-\frac{(N - N_o)^2}{\alpha}\right] \qquad (1.10)$$

Values of σ_a, σ_{t_3} are derived from a model with correlations built into the r clear ground state, viz. $\sigma_{t_3} \approx 0.24\ A^{1/3}$, $\sigma_a \approx 4.9\ \sigma_{t_3}$.

In the production of a series of isotopes the changes in A_F are determined primarily by the N-dependent terms in the liquid drop mass formula. For a fragment of mass A_F this term can be written,

$$\frac{a_s(A_F - 2N)^2}{A_F} - \frac{a_{ss}(A_F - 2N)^2}{A_F^{4/3}} \qquad (1.11)$$

where a_s and a_{ss} are the symmetry and surface symmetry coefficients respectively (Preston, 1975). It is then simple to derive a quadratic dependence of Q_F on $(N - N_o)^2$, viz.

$$Q_F \propto 4\left(\frac{a_s}{A} - \frac{a_{ss}}{A^{4/3}}\right)(N - N_o)^2 = \beta(N - N_o)^2 \qquad (1.12)$$

From these equations we get,

$$\exp(Q_F/\alpha\beta) \tag{1.13}$$

which is equivalent to the result of the thermal model, $\exp(Q_F/T)$, with T replaced by $\alpha\beta$. By inserting the values of σ_a, σ_{t_3} and of the mass formula coefficients, we deduce that T = 9 MeV (or 5 MeV with values of σ neglecting correlations). This derivation of isotope distributions ignores the subsequent redistribution by nucleon capture and evaporation, but the value of 9 MeV is close to the required saturation value of 8 MeV in Fig. 1.8. This parameter in the exponential dependence of σ on Q_F is, however, identified with the onset of the fast abrasion mechanism, rather than with the saturation of nuclear temperature in the slower, equilibrating process. Although this degeneracy in interpretation of the saturation region by fast and slow reaction processes leaves open the question of their respective roles in high energy heavy-ion reactions, it emphasizes that both mechanisms are likely to be operative through the transition region leading to the limit. Therefore this transition region must contain much interesting information on the response of heavy-ions to a collision.

Within the framework of the abrasion model, the transition should be related to the tensile strength of nuclear matter. A formal approach to the break-up of nuclear matter can be derived (Bertsch, 1978) by writing for the stress, S,

$$S = P = \frac{\partial E}{\partial V} = \rho^2 \frac{\partial(E/A)}{\partial \rho} \tag{1.14}$$

with

$$E/A = (\hbar^2/2m)\ k^2 + A\rho + B\rho^2 \tag{1.15}$$

In this equation the three terms represent the kinetic energy and the effects of the ordinary and velocity dependent nucleon nucleus potentials. Then the stress becomes,

$$\frac{P}{\rho} = \frac{2}{5}\hbar^2\ 2\frac{k_F^2}{2m}\left(\frac{\rho}{\rho_o}\right)^2 + A\rho + 3B\rho^3 \tag{1.16}$$

from which information on the tensile strength of nuclear matter is obtained by the condition of maximum stress $dP/d\rho = 0$, equivalent to the classical condition of the sound velocity going to zero. In central collisions the energy per particle comes out at a few MeV/A. This approach, if extended to the type of peripheral collisions we have discussed in above, could be a fruitful way of studying continuum properties of nuclear matter.

Some of the features of Fig. 1.8 may also be present in recent TDHF calculations for $^{16}O + {}^{16}O$ carried up to high energies, which are illustrated in Fig. 1.11 (Dhar, 1979). In a TDHF approach the equations for the single particle wave functions χ_n are given by

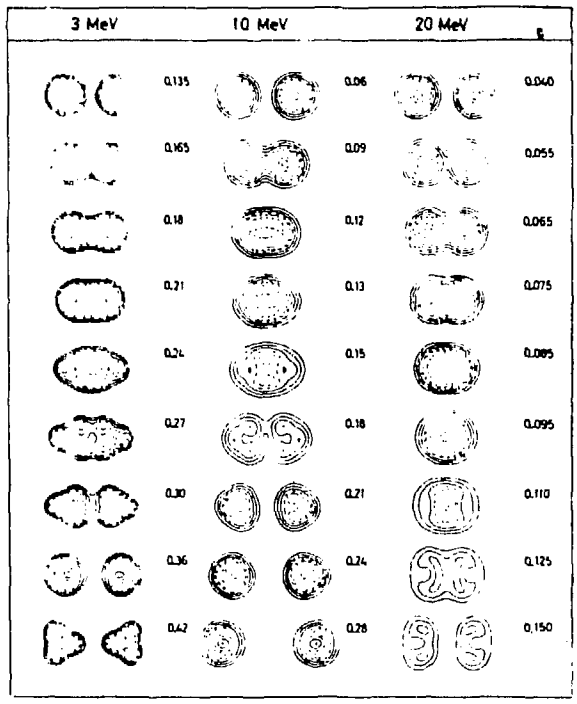

Fig. 1.11

$$i \frac{\partial}{\partial t} \chi_n(r,t) = H(t) \chi_n(r,t) \qquad (1.17)$$

$$H(t) = - \frac{\hbar^2}{2m} \nabla^2 + V(t)$$

and V(t) is an integral over the two-body interaction calculated self-consistently with the single particle wave functions (Negele, 1978). At each instant of time one has to calculate a mean field produced by the influence of all other particles. As the solutions are stepped in time, the self-consistent field is simply the Hartree-Fock potential at the previous step. The initial systems are represented by a product of single particle wave functions calculated in a moving potential; after the collision, one needs a mixture of both sets of wave functions. The computer display of the density distributions of these calculations is shown as a function of time in units of 10^{-21} sec. In the case of E/A = 3 MeV the outermost contours correspond to $\rho = 0.07$ nucleons/fm^3 and 0.04 for the other cases. At the lowest energies we see typical deeply inelastic behavior with the outgoing fragments highly excited in collective oscillations. At 20 MeV/A, however, the ions approach a single sphere configuration at $t \approx 0.09 \times 10^{-21}$ sec with the central density reaching 1.5 times normal; the total energy loss leads to a nuclear temperature of 7 MeV, which is close to the "limiting temperature" of Fig. 1.8. In the Fermi gas model the limit of 8 MeV follows directly by assuming that "A" nucleons participate and carry B*A of excited energy where B has the maximum value of 8 MeV (the binding energy of a nucleon) for the system to survive to

emit a complex fragment. Then, $T = 8$ follows from $8A = (A/8)\,T^2$. Since higher temperatures would lead to a disintegration of the fragment, it is natural to refer to this temperature as that of "nuclear boiling" (Bondorf, 1976). In the TDHF calculation this high temperature leads to a dispersed density distribution, $0.001 \leq \rho \leq 0.02$ nucleons/fm^3.

On the other hand, if we adopt the abrasion model for the description of the high energy data, then the sudden transition from equilibration to fragmentation must contain information on characteristic properties of nuclear matter, such as the relaxation time for spreading the deposition of energy over the nucleus. The initial excitation may be in the form of uncorrelated particle-hole excitations, in which case this relaxation time is related to the Fermi velocity. On the other hand, if the initial excitation is carried by coherent, collective compressional modes, then this time is related to the frequency of these modes, which in turn depends on the speed of sound in nuclear matter (Johansen, 1977). Recent experiments (Youngblood, 1977), determining the frequency of the monopole mode (Pandharpande, 1970) lead to a value of the compressibility coefficient $K \approx 300$ MeV, and an implied velocity of sound $V_s = \sqrt{K/9m}$ of 0.19 c (m is the nucleon rest mass). This velocity and the Fermi velocity in nuclear matter (equivalent to 36 MeV/nucleon) are marked in Fig. 1.8. Although it would be premature to specify which (if either) defines the change of mechanism without a detailed model, the velocity of sound is certainly close to the transition region.

The rapid onset of fragmentation is in agreement with the proposed evolution of Fig. 1.4, in which the boundary between deeply-inelastic and participant spectator processes is constricted to a narrow energy band. The nature of this transition is attracting interest theoretically, both from a microscopic and a macroscopic point of view. In direct reaction models of projectile fragmentation and two-body transfer reactions, the transition to fragmentation occurs at about 18 MeV/nucleon (McVoy, 1979). Following a macroscopic approach, excitation functions can also be interpreted in terms of a generalized concept of critical angular momentum. An energy threshold of approximately 15 MeV/nucleon is predicted at which projectile fragmentation processes set in rapidly at the cost of decreasing cross section for binary transfer reactions. Above this critical energy, few of the projectile fragments can be captured (Siwek-Wilcyzinska, 1979).

New Features at Intermediate Energies

The equivalence of two extreme models for the ^{16}O induced reactions presents an intriguing problem. One model assumes thermal equilibrium by excitation whereas the other infers a fast abrasion process from the nuclear ground state. Both models imply that $\sigma(P_\parallel)$ should equal $\sigma(P_\perp)$, i.e., that the distribution should be isotropic in the rest frame of the projectile, and indeed at 2.1 GeV/nucleon this quality is confirmed within 10% (Greiner, 1975). Recent results at 100 MeV/nucleon give a large anisotropy in the values of $(\sigma_\parallel)$ and $(\sigma_\perp)$ (Van Bibber, 1979). The angular distributions were fitted assuming a Gaussian distribution in the projectile frame of reference:

$$P(p) \propto \exp - \left[\frac{P_\perp^2}{2\sigma_\parallel^2} + \frac{P_\parallel^2}{2\sigma_\perp^2} \right] \qquad (1.18)$$

The solid curves in Fig. 1.12 correspond to the best fit with this expression, which led to a value of $\sigma_o \sim 83$ MeV/c associated with $\sigma_\parallel$ in close agreement

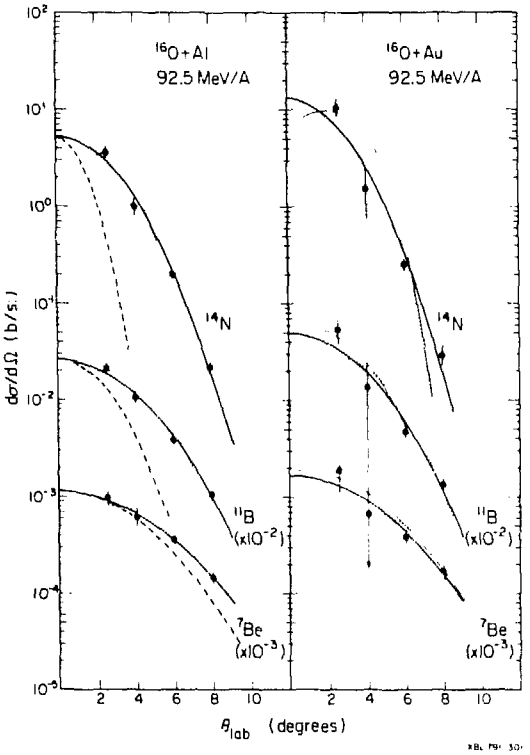

Fig. 1.12

with the results for ^{16}O beams at other energies. The corresponding value associated with $\sigma_\perp$ is in excess of 200 MeV/c for all fragments, and is to be compared in Fig. 1.12 with the dashed line which is constructed for $\sigma_\perp = \sigma_\parallel$ (both corresponding to σ_o = 86 MeV/c).

The increased widths appear to arise from refraction of the particle trajectories in the optical potential, which leads to a momentum dispersion. We can write for the production of fragment (F),

$$\sigma^2_{P_\perp}(F) = \frac{F(A-F)}{A-1}\,\sigma_1^2 + \frac{F(F-1)}{A(A-1)}\,\sigma_2^2$$

where $\sigma_1^2 = 1/2\,(P^2_{i\perp}) = \sigma_o^2$ is the usual term due to intrinsic motion discussed earlier, and $\sigma_2^2 = 1/2\,(P^2_{A\perp})$ is the variance in the projectile (A) momentum at the time of fragmentation. In order to calculate σ_2^2, we derive the classical deflection function in the optical potential, assumed of Woods-Saxon form for the nuclear component (r_o = 1.2 fm, a = 0.6 fm). Another input to the calculation is the ratio σ (fragmentation)/$\sigma_{tot} \approx 0.6$, which defines the range of impact parameters b, over which the deflection function operates. Then $\sigma_2^2 = 1/2\ P_A^2 \int N(b)\ \sin^2\theta(b)\ db$, where $N(b) = 2b/(R^2 - b^2)$ is the weighting factor for impact parameter. The results

for Al and Au targets are shown in Fig. 1.13 in which the evolution of σ (for σ_1 fixed at 84 MeV/c) is shown as a function of σ_2 in section (d), together with the best fit . Note that for $\sigma_2 = 0$, the parabolic form characteristic of relativistic energies is restored, as the effect of refraction becomes negligible.

One might infer from the constancy of σ_2 with fragment mass that the full range of impact parameters is effective for all fragments. Superficially, this result contradicts the predictions of abrasion calculations where the orbits responsible for different final masses sample different regions of impact parameter space (Hufner, 1975). The effect of folding the deflection function with the abrasion calculation is shown in Fig. 1.12 by the fine lines and results in significant differences near 0^{o}. Such measurements could illuminate details of the optical potential for deep incursions into the nuclear interior, and would complement the study of potentials via heavy ion elastic and inelastic scattering and fusion (Birkelund, 1978, 1979). Such measurements have been used to establish the form of the proximity potential at distances ≈ 1 fm inside the strong interaction radius. The status of such measurements is shown in Fig. 1.14, by the proximity function Φ as a function of $S = r - (R_1 + R_2)$; the abrasion of fragments such as Li from ^{16}O could probe into much greater depths. For example, the region of impact parameter space spanned by the calculations of Fig. 1.13 are shown by the shaded areas of the deflection functions in Fig. 1.15.

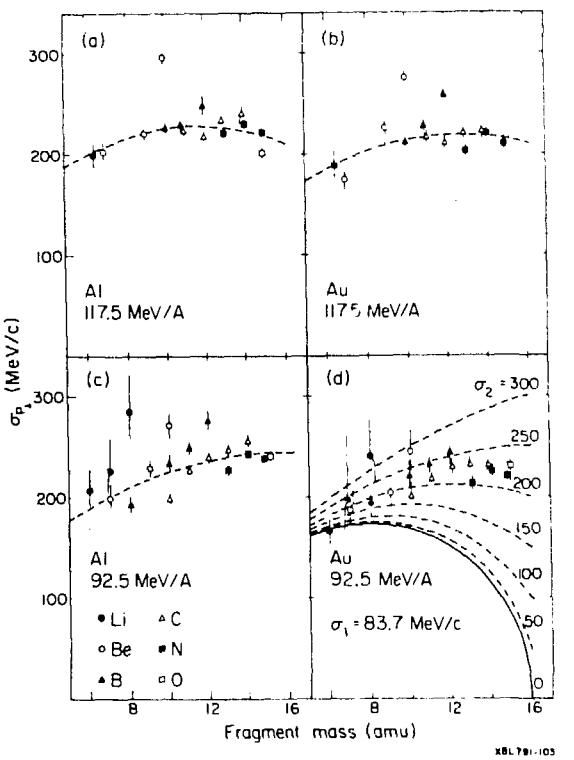

Fig. 1.13

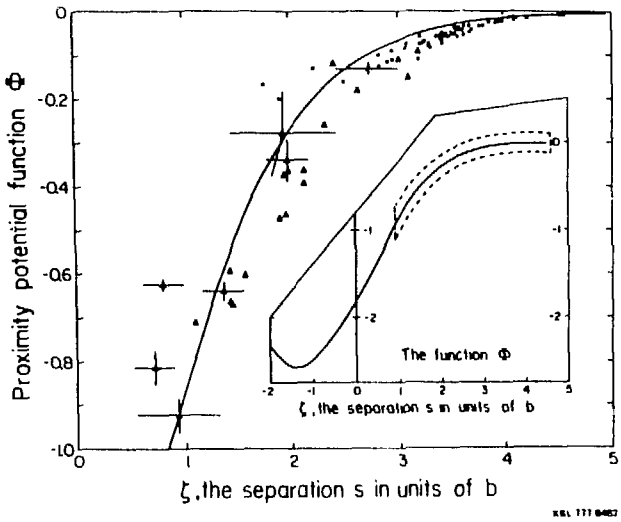

Fig. 1.14

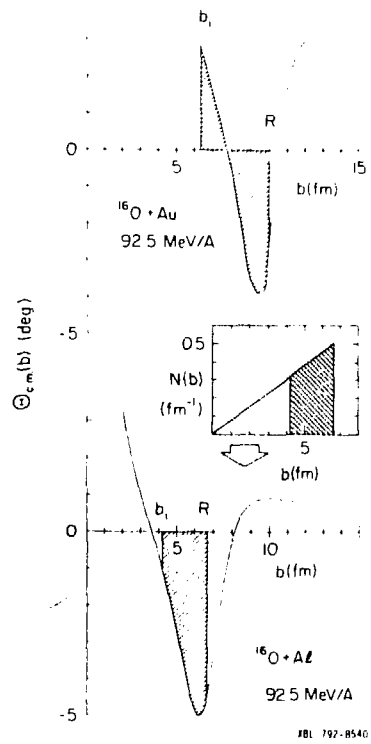

Fig. 1.15

Ground State Correlations

Further insight might be expected from studies with heavier projectiles like ^{40}Ar, for which the characteristic reaction processes of deeply-inelastic scattering are well developed at low energies. Results are now available for

^{40}Ar + Th at 6, 9, 65, 100 and 213 MeV/nucleon (Viyogi, 1979). The isotope identification at 213 MeV/nucleon was achieved by combining multiple ΔE-E identification in a 9 element detector telescope, with magnetic analyses. The energy spectrum for ^{34}S appears in Fig. 1.16, which again has a Gaussian form, peaking at an energy corresponding to the beam velocity. The values of σ_0 deduced from the wide variety of isotopes at the bottom of the figure is 94 ± 5 MeV/c, i.e., equivalent to a Fermi momentum of 210 MeV/c, or a "temperature" of 9.5 MeV. In a thermal model one might expect that the local energy deposit (presumed similar to the ^{16}O projectile) would spread out more, resulting in a lower effective temperature. Since the value is in fact slightly higher than the value of 8 MeV for ^{16}O, one might conclude that the fast abrasion process is the correct description of the dominant reaction mechanism.

On this assumption, let us see what interesting microscopic aspects become accessible for study in these relativistic heavy-ion collisions. As we indicated for ^{16}O, there is a possibility of observing the effect of correlations in the nuclear ground state (Bondorf, 1978a, 1978b). These experiments measure the number of particles in a subvolume of an extended Fermi system (Bertsch, 1979). In order to study this effect calculations have been done with a microscopic model (ignoring correlations) and a macroscopic model including correlations arising from the zero point motion of the giant dipole mode (Morrissey, 1979).

The microscopic approach was based on the intranuclear cascade model. Individual projectile and target nucleons move at uniform velocities between collisions, the position and outcome of each collision in a given cascade

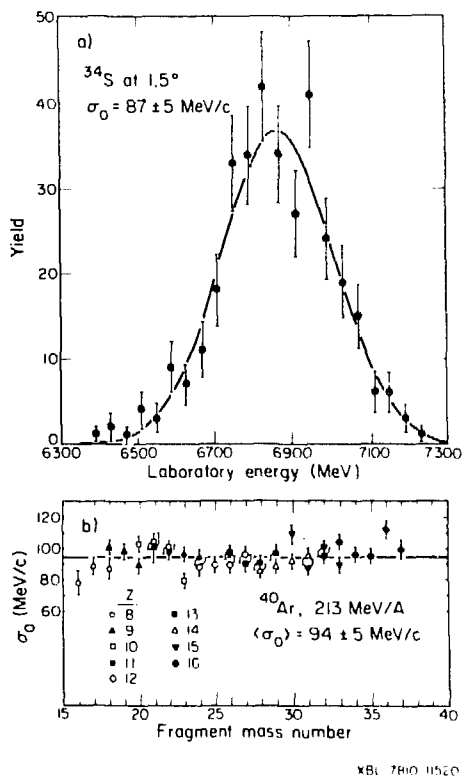

Fig. 1.16

determined by the random sampling of probabilities derived from elementary cross sections. Meson production was included via the isobar model (Harp, 1973), and the Fermi motion was included in projectile and target. The nucleons were uncorrelated insofar as the probability of the colliding partner being a proton or a neutron was selected at random.

The effects of the correlations were incorporated into a macroscopic abrasion model. The fluctuations in the number of swept out nucleons arises from the zero point motion of the giant dipole model, which is an out-of-phase vibration of protons and neutrons (Morrissey, 1978). (This calculation can be viewed as the leading term of the correlated model discussed earlier, which actually included very high orders of zero point multipole vibrations, from $\ell = 0$ to $\ell = 9$). A comparison of the primary fragment distributions is given in Figs. 1.17(a) and (c), in which the dramatic narrowing of the distributions due to the correlations is evident. This effect is, however, largely washed out by the subsequent decay of the primary fragments, which, as shown in Fig. 1.18, are highly excited (up to 200 MeV for 6 nucleons removed from the projectile). The statistical de-excitation focuses the primary distributions back into the valley of stability, and the end products, are disappointingly similar (see Fig. 1.17(b) and (d)). The results are however in fair agreement with the data; a quantitative comparison of the cascade (histogram) and abrasion model with correlations (solid line) for isotopes of Na, Ng and Al is given in Fig. 1.19.

Although it is not possible to claim at this stage that ground state correlations have been observed unambiguously, there is hope that the use of more neutron excess projectiles will open up this interesting application of relativistic heavy ion collisions. Look, for example, at the case of ^{48}Ca + ^{12}C in Fig. 1.20 (Morissey 1979). Here the secondary decay processes are

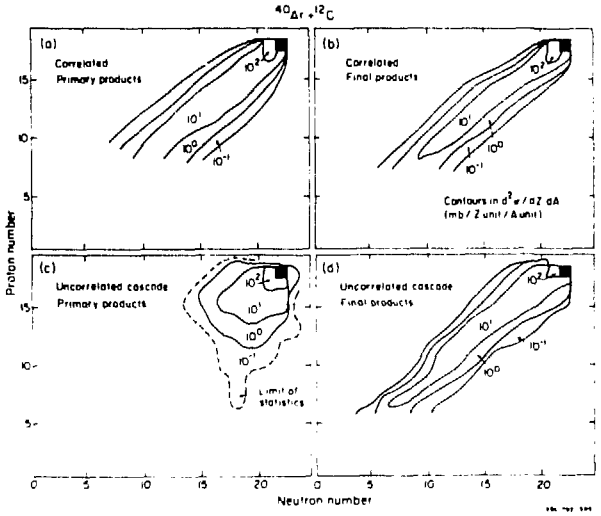

Fig. 1.17

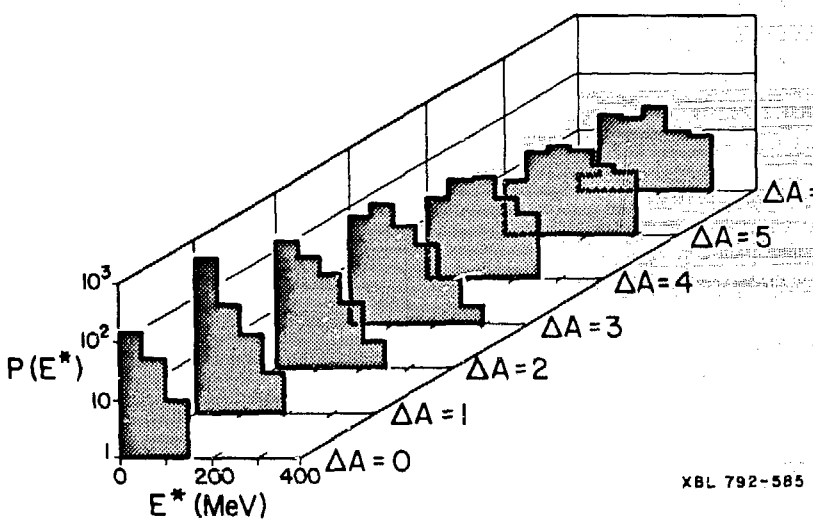

Fig. 1.18

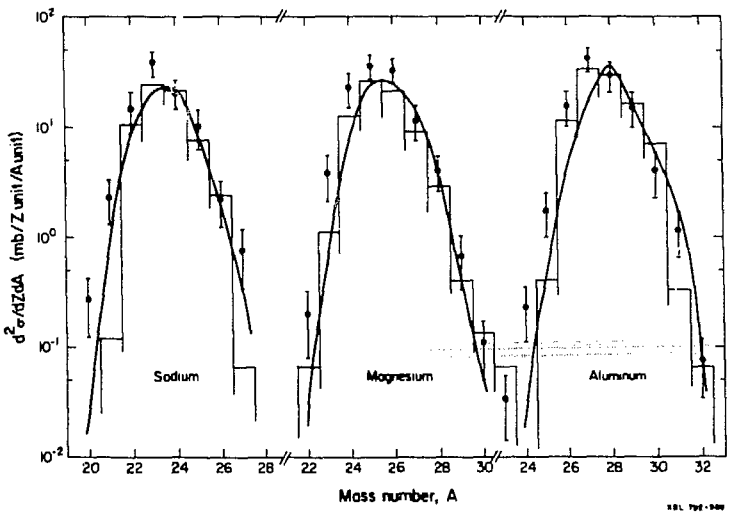

Fig. 1.19

unable to obliterate completely the memory of the primary distribution, which remains very narrow, particularly for products close to the projectile.

At this point it will be constructive to examine the role of mass distributions in the broader context of heavy ion reactions at low, intermediate and high energies. In Fig. 1.21 the distribution of magnesium isotopes is compared at a very low energy of 5 MeV/nucleon (Volkov, 1978) and at 200 MeV/nucleon. We notice that the peak of the distribution shifts from an N/Z value characteristic of the dinuclear complex in deeply inelastic scattering, to a value closer to the projectile due to the abrasion process (remember that both distributions are perturbed by the secondary decays) (Bondorf, 1973). The gaussian distribution of the form,

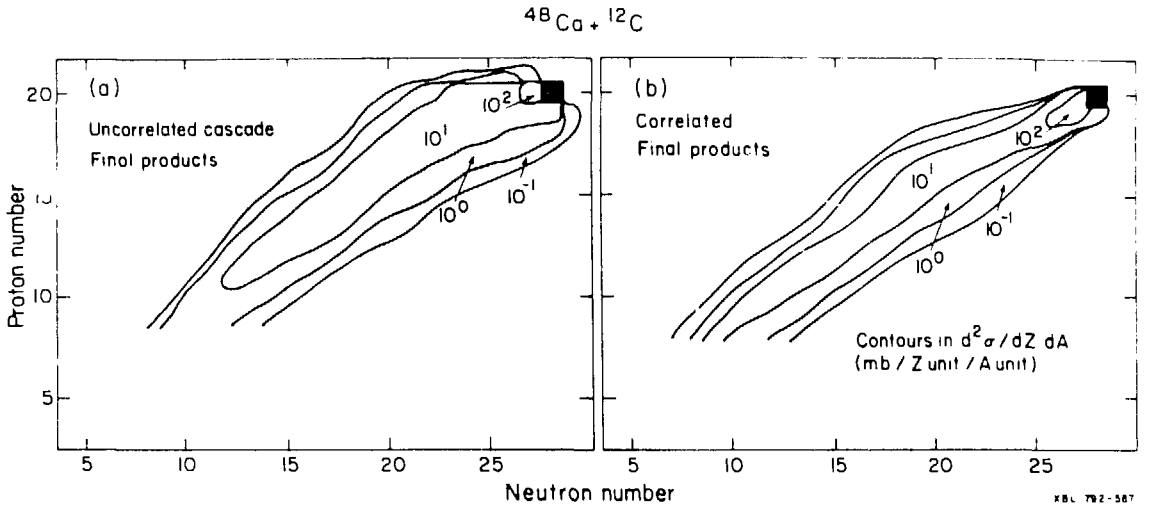

Fig. 1.20

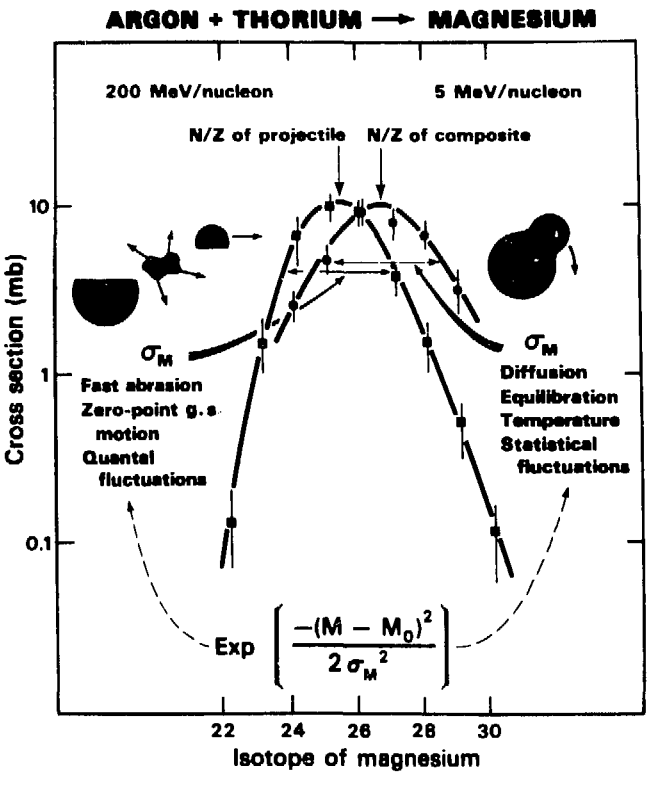

Fig. 1.21

$$\exp \frac{-(M - M_o)^2}{2\sigma_M^2} \tag{1.20}$$

has a dispersion σ_M, which in one case describes the diffusion, equilibration and temperature due to statistical fluctuations, whereas at high energies it describes zero point quantal fluctuations. An interesting question concerns the evolution of one curve into the other. Will this also happen suddenly as the temperature approaches 8 MeV, just like the ^{16}O case (see Fig. 1.8)? Here there may be microscopic features to be studied unique to high energy heavy ion reactions.

We have seen that the giant dipole mode may be important in high energy collisions; it is also expected to play a role in deeply-inelastic scattering, particularly in the equilibration of the neutron excess degree of freedom, which determines the isotope distributions (Brosa, 1978). If we describe the neutron excess mode by an harmonic oscillator, it has to be considered in a heat bath at temperature T (Berlanger, 1978). Then the variance of the atomic number distribution for fixed mass asymmetry is,

$$\sigma_2^2 = \frac{1}{B\omega^2} \frac{1}{2} \hbar\omega + \frac{\hbar\omega}{\left(\exp \frac{\hbar\omega}{T} - 1\right)} \tag{1.21}$$

where B is the inertia connected to the mode and ω is the collective frequency. Two limiting cases are of great interest: when $\hbar\omega << T$, $\sigma_Z^2 \approx T/B\omega^2$ and the dispersion increases as $\sqrt{T}$; in such a case, we deal with statistical fluctuations, and the basic effect is nicely illustrated in Fig. 1.22 for Xe + Bi, where the charge dispersion increases with energy

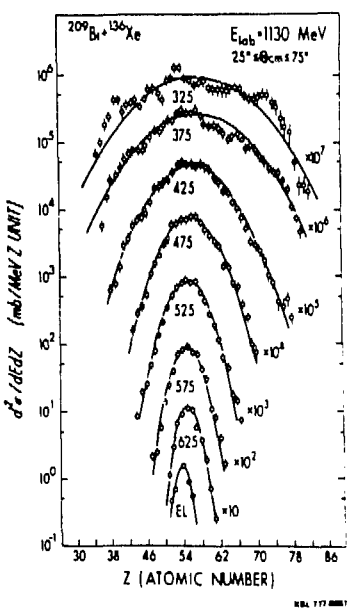

Fig. 1.22

loss. On the other hand, when $\hbar\omega >> T$, we get $\sigma_Z^2 = 1/2\ \hbar/B\omega$ and σ_Z is independent of temperature. The implication is that we observe only a zero point motion, arising from quantal rather than statistical fluctuations, just as in our high energy example. The experimental results for σ_Z in the $^{86}Kr + ^{92}Mo$ system as a function of the dissipated kinetic energy are shown in Fig. 1.23. The dispersion reaches a plateau independent of temperature, implying that the zero point motion of the collective mode of the dinuclear complex is observed. In the high energy cases discussed earlier, quantal fluctuations of the dipole mode in the projectile rather than in the dinuclear system, were at work. It is intriguing to note, however, that the value of T in the above example is 8.6 MeV, very close to the "limiting temperatures" we discussed earlier!

Microscopic Aspects

It is becoming clear that giant collective modes are crucially important in understanding the nature of peripheral heavy ion collisions over a wide range of energies. It may therefore also be constructive to look at the direct excitation of giant resonances in heavy ion collisions. The inelastic excitation of ^{16}O on ^{208}Pb at 20 MeV/nucleon in Fig. 1.24 (Doll, 1979) shows the excitation of low lying collective states, the giant quadrupole at 10.8 MeV, and the structure at approximately 19 MeV, attributed to L = 3 and 5 multipoles. The assignment of $\ell = 3,5$ is inferred partly by the indirect comparison with the theoretical response function shown at the bottom of the figure. The stronger excitation of these high multipolarities in heavy ion scatterings, compared to hadron scattering or electron scattering experiments,

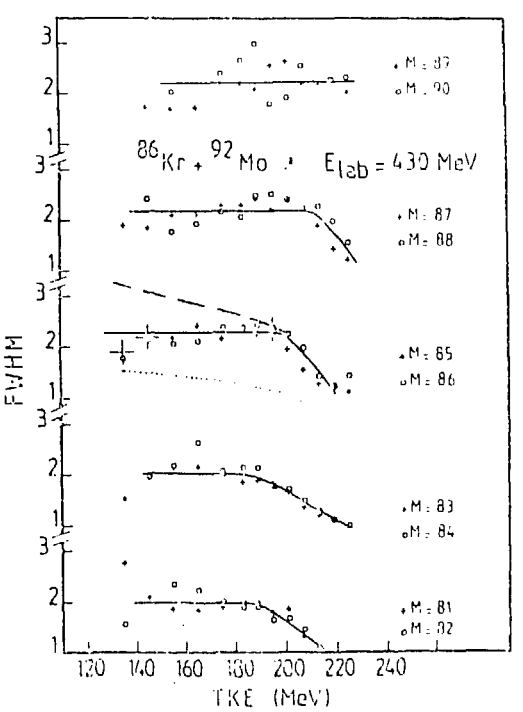

Fig. 1.23

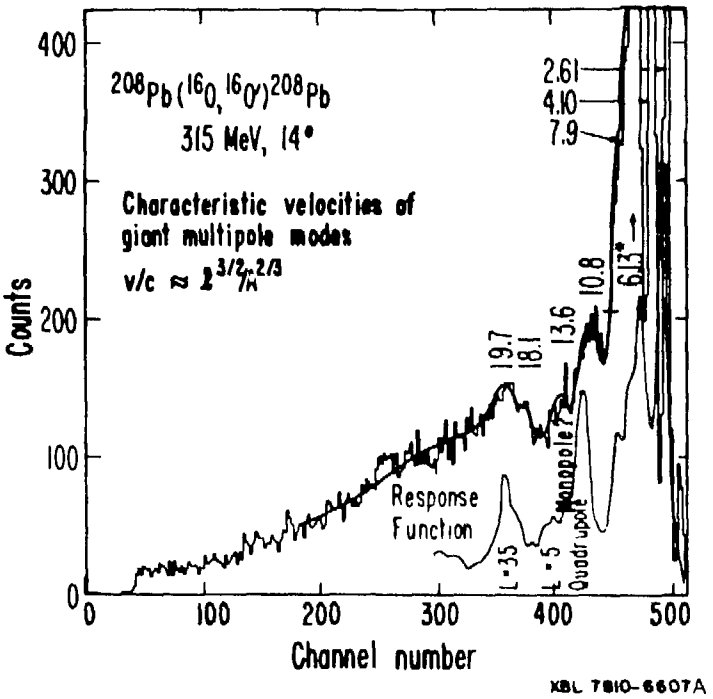

Fig. 1.24

may stem from a better matching of the collision time to the characteristic frequency (Bondorf, 1974) of the mode ($\ell^{3/2}/A$). The results of DWBA calculations for ^{16}O on ^{208}Pb are shown in Fig. 1.25 (Bertrand, 1978). For

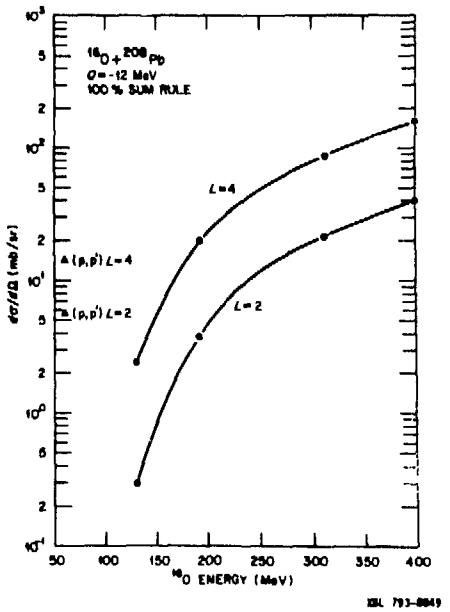

Fig. 1.25

comparison the cross sections obtainable with 60 MeV protons are also plotted, and the exciting prospect is the increasing cross sections for exciting high multipolarities with very high energy heavy ions. Studies of peripheral collisions over a wide region of incident energy, where the cross section for primary excitation is increasing rapidly, while the cross section for deeply inelastic scattering is decreasing, may also help to elucidate their role in deeply inelastic processes (Broglia, 1978).

The giant dipole continues to exert an important influence even at energies of 1 and 2 GeV/nucleon. The effect has been revealed by a deviation of high energy peripheral fragmentation cross sections from the trends of two high energy particle physics concepts. The first feature is called "limiting fragmentation" (Benecke, 1969) or "scaling" (Feynman, 1969), which means that a distribution of products in the rest frame approaches a limiting form as the bombarding energy increases. We have shown earlier that for ^{16}O projectiles the distribution approaches an asymptotic form already at energies of 30 MeV/nucleon, and some caution should therefore be exercised on the role of truly limiting high energy concepts!

The second feature is "factorization" of the cross sections into a projectile and a target term (Frazer, 1972; Boggild, 1974). For the reaction A + T → F + anything,

$$\sigma_{AT}^{F} = \sigma_{A}^{F}\gamma_{T} \quad . \tag{1.22}$$

where γ_T depends only on the target nucleus. A dramatic illustration (Cumming, 1974) of both concepts appears in Fig. 1.26, which compares the yields of target fragments produced by 3.9 GeV/A nitrogen ions (upper curve) and 3.9 GeV/A protons (lower curve). (The data are displaced by a factor of ten for display.) However, other experiments indicate that the distributions

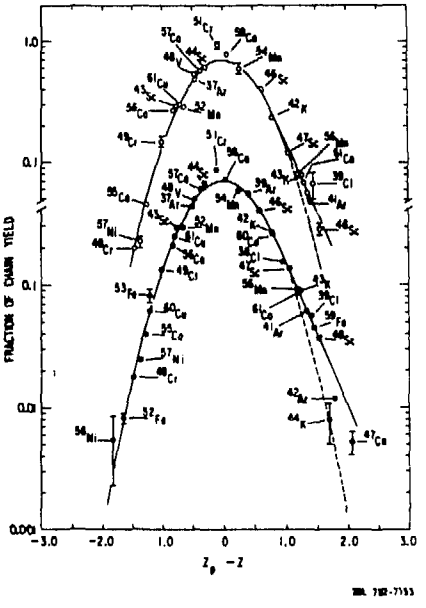

Fig. 1.26

only become similar to those for protons of the same total energy as the heavy ion, rather than of the same velocity, which could argue that the heavy ion acts collectively with the target like a single entity (Morissey, 1978). The strongest deviations from the factorization hypothesis are the one-nucleon loss cross-sections with ^{16}O and ^{12}C on high Z targets (Heckman, 1976). The deviation is explained as the Coulomb dissociation of the projectile in the electric field of the target. The projectile is excited to the giant dipole resonance which then decays by particle emission. The very peripheral nature of the collisions implies that the fragmentation of the projectile is a consequence of the action of a field of force emanating from the nucleons in the surface of the target. Even at very high energies, the limitations on energy and momentum transfer make peripheral relativistic heavy ion collisions essentially a low energy phenomenon. In the language of nuclear physics, both factorization and limiting fragmentation are examples of Bohr's independence hypothesis for decay products of a compound nucleus. Factorization is also expected from simple direct reaction models (Jackson, 1977). These different concepts must be tested further in experiments on coincidences between heavy fragments and evaporated light particles or γ rays (Shibata, 1978). Nevertheless the subject of peripheral collisions of relativistic heavy ions is the best understood theoretically.

Although the primary motivation for the study of relativistic peripheral heavy ion collisions remains the search for new phenomina, we have mainly discussed more traditional areas. Such a pattern is frequently characteristic of research. The search (so far unsuccessful) for superheavy elements led to a new reaction mechanism known as deeply inelastic scattering. The study of peripheral collisions over the whole energy range has been analyzed by a number of theoretical techniques, well tested in the familiar domains of nuclear and particle physics. At the same time, new insights into these traditional high and low energy limits have been gained, which demand new reaction theories to describe the evolution of heavy ion reactions from a few MeV/nucleon up to several GeV/nucleon. It is also possible that peripheral collisions may reveal exotic aspects of heavy ion reactions, such as effects of compression, through an understanding of data such as in Fig. 1.3. Nevertheless the greater hope is believed to be in more central collisions, to which subject we now proceed.

CENTRAL COLLISIONS

"I shall make a Star Chamber matter of it."

Shakespeare,
The Merry Wives of Windsor

Introduction

The limit of a central collision corresponds to two nuclei hitting head-on with small impact parameter. A probable example of such an event is shown in Fig. 2.1, taken in a steamer chamber. The collision is of Ar + Ca at 1.8 GeV/nucleon (Schroeder, 1976), and we see that there is a star explosion; the total multiplicity of charged particles ranges up to the number in the initial system, suggesting that the nuclei are completely disintegrated. The hope is that novel states of matter will manifest themselves in the extreme conditions of temperature and pressure that are most likely to be present at the early stages of the collision. Therefore, one very much hopes to "make a star chamber matter of it" but there are many obstacles--the most significant

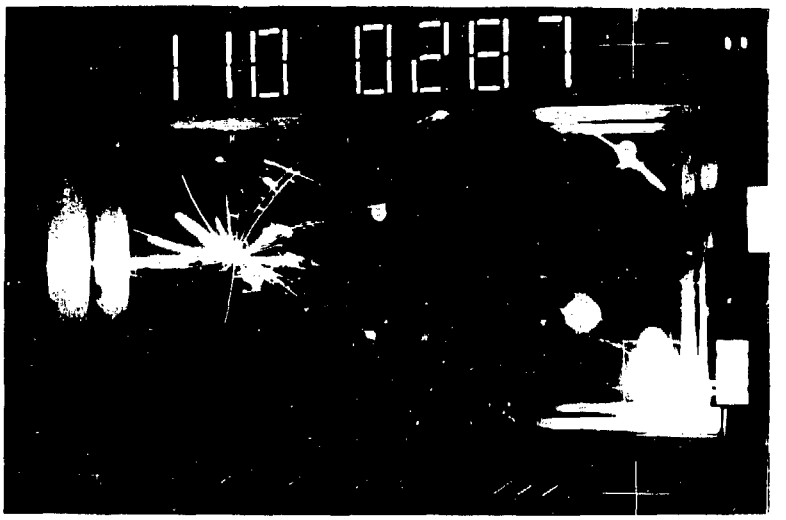

XBB 7511-8445

Fig. 2.1

being that only asymptotic states can be observed experimentally. As in our discussion of peripheral reactions, we shall proceed from the low energy perspective, to see how the spectacular events of Fig. 2.1 evolve from the more familiar central collision processes of fusion and fission along the bottom regions of Fig. 1.4.

The Low Energy Perspective

Some of the paths taken by low energy heavy ion collisions are shown in Fig. 2.2 (the time scale is in units of 10^{-22} sec) (Lefort, 1976). It illustrates how the composite may proceed to compound nuclear formation, possibly ending in symmetric fission, and also to the new path of deeply inelastic scattering where the composite system never fuses completely but separates on a short time scale into two fragments reminiscent of the initial ions. A schematic division of the reaction cross sections as a function of ℓ is given by the sloping line which represents the unitarily limit $\sigma = \pi R^2(2\ell + 1)$. For high partial waves, direct reactions occur; then at closer impacts come the deeply-inelastic processes and finally the compound nucleus formation. For almost head-on collisions it is possible, according to recent speculations (Negele, 1978; Bonche, 1979), that the nuclei either bounce off or pass through each other, instead of fusing.

Some insight comes (Vigdor, 1979) from the $^{16}O + ^{40}Ca$ reaction as a function of energy (see Fig. 2.3). Initially, the fusion cross-section follows the prescription $\sigma_f = \pi R^2(1 - V/E)$ for the total reaction cross section, but at a critical energy begins to deviate. It is believed that beyond this point some partial waves are not allowed to participate in fusion, because they do not allow the nuclei to come within the critical fusion distance of $1.00\,(A_1^{1/3} + A_2^{1/3})$ fm. The cross-section is drained off instead into deeply inelastic scattering. At still higher energies the fusion cross-section again decreases possibly on account of surpassing the liquid drop limit (Cohen, 1974) so that the system can no longer sustain the angular momentum (Stokstad, 1977), and flies apart in fission. Another intriguing explanation comes from TDHF calculations, which suggest that in the energy

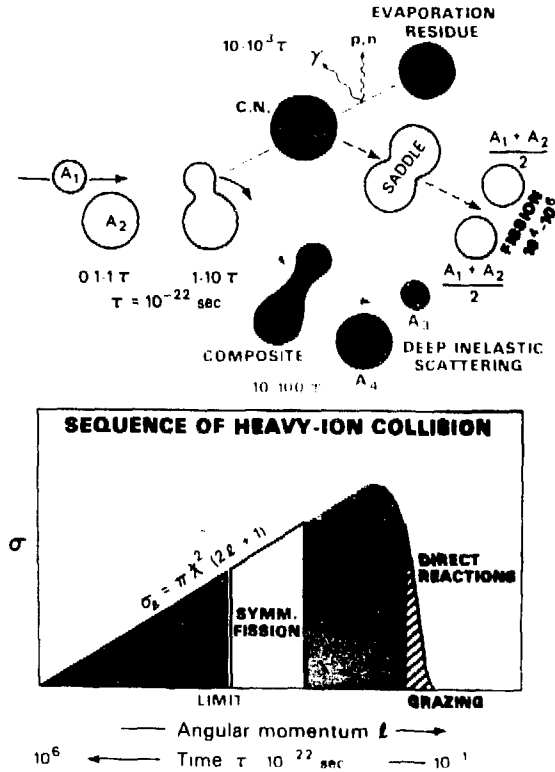

Fig. 2.2

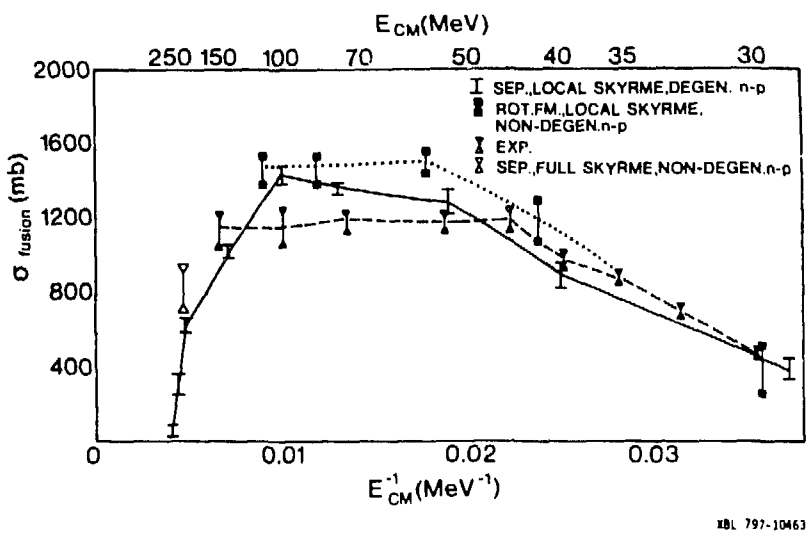

Fig. 2.3

region of 20 MeV/nucleon the nuclei become transparent (Bonche, 1979). (The TDHF results shown on the figure are preliminary.) It is also possible, however, that new processes set in, such as the sudden fragmentation and pre-equilibrium emission suggested by the TDHF calculations at this energy (Fig. 1.11), which remove cross section from the fission channel.

The question of transparency is of fundamental importance to relativistic heavy ion collisions, since high densities cannot be achieved if nuclei pass through each other. The results of a recent semi-classical analysis indicate that at an energy per nucleon of 250 MeV, composite projectile collisions may be more transparent than proton collisions with the same target nucleus (DeVries, 1979).

In order to see how fusion begins to fade into the higher energy catastrophic processes, we need an operational definition. One criterion is the stipulation of complete momentum transfer from the incident projectile, which can be checked for heavy nuclei by measuring the fission fragments following fusion. These can be used to reconstruct the momentum of the recoiling fissioning nucleus, and the results of several measurements at low energies (<10 MeV/nucleon) confirm that there is indeed 100% momentum transfer. (See the example (Viola, 1976) of ^{20}Ne + U in Fig. 2.4; the data are plotted as a function of the angle θ^{AB} between the fission detectors.) At 20 MeV/nucleon the situation appears to be different, as shown by the experiment on fission fragments in coincidence with a leading particle in the reaction ^{16}O + $^{238}U \rightarrow X$ + fission in Fig. 2.5 (Dyer, 1979). The figure shows that both for the inclusive measurement and for a proton detected as X, the momentum transfer is incomplete. This experiment also gives an elegant signature for the division between peripheral and central collisions in heavy ion reactions; for lithium as the leading fragment the reaction appears to be almost completely perpheral, with a very small momentum transfer. Similar studies have not yet been undertaken at relativistic energies, where the technique may also serve as a measure of impact parameter.

Further insight comes from the energy spectra of light particles emitted in coincidence with the fission fragments (Awes, 1979). As shown in Fig. 2.6 both for peripheral ($\theta_{AB} > 160^o$) and central collisions ($\theta_{AB} < 160^o$), the energy spectra of p, d, t and α particles have an exponential tail of the form exp(-E/T) with a slope parameter T of 13 MeV. How are we to interpret these results? Recently it has been suggested that the "prompt emission" of

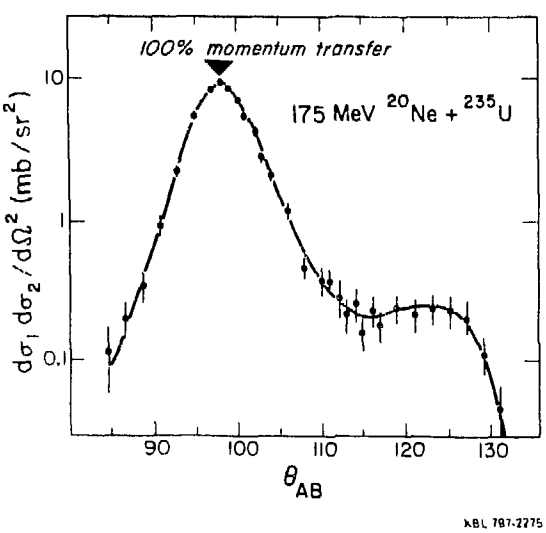

Fig. 2.4

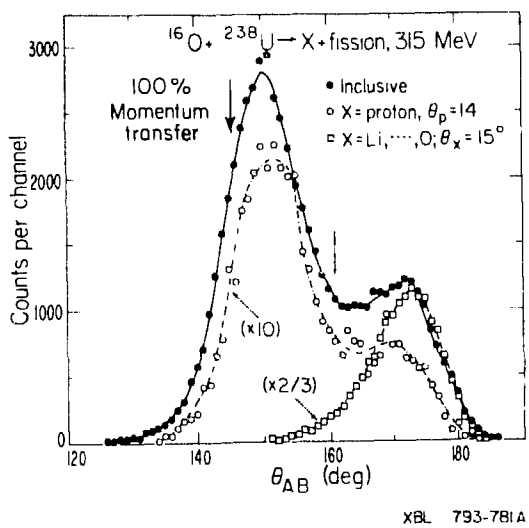

Fig. 2.5

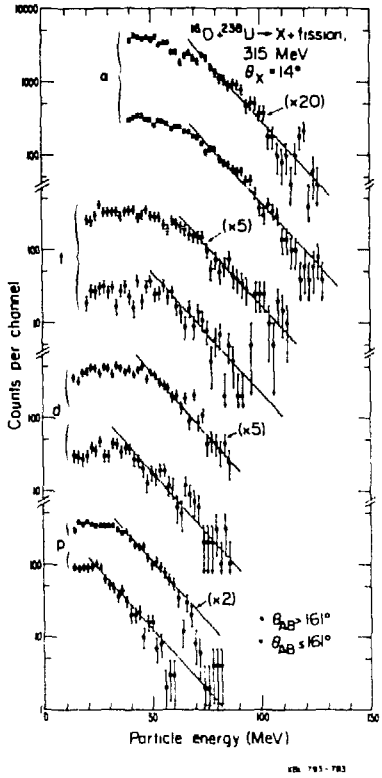

Fig. 2.6

energetic light particles should become an important aspect of heavy ion reactions at energies of a few tens of MeV/nucleon (Bondorf, 1978; Robel, 1979). These promptly emitted particles (PEPS) should be produced at a very early stage of the collision, and could yield energy spectra rather independent of the final fate of the colliding nuclei. Quantitative comparisons of PEP production with fast neutrons emitted in fusion reactions (Westerberg, 1978) have already been made.

In general the production of fast light particles, i.e., pre-equilibrium emission, has not received extensive study in heavy-ion reactions (Blann, 1976), although it is well known in light ion reactions. The reason becomes clear from a comparison of two typical reactions in Fig. 2.7. In light ion reactions, the average energy loss (Δ) per collision is large and the number of collisions (N) for complete dissipation of the energy by excitation of particle-hole states is small. Furthermore, the fluctuations $\delta E = \sqrt{N}\,\Delta$ are large and comparable to the energy E. The opposite is the case for low energy heavy ion reactions. Only small energy dissipation occurs per step, and the low-lying excitations are unlikely to decay by pre-equilibrium emission. Let us now consider how the picture changes at higher energies of 20 MeV/nucleon, by considering some relevant time scales. We shall see that light particle pre-equilibrium emission becomes a vital connecting link between low and high energy phenomena.

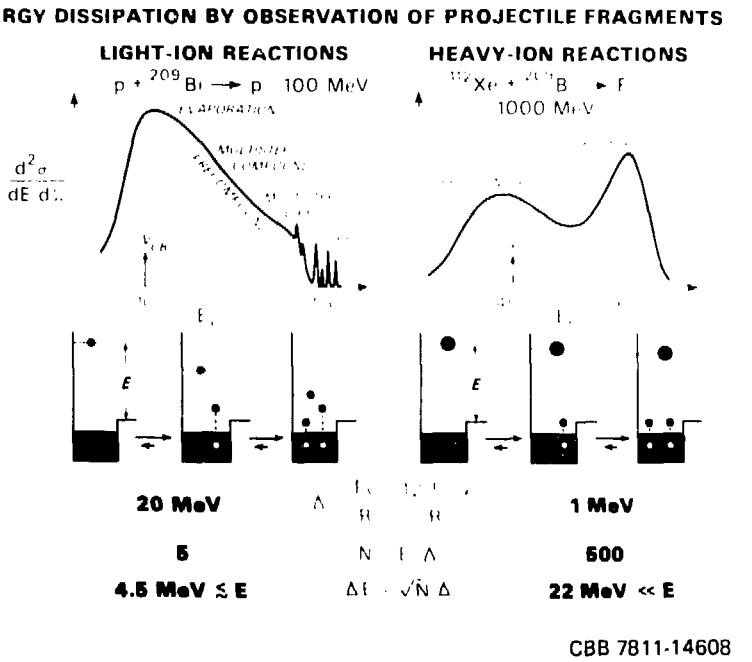

Fig. 2.7

Time Scales in Heavy Ion Collisions

We can estimate the time it takes an equilibrated nucleus to emit a particle. An empirical fit to the measured widths of compound nuclei for A = 20-100 yields (Bohning, 1970);

$$\Gamma(\text{MeV}) = 14 \exp(-4.69 \sqrt{A/E^*}) \qquad (2.1)$$

Relating the temperature T to the excitation energy by $E^* = aT^2$, where a = A/8, we have,

$$\tau_{\text{particle}} \approx 0.5 \exp(13/T) \qquad (2.2)$$

where T is in MeV and τ is in units of 10^{-22} sec. An excitation energy of 3.25 MeV/A yields a temperature of 5 MeV and a lifetime of 7×10^{-22} sec. If local temperatures of this magnitude are produced in heavy-ion collisions, then the lifetime for particle emission is so short that the rotating di-nuclear complex will emit particles before it scissions. We say local temperatures because total center of mass energies in deeply-inelastic experiments are typically 10 MeV per projectile nucleon, and therefore the achievement of say 3 MeV/nucleon in some region requires a concentration of energy into a "hot-spot" (Stokstad, 1977).

Delving slightly deeper we can write the relaxation time for dissipating the initial energy deposition as (Weiner, 1977);

$$\tau_R = \frac{R^2}{\chi} = \frac{R^2}{v_F \Lambda} \quad , \quad \chi = \frac{K}{\rho c_p} \tag{2.3}$$

Here v_F is the Fermi velocity, Λ is the mean free path for nucleon-nucleon scattering, K is the thermal conductivity, ρ is the density and c_p the specific heat of nuclear matter. Expressions for K and c_p can be derived from the Fermi gas model (Tomonaga, 1938). Thus,

$$K = \frac{7}{48\sqrt{2}} \frac{\varepsilon_F^{3/2}}{\sqrt{m}\, TQ} \quad , \quad C_p = \frac{1}{2} \frac{\pi^2 T}{\varepsilon_F} \tag{2.4}$$

where ε_F is the Fermi energy, T is the temperature and Q is the effective nucleon-nucleon cross section ($\approx$27 mb). For a temperature of 1 MeV, τ_R is 4×10^{-22} sec. From the above equations, τ_R varies as T^2 (essentially because the mean free path decreases as more nucleons are excited above the Fermi level) and at high enough temperatures, becomes longer than the time for particle emission. These trends are illustrated in Fig. 2.8 (Kind, 1953). As the incident energy increases and the temperature approaches 7.5 MeV, we reach a point where the compound nuclear lifetime is less than the relaxation time, which is just the condition for the formation of a hot-spot. These concepts may prove very relevant to the rapid onset of abrasion, and the approach to a limiting temperature which we discussed in Lecture 1 (see Fig. 1.8).

The binding energy of the nucleus also sets an upper limit for the existence of a compound nucleus, the nuclear boiling point. Quantitatively for central collisions this limit can be expressed as,

$$\varepsilon_{boil} \leq \varepsilon_{excit} \tag{2.5}$$

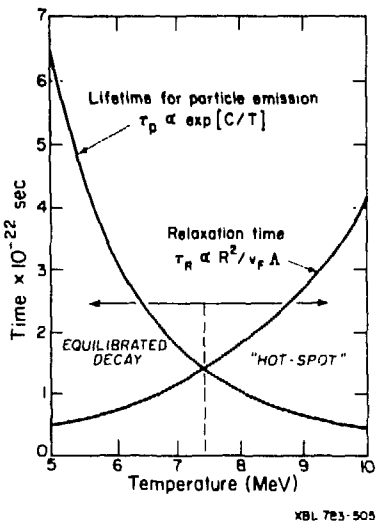

Fig. 2.8

where $\varepsilon_{excit} = \varepsilon_{LAB} = A_1A_2/A_1 + A_2)^2$ and $\varepsilon_{boil} = 8$ MeV. In this energy region many more break-up channels open up, and the nucleus may break into large chunks by multinucleon fragmentation. One can think of the analagous explosions of ordinary condensed matter, like a liquid or a solid, which result in a broad mass distribution well known from soil mechanics (Bondorf, 1978), as shown in Fig. 2.9. The average mass of the fragment (M_F) decreases with the increase of available energy and momentum. In the case of the explosion of ordinary matter, the dispersion δm depends on how the energy and momentum are distributed. For a possible analogy with nuclear fragmentation, it is illuminating to look at the Z-distribution of fragments (Beiser, 1979) emitted in the collision of $^{40}Ar + {}^{232}Th$ (see Fig. 2.10).

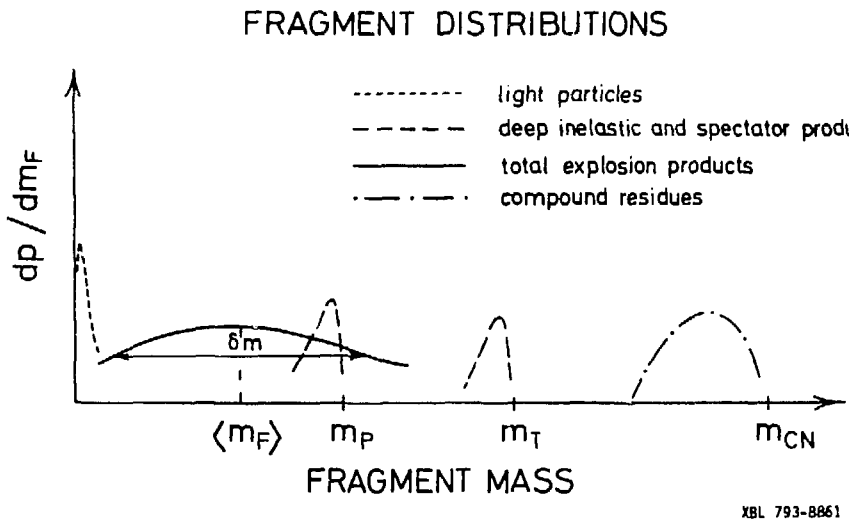

Fig. 2.9

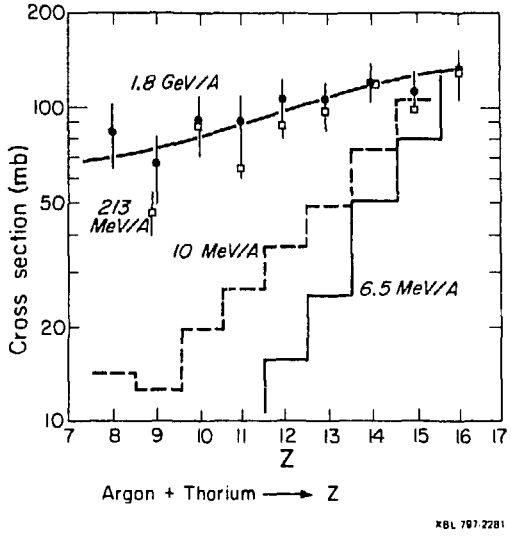

Fig. 2.10

At low energies of 6.5 and 10 MeV/nucleon the Z, or equivalently the mass, dispersion is gaussian (Volkov, 1978) governed by statistical diffusion processes in deeply inelastic scattering; at 200 MeV/nucleon and 1.8 GeV/nucleon the distribution of fragments from Argon to oxygen becomes essentially flat. This feature is also characteristic (Westfall, 1979) of Fe fragmentation at 1.8 GeV/nucleon. Could this mark the onset of an explosive behavior, in this case for a peripheral collision? A related piece of evidence may be the increase in multiplicity of central collisions at 75-100 MeV/nucleon, which is observed (Kullberg, 1978) in emulsion experiments.

An important condition for the occurrence of an explosion is that the available energy should be transmitted to the whole system, requiring a time of the order of the nuclear radius divided by the speed of transverse communication. At low energies this transmission may go by compression, and the communication then depends on t(sound). Using v(sound) = 0.2c, and a traversal distance of 10 fm, t(sound) is ≈50 fm/c, compared to the passing time (2R/v) of 50 fm/c at 50 MeV/nucleon. We are led from the discussions in this section to add the time regions shown (Bondorf, 1978) in Fig. 2.11 to the heavy ion reaction phase diagram of Fig. 1.4. At 10 MeV/nucleon fast emission of light particles sets in (PEPS and Fermi Jets), while at 15-20 MeV/nucleon spatial localization leads to hot-spot emission. The regions of nuclear boiling and compression precede the high energy phenomena, such as the nuclear fireball. All these effects herald the onset of explosive reactions, and in the next section we consider some of the present evidence for spatial and temporal localization in heavy ion collisions.

Spatial, Temporal Localization and the Onset of the Nuclear Fireball

Inclusive proton energy spectra from the collision of ^{16}O on Au at 20 MeV/nucleon (the energy we have frequently discussed as giving intimations of new phenomena) are shown in Fig. 2.12 (Symons, 1979a). These spectra extend up to very high energies and are reminiscent of pre-equilibrium emission (Blann, 1975). The effective temperature is ≈12 MeV, similar to that observed for light particles in the fission coincidence experiment (Fig. 2.6). For a theo-

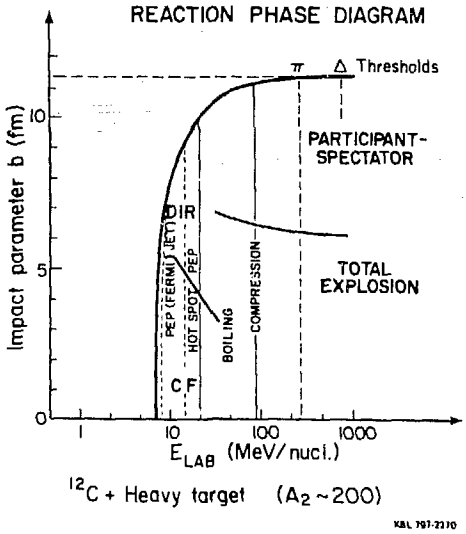

Fig. 2.11

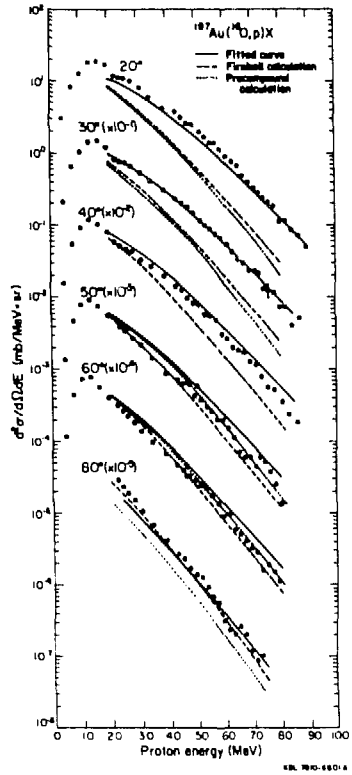

Fig. 2.12

retical analysis with a pre-equilibrium model we need to know the number of excitons in the initial channel. There is a well established prescription in light ion reactions; the cross section for emission of a particle β is,

$$\frac{d\sigma_\beta}{dE}(E) \propto E\sigma_\beta(E)\, U^{p+h-\beta-1} \qquad (2.6)$$

where U is excitation energy of the residual nucleus, σ_β is the inverse cross section for particle β at energy E (Griffin, 1967). Then a plot of

$$\log\left[\frac{d\sigma_\beta(E)}{dE}/E\sigma_\beta\right] \quad \text{vs} \quad \log U$$

gives the slope S = p + h − β − 1 where p + h is the number of particles and holes. Such a plot is shown (Wu, 1979) in Fig. 2.13 for deuteron and alpha induced reactions; the associated numbers of particles particles and holes (p + h), are 4 (i.e., 3 particle-1 hole) and 6 (5 particle-1 hole) respectively. The initial excitation creates a particle-hole state, which combines with the incident nucleons. The same analysis applied to ^{16}O as a projectile leads us to expect at least 18 excitons, and the graph in fact gives 25! The calculated angular distributions and energy spectra (Mantzouranis, 1976), shown by the dotted lines in Fig. 2.12, are in reasonable agreement with the data.

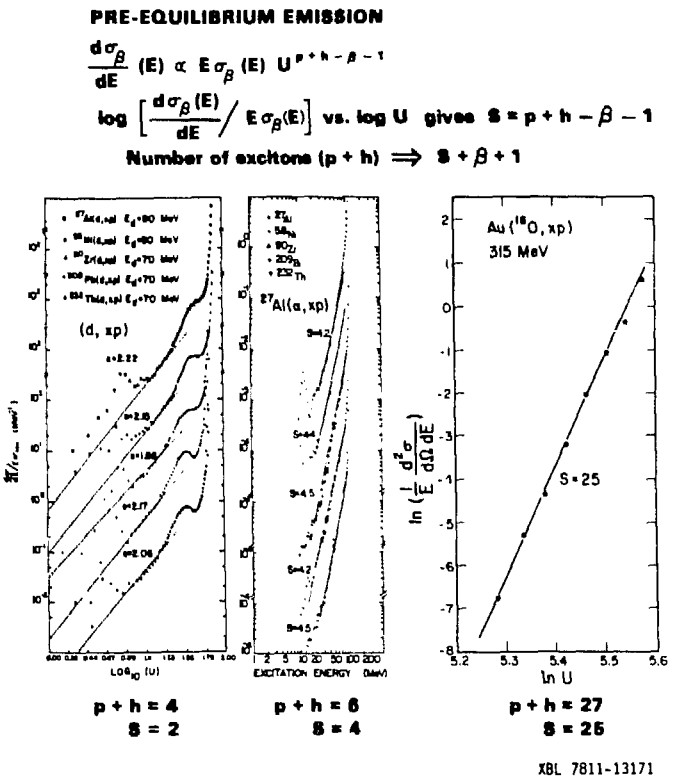

Fig. 2.13

We note that compound nuclear evaporation could not account for these spectra, since, by extending up to energies of 80 MeV with substantial cross-section, they require temperatures much too high (the center of mass energy of 200 MeV above the barrier leads to T $\approx$ 2.9 MeV, from the expression $E^* = A/8\ T^2$; then we expect a decrease of 10^9 in cross-section between 10 and 70 MeV compared to the observed factor of only 10^3. What type of source, one might therefore ask, is responsible for the emission of these particles (Ball, 1978)? Some insight comes from a plot of the constant invariant cross-section in the parallel and perpendicular velocity plane (Fig. 2.14). The data are well described by circles centered around a velocity midway between the compound nucleus and projectile (denoted V_{CN} and V_{16_O}) as would be expected for evaporation from a system moving with this velocity. Transforming to the laboratory frame:

$$\sigma(\theta_L, E_L) = \sqrt{E_L}\,\sigma_{INV}\, e^{-(E_L - 2a\sqrt{E_L}\cos\theta_L + a^2)/T} \qquad (2.7)$$

where T is the source temperature, and "a^2" is the energy of a proton with the velocity of the frame. The best fits to the data are shown by the full lines in Fig. 2.12, and correspond to a source at temperature 8.1 MeV moving with a velocity of 0.1 c in the laboratory.

Once again the "limiting temperature" of 8 MeV has appeared, this time for light fragment emission rather than in describing the evolution of peripheral fragmentation reactions towards the fast abrasion limit in Fig. 1.8. We recall also the significance of this temperature in delineating the onset of "hot-spot" formation in Fig. 2.8. The formation of hot-spots in heavy ion

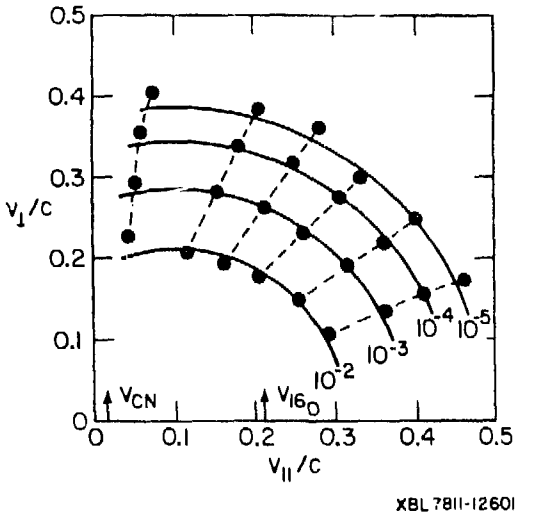

Fig. 2.14

collisions has been discussed recently on formal theoretical grounds (Gottschalk, 1979). It is known, for example, that at an incident energy smaller than 80 MeV/nucleon, the longitudinal momentum decay length is only 1.5 fm (Sobel, 1975). Thus if in this energy region, a hot spot is created, it is stopped almost immediately. The hot, compressed zone might then emit nucleons before the equilibration with the surrounding nuclear medium is achieved. The results (Garpman, 1979) of a model, which parameterizes the hot zone by the size and compression, shows that at the energy of 15 MeV/nucleon of the above example of ^{16}O or ^{197}Au, the data are consistent with a large hot spot and low compressibility. For higher incident energies, the hot-spot can move through the cold nuclear medium, heating it up and leaving the system as a fireball. An understanding of the origin of the particles and the evolution with energy should yield information on spatial and temporal localization in nuclear reactions, as well as on the thermal conductivity of nuclear matter (Weiner, 1974,1976,1977). At low energies a conceptual link must also be established with high energy light particle emission in hydrodynamical and TDHF models (Wong, 1977; Bonche, 1976).

The presence of "pre-equilibrium tails" in the spectra of particles emitted in very high energy proton induced reactions is also of long standing interest. The example in Fig. 2.15 (Westfall, 1978) for p + C → fragments, ranging from ^4He up to C, at 4.9 GeV shows two temperature components in the spectrum. The lower component (dashed curves) corresponds to a temperature of 8 MeV, and presumably can be identified with the "limiting temperature" we have discussed earlier for peripheral collisions. The high energy tail (solid line) is equivalent to T = 14 MeV, and may originate from more central collisions. (The association with thermal concepts should be treated with caution, however, since we have already shown that the lower component of 8 MeV may simply reflect the ground state motion of the system). The behavior exhibited in Fig. 2.15 holds up to much higher energy protons of 400 GeV, and for fragments as massive as silicon, according to recent gas jet target experiments at Fermilab (Gaidos, 1979).

There may even be analogies with high energy studies of hadronic matter in p + p collisions. In Fig. 2.16, proton data at 100 GeV/c (Weiner, 1976) are

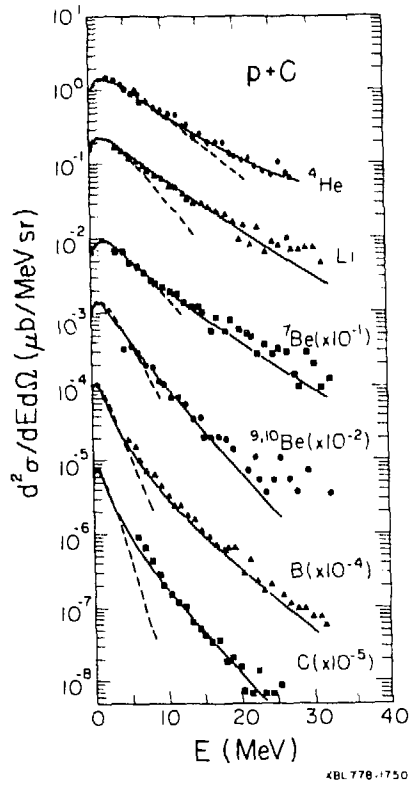

Fig. 2.15

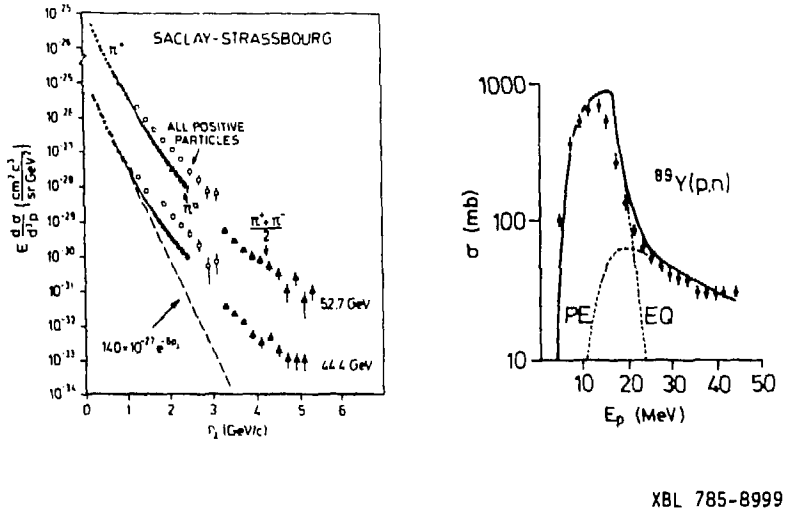

Fig. 2.16

compared with the ^{89}Y(p,n) reactions at low energies of 30 MeV. Both spectra have a "low temperature" component, which for the p + p case, is roughly m_π, the limiting temperature of hadronic matter discussed in the introduction to these lectures. The pre-equilibrium tail has been used to derive the

conductivity and transport properties of hadronic matter, using concepts first formulated by Fermi (1950) to understand the violent processes occurring in proton-proton collisions. As suggested in this section, the analogous component in low energy reactions can provide the same information on nuclear matter (Ho, 1977). The common meeting ground of high and low energy concepts may be the nuclear fireball (Gosset, 1977), which has played an important role in understanding relativistic nucleus-nucleus collisions. The next section is devoted to a discussion of the basic concepts of this model.

Models of Particle Emission in Central Relativistic Collisions

No rigorous framework has yet been found to describe an event like that of Fig. 2.1! We proceed by turning to model calculations, which hopefully provide the background to reveal the important dynamical features. There is at present a complete zoo of models: Fireball, Firestreak, Hydrodynamics, Row on Row, Cascade, Hard Spheres, and Coherent Tube to name a few (For a review, see Gyulassy, 1977). These models range from macroscopic fluid dynamics--which imply that the interaction time is sufficiently long for equilibration to occur, and for thermodynamics and an equation of state to apply--down to single nucleon-nucleon scattering! Although each model can claim some successes, the fact is that a complete theoretical explanation remains to be developed. Even in the low energy domain (<300 MeV/nucleon) according to a careful analysis (Bodmer, 1977) by Bodmer; "Neither the simplifications of hydrodynamics nor that of microscopic descriptions appropriate for dilute systems (Boltzmann equation, Uehling-Uhlenbeck equation, cascade calculation) are adequate. Hydrodynamics, if used, should include dissipation, and at least the Navier-Stokes equations should be used. Quantum mechanical effects, although perhaps not of dominant importance at higher energies (>300 MeV/nucleon) are probably not negligible. It is thus not clear that there are any fully justified simplifications of the nuclear many body Schrodinger equation appropriate for high energy heavy ions collisions at not too high energies." We shall select two representative models, the fireball and the hard single scattering model as two extremes and test their success against the data. But first it is instructive to see why two superficially dissimilar models can make contact with the data, by considering some time scales for heavy ion collisions at several hundred MeV/nucleon.

a) τ_{int} = duration of individual nucleon-nucleon collisions,

$$= \text{force range} \approx h/m_\pi c \approx 1\text{-}2 \text{ fm/c}.$$

b) τ_{relax} = relaxation time between nucleon-nucleon collision,

$$= \lambda/v \approx 2 \text{ fm}/(0.5\text{-}0.75)c \approx 3\text{-}4 \text{ fm/c}.$$

c) τ_{coll} = collision time,

$$= \ell/V \approx 10 \text{ fm}/(0.5\text{-}0.75)c \approx 10\text{-}20 \text{ fm/c} \quad .$$

While there are no gross differences in the time scales, the following inequality holds:

$$\tau_{INT} < \tau_{rel} < \tau_{coll}$$

If $\tau_{rel} \ll \tau_{coll}$, then hydrodynamics would hold with an equation of state and collective effects. If $\tau_{int} \ll \tau_{rel}$, only two-body collisions are important, with no collective effects. The real situation is intermediate.

An example of proton spectra from the collision of Ne on U at 250 MeV/nucleon appears in Fig. 2.17, which shows that the spectra have Maxwellian shapes, corresponding to high temperature (Gutbrod, 1978). These spectra have been elegantly explained with a fireball model (Gosset, 1977), illustrated schemically in Fig. 1.9. The model is an extension of the abrasion-ablation picture used previously for peripheral reactions. In the more central collision, nucleons swept out from the target and projectile form a quasi-equilibrated fireball at high temperature, equal to the available energy per nucleon. The velocity of the fireball is assumed to be that of the center of mass system of the nucleons swept out. The fireball expands isotropically in its center of mass system with a maxwellian distribution in energy.

Assuming spherical nuclei and straight-line trajectories, the participating protons, as well as the division of swept out nucleons between projectile and target, are shown in Fig. 2.18 for Ne on U. At the bottom is the effective weight, $2\pi b N_{proton}$, given to each impact parameter. The velocity of the center of mass of the fireball is then given by,

$$\beta_{CM} = \frac{P_{LAB}}{E_{LAB}} \quad \frac{N_p\, t_1 (t_1 + 2m)^{1/2}}{(N_p + N_t)\, m + N_p t_i} \tag{2.8}$$

where P_{lab} is the lab momentum, E_{lab} the total energy, t_i the projectile incident energy/nucleon, and m the nucleon mass. The total energy in the center of mass of the fireball is,

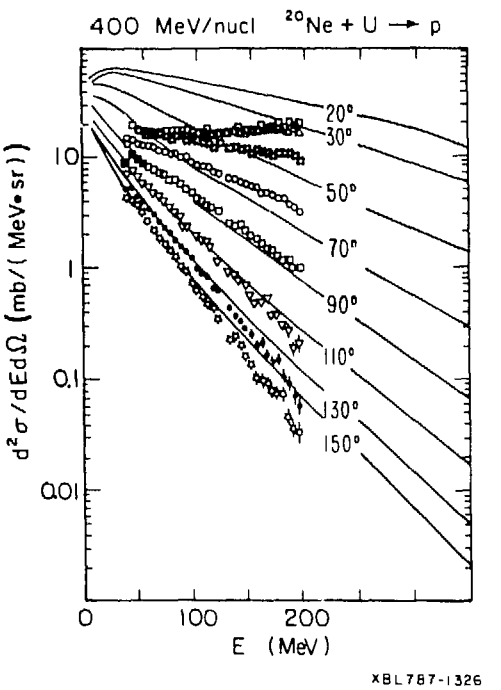

Fig. 2.17

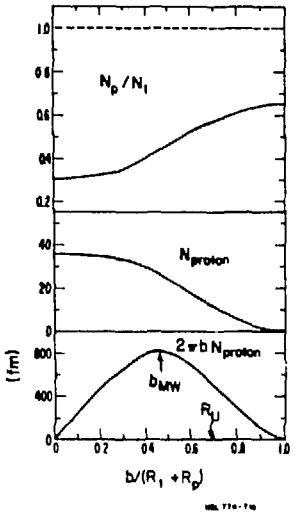

Fig. 2.18

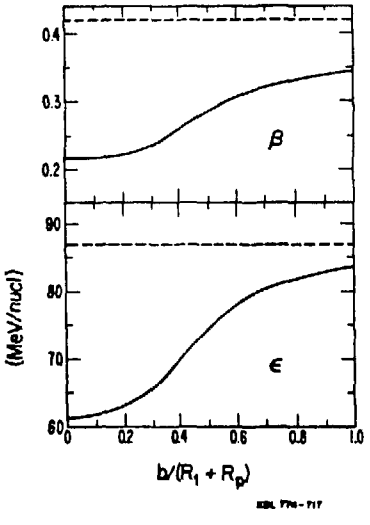

Fig. 2.19

$$E_{CM} = \left[E^2_{lab}\right] - \left[P^2_{lab}\right]^{1/2} \qquad (2.9)$$

If one assumes there are sufficient degrees of freedom in the fireball, and that there is a mechanism to randomize the available energy, one can define a temperature T, which can be expressed (non-relativistically) by, $E = 3/2\ T$ where E is the available kinetic energy per nucleon in the center of mass, i.e., $(E_{cm}/N_t + N_p)$. The quantities β and E (calculated relativistically) are given in Fig. 2.19 as a function of impact parameter. The momentum distribution of the fireball nucleons in the center of mass is then:

$$\frac{d^2N}{p^2 dp d\Omega} \propto (2\pi mT)^{-3/2} \, e^{-p^2/2mT} \qquad (2.10)$$

where p is the momentum of a nucleon in the center of mass. Using the earlier expressions, this distribution can be transformed to an energy distribution in the laboratory, which must then be integrated over impact parameter, weighted appropriately (Fig. 2.18). Typical values of β and T can be derived from Fig. 2.19 at the point of maximum weight ($\beta \approx 0.25$ and $T \approx 50$ MeV). An extension of the fireball model, taking temperature and velocity gradients into account, is the firestreak model (Myers, 1978), which divides the interaction region into a series of tubes. Each tube-tube collision is treated with the fireball model. The firestreak was used to make the theoretical predictions shown in Fig. 2.17. At forward angles the model is not very successful. We should not be disappointed because many features of the dynamics are missing—e.g., there are no compression effects and no viscosity included. One should also note that in collisions of much more massive nuclei like Fe in nuclear emulsions, the clean-cut participant spectator model fails badly (Bhalla, 1979). It is also possible, however, that trivial effects are responsible for the forward angle discrepancies.

We recall that the concepts of a localized emitting source were also used to describe the proton emission at 20 MeV/nucleon in Fig. 2.12. The figure also shows the fireball predictions with a source velocity of 0.06c. The quality of agreement is at least comparable to the results at relativistic energies; as we noted in the previous section, the reconciliation of this model with hot-spot and pre-equilibrium descriptions at lower energies presents a theoretical challenge (Weiner, 1979).

At the opposite extreme to the fireball model is the single scattering model, in which internal nucleons with off-shell momenta overcome the average binding potential and scatter to on-shell final states (Hatch, 1979). Instead of using the Fermi momentum distribution for the struck nucleons, it is considered more realistic to emphasize the high momentum behavior of the distributions, which are described by an exponential fall-off. (This tail may also be consistent with collective effects in the nucleus--possibly raising a caveat that this model may not be purely hard nucleon scattering after all!) A comparison of this "parameter-free" calculation with several systems at 800 MeV/nucleon is given in Fig. 2.20. The agreement is certainly comparable to that of the firestreak model. However, the proton spectra at back angles in the heavier C + Pb system, and in the low momentum regions of all spectra, are not well reproduced, indicating the presence of more complicated multistep (pre-equilibrium or equilibrium?) processes.

These two extreme models--fireball and hard nucleon-nucleon scattering—represent two attempts at understanding complicated processes which occur in relativistic heavy-ion collisions. A legitimate question is, why do they both work (Hufner, 1978)? Consider a typical nucleon-nucleon event with initial momenta $\langle\bar{p}\rangle_p$ and $\langle\bar{p}\rangle_T$, and $\langle\bar{p}\rangle'_p$, and $\langle\bar{p}\rangle'_T$ afterwards. Then conservation laws give,

$$\langle\bar{p}\rangle'_p = (1 - \alpha)\ \langle\bar{p}\rangle_p + \alpha\langle\bar{p}\rangle_T \qquad (2.11)$$

$$\langle\bar{p}\rangle'_T = \alpha\langle\bar{p}\rangle_p + (1 - \alpha)\langle\bar{p}\rangle_T \quad .$$

where

$$\alpha = \langle \sin^2 \frac{\theta_{cm}}{2} \rangle$$

is essentially the fractional momentum loss per collision. The parameter determines how quickly the two moments of the nucleons approach one another, and essentially determines the cascade. The inverse $1/\alpha$ fixes the number of collisions to reach equilibrium. For an isotropic cross section, $\alpha = 1/4$, and $n_{thermal} = 4$. It is also known from the theory of heat that if 100 particles are put in a corner of phase space and released, it takes only 3 collisions for the system to reach equilibrium (Kittel, 1958). With this constraint it is relatively easy to calculate that in the collision of C + C, the contributions of direct, intermediate and thermal collisions are approximately equal. The components due to 2,3 scatterings can also be calculated with intranuclear cascade codes (Randrup, 1979). It is found that the component due to four or more scatterings rapidly approaches a Gaussian distribution, a property of the Central Limit Theorem in statistics. Once a Gaussian momentum distribution is reached, then the two parameters (center and width) are completely determined by energy and momentum conservation. The

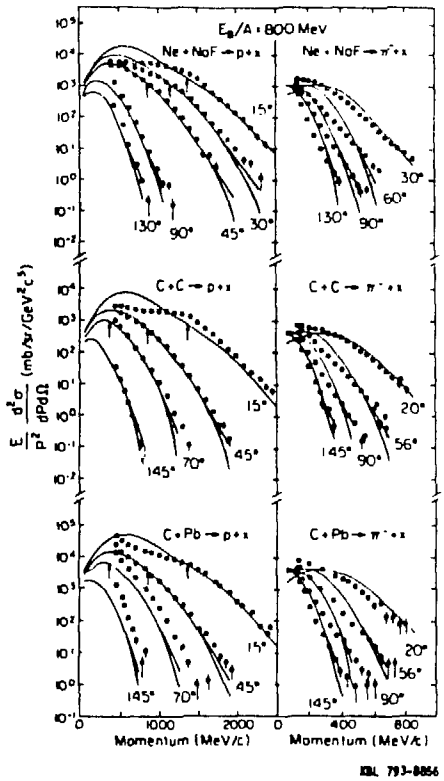

Fig. 2.20

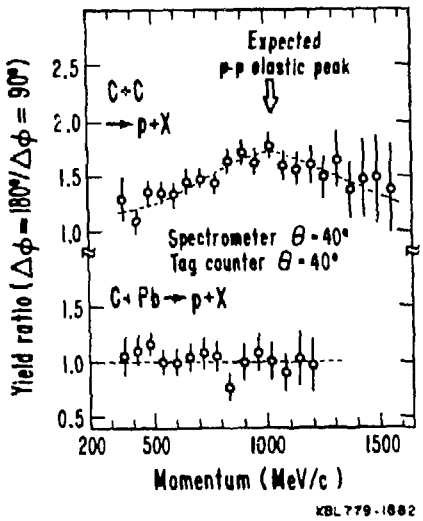

Fig. 2.21

end result is identical for all models, which amounts for their comparable success in describing the data (Chemtob, 1979).

The direct contribution has actually been isolated in a two-particle correlation experiment (Naganiya, 1979). In addition to the main counter telescope at azimuthal angle $\phi = 0$, three additional tag counters were placed at $\phi = \pm 90, 180^{\circ}$. The quantity C, defined as the coincidence rate with the in to out-of-plane tag counters is shown in Fig. 2.21. For a thermal event $C = 1$, whereas $C > 1$ favors coplanar emission. This is clearly observed for C + C, but not for C + Pb, where the direct effect may be reduced by shadowing of the heavy target spectator. Using the simple counting approach outlined above, one also finds the direct component should be negligibly small for C + Pb.

The Heart of the Matter

It is obviously an understatement to say that single particle inclusive measurements of central collisions, i.e., the detection of one particle out of the splendor of the event in Fig. 2.1, must surely suppress much information! In order to inspect more closely the fireball and equilibration features as revealed by single particle inclusive and exclusive data, we construct a plot which helps to sort out the velocity and isotropy of the emitting sources. It is convenient to characterize the distribution of longitudinal momentum by the rapidity variable:

$$y = \frac{1}{2} \ln \frac{(E + P_{\parallel})}{(E - P_{\parallel})} \qquad (2.12)$$

where E and $P_{\|}$ are the total energy and longitudinal momentum of the particle. This variable transforms in Galilean fashion for different frames. (Nonrelativistically it becomes the parallel velocity component, shown in Fig. 2.14.) Contour plots of the invariant cross-section $1/P\ d\sigma/d\Omega dE$ in the Y vs $P_{\perp}/mc$ plane are then formally equivalent to the plot of 2.14 (which is intuitively more comprehensible!) and are shown for Ar + KCl and Ar + Pb in Fig. 2.22 (Nagamiya, 1979a).

Each contour line connects the same invariant cross-sections, and two adjacent thick curves differ by one order of magnitude. The projectile and target rapidities are indicated by $Y_P(= 1.23)$ and $Y_T(= 0)$. The line $(Y_P + Y_T)/2$ $(= 0.61)$ corresponds to the direction at 90° in the nucleon-nucleon center of mass frame, whereas Y_{cm} is the rapidity of the total CM frame. According to the fireball model the protons are emitted isotropically in the CM frame of fireball, which is indicated by Y_{FB} (it coincides with the nucleon-nucleon system for equal mass target and projectile). In the small P region we expect the emission to be highly influenced by peripheral projectile and target fragmentation, which are clearly hinted at for Ar + Pb. However, the regions far removed from $(Y, P_{\perp}/m_pc) = (Y_p,0)$ and $(Y_T,0)$ are due to high momentum transfers. We see that for both systems the distributions do appear to approach the form expected of isotropic emission in the fireball frame of reference.

An elegant indication that the same physics may be contained in the macroscopic fireball model and in the microscopic model of a full cascade calculation, is given (Smith, 1978) by making a rapidity plot of the output from the cascade (see Fig. 2.23) for Ne + Pb → protons at 800 MeV/nucleon. The development of the fireball in coordinate space (left) and in momentum space (right) is evident. As we mentioned previously, a detailed analysis also

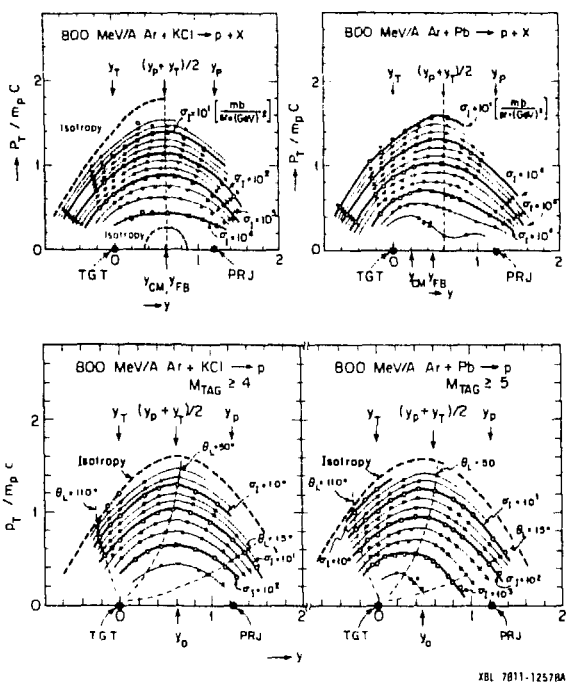

Fig. 2.22

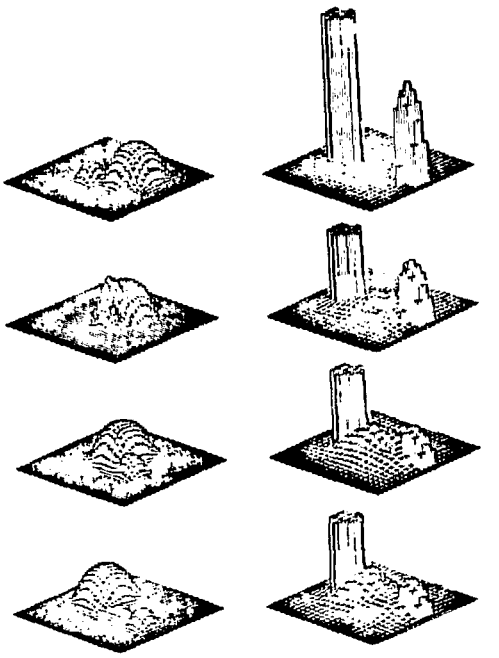

Fig. 2.23

shows that complete thermalization is achieved, after only a few nucleon-nucleon collisions (see also, Smith, 1977).

Data obtained with the very different techniques of stacked Lexan foil detectors, however, give evidence for emission of complex fragments from a source moving with low velocity and high temperature, which cannot be accommodated in the framework of a fireball (Stevenson, 1977; Price, 1977, 1978). These fragments appear to originate through non-equilibrium emission from a system like the entire target, where the internal energy does not have to reach the value of 3/2 T per nucleon. The radial emission velocity in the source frame is strongly correlated with the source velocity, independent of the mass of the fragment observed. This behavior is uncharacteristic of a thermalized source. Various cooperative, non-thermal processes can be imagined, amongst which are compressional wave phenomena or the release of preexisting clusters. In high energy hadron-hadron collisions it is known that the time required for the formation of multibody final states is so long that in a hadron-nucleus process the nucleons in the path of the incident hadron can be viewed as acting collectively, and in a first approximation can be regarded as a single object—an effective target. Similarly a nucleus-nucleus collision at high energy is regarded as a simultaneous collision between an effective target and projectile (Ta-Chung, 1978).

One must remember that these superficially different approaches have so far all been applied to single particle inclusive data. There is still hope that an event like the explosion of Fig. 2.1 represents the decay of an equilibrated, high density piece of nuclear matter. To get closer to the heart of the matter, to make a more stringent test of the different theoretical approaches, it is necessary to look at more exlusive data.

Multiplicity Selection

The multiplicity of particles in an event can be measured from streamer chamber data, of the type illustrated in Fig. 2.1. It can also be determined with an apparatus such as that shown in Fig. 2.24, which is an array of 80 scintillators covering the forward hemisphere in three rings A, B, C and an arrangement of single fragment telescopes inside the scattering chamber (Poskanzer, 1978). The events in the telescopes can then be registered with associated high and low multiplicity, which we believe will indicate small and large impact parameters. How well founded is this hypothesis? Certainly, the possible multiplicities can be very large. To give a glimpse of the challenge ahead with future higher energy accelerators, some events in cosmic ray interactions are known to produce multiplicities of 500 (Rybicki, 1963; Jacobsson, 1978)!

At presently attainable energies the numbers are less staggering, with multiplicities ranging up to ten or twenty (Bannik, 1978). The measured negative pion multiplicity for Ar + Pb_3O_4 at 1.8 GeV/nucleon appears in the upper part of Fig. 2.25 (Fung, 1978). The solid lines are the fireball model predictions (Gyulassy, 1978) with no cut off in impact parameter (1) and with a cut off at 9.6 fm for ^{208}Pb and 5 fm for ^{16}O (curve labelled (2)). The separate contributions from lead and oxygen are also shown; the triangles represent the prediction of an analytical cascade model (Vary, 1978). In passing we note that yet another independent approach to describe the data by the Coherent Tube Model is also successful (Afek, 1978). A restriction of the operating range of contributing impact parameters is likely to reveal greater sensitivity. The lower half of the figure gives a theoretical decomposition of the multiplicity with impact parameter. The relationship between M and b is almost linear, but the individual Poisson distributions, associated with

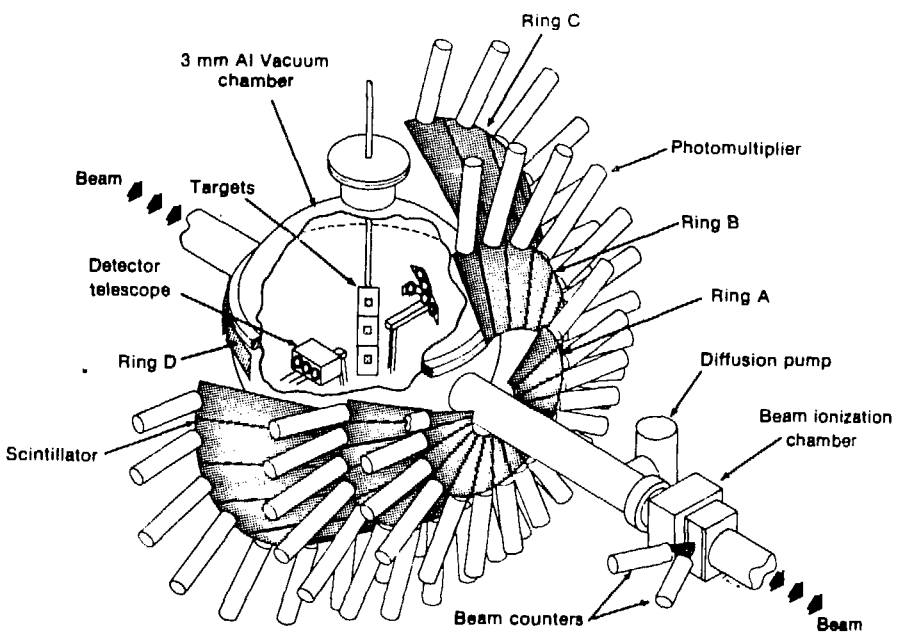

Fig. 2.24

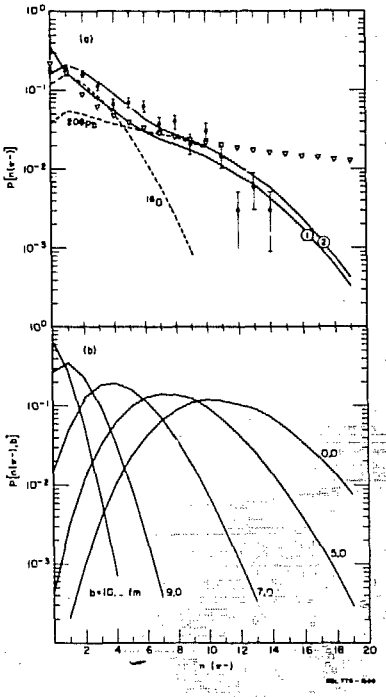

Fig. 2.25

different impact parameters, are wide and overlapping. In particular the sensitivity is small for b < 5 fm. The best recipe for isolating head-on central collisions is therefore to demand extreme multiplicities, e.g., M > 18, where b = 5 fm is suppressed relative to b = 0 by a factor of twenty (unfortunately, only 1% of the cross section would remain!).

If the developing fireball would trigger the propagation of density shock waves through the spectator medium, one might expect the isotropic emission pattern of the rapidity plot to be radically modified (Stock, 1978). Returning to Fig. 2.22, the lower sections show the effect of imposing a multiplicity trigger (of approximately 4) and one can indeed see a modification of the pattern. In particular, the distributions from a two targets become more similar, and the contributions of the contours centered at projectile and target rapidities have been eliminated. Clearly a great deal of difficult, complex experimentation lies ahead, but an impressive attack on the dramatic events of Fig. 2.1 has certainly been launched. Other discussions of theoretical methods to isolate impact parameters are given by Bertsch (1978) and of the significance of multiplicity distributions by Knoll (1978).

The Emission of Composite Particles

The energy spectra of composite particles emitted in relativistic heavy ion collisions have been calculated with two models, the coalescence model (Westfall, 1976) and the firestreak model (Gossett, 1978). In the latter the interaction is assumed to be localized in the overlapping volume of the target and projectile nuclei, which is divided into streaks; in each streak the matter is treated as a thermodynamic system in chemical equilibrium, so that

relative yields and momentum distributions for pions and nucleons can be calculated.

To calculate the fragment cross-sections with the coalescence model, we must determine the probability of condensation of the nucleons, which is assumed to take place if they are within a coalescence radius p_o. the probability of finding a nucleon in a sphere in momentum space of radius p, centered at p is (Feshbach, 1977):

$$P = \frac{4\pi p_o^3 \gamma}{3M} \frac{1}{\sigma_o} \frac{d^2\sigma_1(p)}{p^2 dp d\Omega} \tag{2.13}$$

where M is the nucleon multiplicity, σ_o the total cross-section and γ the relativistic factor. The first factor is the momentum sphere volume and the second the relative probability of finding a nucleon with momentum (p). The probability of finding A_F nucleons is then:

$$P(A_F) = \binom{\bar{M}}{A_F} P^{A_F}(1 - P)^{\bar{M}-A_F}$$

$$\approx \frac{(\bar{M}P)^{A_F}}{A_F!} e^{-\bar{M}P} \doteq \frac{1}{A_F!} \left(\frac{4\pi p_o^3 \gamma}{3\sigma_o}\right)^{A_F} \left(\frac{d^2\sigma_1}{p^2 dp d\Omega}\right)^{A_F} \tag{2.14}$$

where A is the fragment mass number. To obtain the cross-section we take the probability of finding (A_F-1) nucleons in the momentum sphere (p_o) times $1/A_F$ of the cross-section for the emission of one additional particle:

$$\frac{d^2\sigma A_F}{p^2 dp d\Omega} = \frac{1}{A_F!} \left(\frac{4\pi p_o^3 \gamma}{3\sigma_o}\right)^{A_F-1} \left(\frac{d^2\sigma_1}{p^2 dp d\Omega}\right)^{A_F} \tag{2.15}$$

Once the nucleon emission cross-section σ_1 is known (so far measured only for protons) the cross-section for a composite particle is easily calculated. The magnitude of p_o is an adjustable parameter and r_o is calculated from

$$\sigma_R = \pi r_o^2 (A_T^{1/3} + A_P^{1/3} - \delta)^2 \qquad (2.16)$$

Some typical results for Ar + Pb → d, ^{3}He are shown in Fig. 2.26 in which the agreement with the data is superb (Lemaire, 1979). Note that the fire-streak predictions (solid line) are less successful. In this model the relationship between nucleon and composite particle cross-section predicted by the coalescence model does not hold when a wide kinematic region is encompassed, because each streak contributes with a different temperature. The agreement with the coalescence model must therefore be considered quite significant and

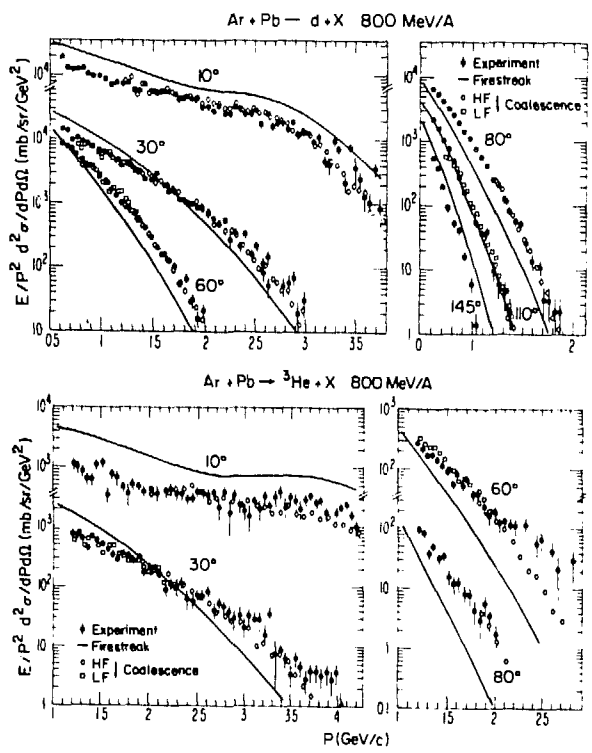

Fig. 2.26

any other successful model must contain the relationship to nucleon data of the coalescence model.

At least one interesting and profound new fact emerges when the values of p_o are related to the size of the emitting source (the fireball)? If chemical equilibrium is reached during the expansion of the fireball it is possible to relate the value of p_o to the size of the fireball at the freeze out density (Mekjian, 1978, 1978a).

$$V \propto \frac{3h^3}{4\pi p_o^3} \tag{2.17}$$

Expressing the volume in terms of the radius of an equivalent sphere $R = a(A_p^{1/3} + A_T^{1/3}) + b$, with $a = 0.24$, $b = 1.9$ fm for the deuterons and 1.5 fm for tritons and ^{3}He, the analysis leads to values of R from 3.4 to 4.3 fm. It is fascinating to note that an attempt to measure the source dimensions in an experiment with 1.8 GeV/nucleon Argon on Pb by means of pion interferometry (Fung, 1978) gave a very similar value of 3.3 fm!

There is hope that a quantitative information can be retrieved from the apparent staggering complexity of heavy ion central collisions, setting our course for the last lecture on the search for the exotic.

THE SEARCH FOR THE EXOTIC

> "Ogni linguna per certo verria meno, per lo nostro sermone e per la menta ch'hanno a tanto comprender poco seno."
>
> Truly all tonges would fail, for neither could the mind avail, nor any speech be found for things not to be named or understood.
>
> Dante, The Divine Comedy

Introduction

Since the discovery of nuclei in 1911, we have studied them primarily under conditions in which the nuclear density is close to the equilibrium value, the excitation energy or temperature is relatively low, and in general the nuclei are confined close to the valley of stability. However, with the development of accelerators capable of delivering heavy nuclei at relativistic speeds, we are now beginning to explore the relaxation of these traditional constraints, and to search for the exotic.

The search for the exotic in relativistic heavy ion collisions is reminiscent of the hunt of the Unicorn in bygone times. Although there was a considerable element of doubt about the existence of this elusive beast, the illustration of "The Unicorn Under Attack," from a famous tapestry in Fig. 3.1, spares no attention to detail. The hunters carry very real spears and every leaf on every tree is correctly depicted. The search for exotic phenomena is also deadly serious--otherwise the planned construction of the apparatus for the hunt shown in Fig. 3.2 could never be contemplated (Gutbrod, 1979). The instrument consists of a plastic ball in coincidence with a plastic wall. The

The ball consists of 680 modules of Phoswich ΔE-E detectors (Wilkinson, 1952) to detect the central explosion fragments in coincidence with leading particles identified by time-of-flight between the entrance beam counters and a wall of 160 scintillators which also measure position. In this lecture, as the Walrus said,

"The time has come--...,
To talk of many things:
Of shoes--and ships--and sealing wax--
Of cabbages—and kings—
And why the sea is boiling hot--
And whether pigs have wings."

Lewis Carroll,
Through the Looking Glass

This verse is reminiscent of discussions of the state of relativistic heavy ion collisions. The concepts often border on the fantastic compared to conventional theories of nuclear physics. Nevertheless some have become accepted into our everyday thinking; others remain subjects for imaginative debate! In this lecture, I shall not talk of too many things, and I fear that the glimpses of the exotic that I am able to give will be seen "through the glass darkly." I shall restrict myself to the search for various limits in relativistic heavy ion collisions: the Limits of Temperature and Pressure, the Spatial and Temporal Limits, and finally the Limits of Nuclear Matter and of Nuclei.

The Limits of Temperature and Pressure

The limiting temperature of hadronic matter ($T \approx m_\pi$) may be reached in high energy heavy-ion collisions (Glendenning 1978) (as mentioned briefly in lecture 1) and may already have been observed in high energy hadron collisions (Laasanen, 1977). The ultimate hope is tht some unusual thermodynamic property of matter at high baryon density might be used as a signal for new states of matter. But, as with other new kinds of phase, the biggest question is what effect this phenomenon would have on the particles remaining after the expansion has lowered the density. The novel states are conjectured to form as the density increases and more nucleons come within the range of the nuclear force. Long range correlations can then develop, resulting in phase transitions, which model calculations indicate will occur when $\rho > 2\ \rho_o$. In particular, phase transitions leading to density isomers and pion condensates have been extensively studied (Stocker, 1979; Hoffman, 1979; Lee, 1975). Speculations also suggest that at high density, nucleons may lose their identity and merge into a new state of quark matter (Chin, 1978; Chapline, 1977). As an indication of some of these exciting possibilities, Fig. 3.3 shows the anticipated equation of state (Nix, 1977). In the absence of special effects the energy would simply increase monotonically with density (beyond the point of normal nuclear matter). Since pressure in a hydrodynamical model is proportional to $dE/d\rho$, a change to negative slope would imply negative pressure, e.g., condensation to abnormal matter.

Perhaps it is useful at the outset to estimate the possible densities resulting from a heavy-ion collision (Goldhaber, 1978). Uranium is a sufficiently large nucleus that a nearly head-on collision (≈0.1 b out of ≈7 b total reaction cross section) may be described as a meeting of two slabs 15 fm thick with $\rho \approx 0.15\ \text{fm}^{-3}$. The Lorentz contraction increases ρ and decreases the

CBB 781-447

Fig. 3.1

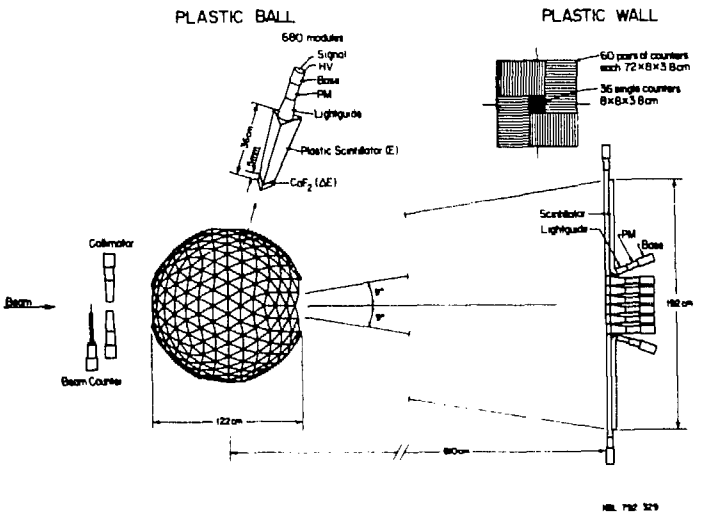

Fig. 3.2

thickness by a factor $\gamma = W/2M$; the combined system will eventually be confined to a thickness $15/\gamma$, since the back of either slab must proceed half way to the meeting plane before even a light signal from that plane could reach it. At one moment the density would be 2γ times normal. To get a maximum

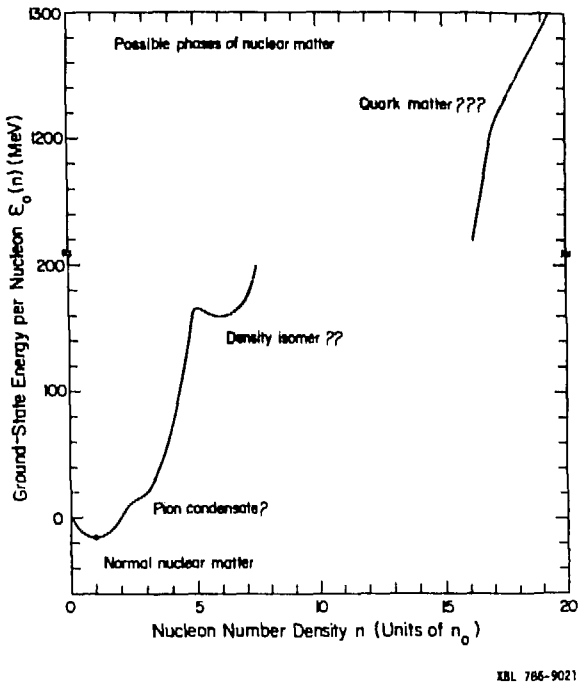

Fig. 3.3

estimate of ρ, one notes that a 40 mb nucleon-nucleon cross section leads to N = 9 interactions in crossing the slab, and the mean fraction of momentum retained by the nucleon is $1/N + 1$ which is also $\approx\gamma$. Therefore the density increase could be as high as 10 times normal. Calculations indicate that a transition to quark matter will call for densities 10 to 20 times above normal (Chapline, 1977; Nix, 1977). It is estimated that beam energies per nucleon between 10 and 25 GeV are necessary for this end (see Eq. (4) of Iwe, 1978).

More quantitative calculations of the attainable densities are also given by a variety of theoretical approaches. In classical microscopic calculations (Bondorf, 1976a; Bodmer, 1977) the nuclei are described as a collection of particles which move according to Newton's laws. The heavy ion collision is simulated by calculating each nucleon-nucleon collision successively. The distribution of nucleon positions and velocities vary as a function of time, and they are averaged according to some ad hoc specifications in order to have smooth functions of densities. For head on collisions of uranium on uranium at a few hundred MeV/nucleon, three times normal density is reached. Comparable densities are also attained in more detailed cascade calculations (Smith, 1977), an example of which for calcium on calcium at 1 GeV/nucleon is shown in Fig. 3.4 (Cugnon, 1979). In general, approaches based on relativistic hydrodynamics predict higher compressions (Amsden, 1977; 1978).

In spite of the specific predictions of theory on the subject of compression and density, the experiments at this point are rather vague. None of these exotic effects have yet been observed, and my task is now to describe the first experimental attacks. Whether exotic phenomena occur or not, an immediate goal of relativistic heavy ion physics is to learn about the equation-of-state $W(\rho,T)$ as a function of ρ and T. The only fact known about W today

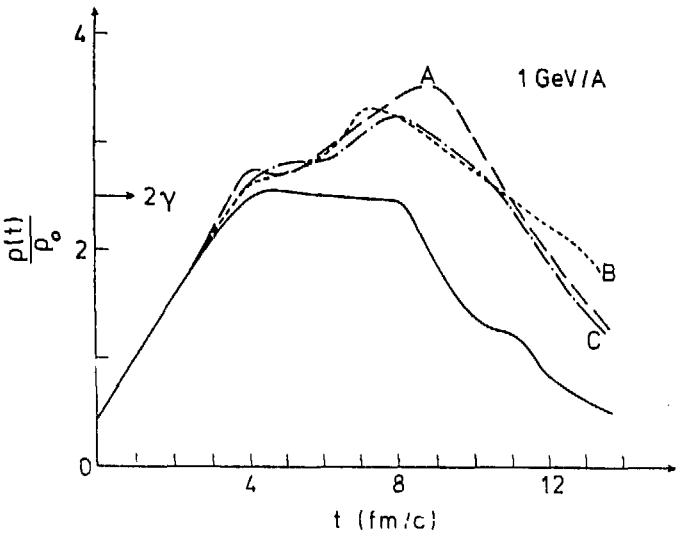

Fig. 3.4

is that $W(\rho,0) = -16$ MeV $(\partial W/\partial\rho) = 0$ (at ρ_0 and $T = 0$) and that the incompressibility,

$$K = 9\ \rho_0^2\ \partial^2 W/\partial\rho^2 \qquad (3.1)$$

is determined to be in the region of 200 MeV from studies of the monopole vibration (Bertrand, 1978; Youngblood, 1977). The determination of W over any finite region of the (ρ,T) plane would vastly expand our knowledge of nuclear physics.

We return to the rapidity plots which were discussed in lecture 2 as a vehicle for isolating the localized nuclear fireball. Figure 3.5 is a projection of proton and pion kinetic energies (see Fig. 2.24) along the line of mid-rapidity $(y_p + y_T)/2$, for several systems (Nagamiya, 1979). The invariant cross sections have the form $\exp(-E_k/E_0)$ from which we inferred in lecture 2 the existence of a thermally equilibrated fireball. However, in this model the total available energy in the overlap region between target and projectile is completely thermalized, and the calculated temperature should be given by $E^* = 3/2\ T$, leading to $T \approx 115$ MeV for the systems presented. The observed temperatures are much lower (≈75 MeV). Figure 3.6 shows the radical departure from the ideal gas formula at several energies (Nagamiya, 1978). Both figures also show that the pion temperatures are consistently below the proton temperature--again at variance with a purely thermal model. (In Fig. 3.5 the predictions of the macroscopic firestreak and the microscopic hard scattering models are also shown--c.f., lecture 2.) The difference in π-p temperatures cannot be solely due to the cooling effect of pion production, since only one pion is created for every 10 protons, with a mean energy (including the rest mass) of 240 MeV. Assuming equal numbers of $\pi^{\pm}$ and π^{o}, about 35 MeV per baryon goes into producing and accelerating pions, lowering the temperature to only 90 MeV (Siemens, 1979).

The additional cooling has been attributed to a "blast wave" (Siemens, 1979). It is a matter of ordinary experience that the sudden creation of hot, dense

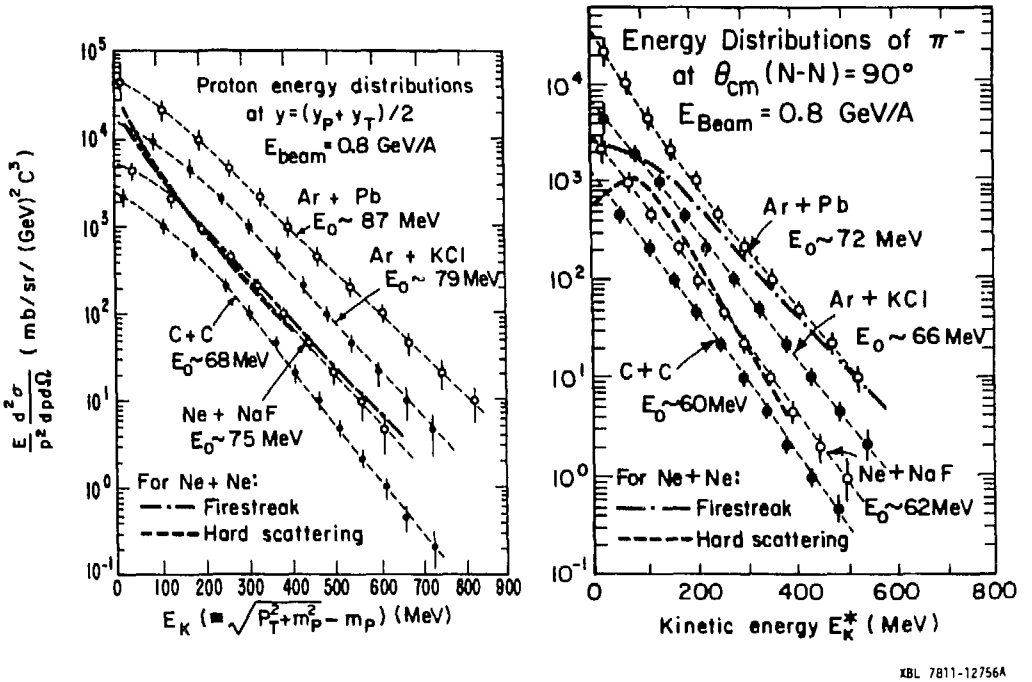

Fig. 3.5

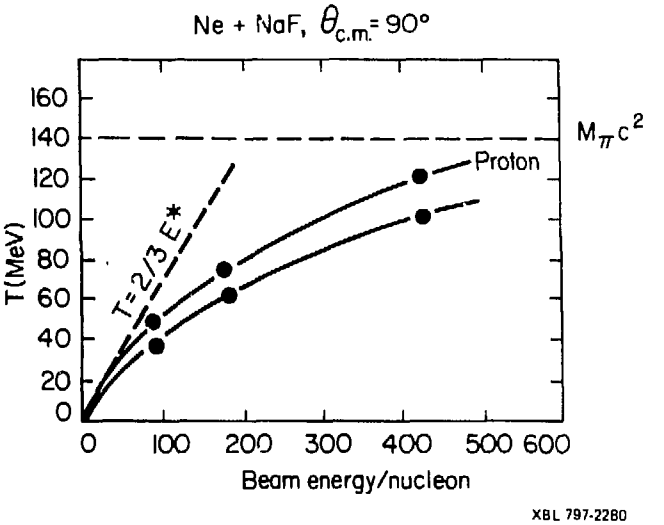

Fig. 3.6

matter leads to an explosion (bombs, blasting caps, supernovae). Due to the pressure wave, particles acquire a net flow velocity outwards, the energy for which comes primarily from the kinetic energy of the random (thermal) relative motion (Kitazoe, 1976, 1979). Since I cannot show a picture of this happening in a nuclear collision, perhaps the reader will be content with a possible cosmological analog, the case of the Crab Nebula itself (Fig. 1.1) or the

Planetary Nebula in Aquarius (Fig. 3.7). The characteristic features of an explosion are (a) the peaking of the velocity distribution about the mean radial velocity, in contrast to the fully thermalized distribution which is largest for the slowest particles in the fireball frame, and (b) the reduction of the intrinsic temperature due to the cooling of the expansion.

These features appear to be required to explain the data of Fig. 3.5. The appearance of the peak is suggestive for the π^+ data at 15 MeV; it could also be due to Coulomb effects and a comparison of π^+ and π^- would clarify this point. Since for protons the mean thermal velocity is smaller than for pions at the same temperature, the peaking of protons at the blast velocity should be more pronounced, as observed. By considering (Siemens, 1979) a spherically symmetric fireball expanding at velocity β, temperature T, the momentum space density of particles of momentum ρ and energy E is,

$$\frac{d^3n}{dp^3} = \frac{N \exp(-\gamma E/T)}{Z(T)} \left[\left(\gamma + \frac{T}{E}\right) \frac{\sinh\alpha}{\alpha} - \frac{T}{E} \cosh\alpha\right]$$

where $\alpha = \gamma\beta p/T$ and Z(T) is a relativistic Boltzmann factor of the normalization. For large p the distribution is a Boltzmann form with apparent temperature,

$$T_{app} = \left(\frac{-d \ln \sigma}{dE}\right)^{-1} \approx T\gamma^{-1}(1 - \beta E/p)^{-1} \qquad (3.3)$$

Therefore the pions ($p \approx E$) should indeed be cooler than the protons ($p < E$). The predictions are shown in Fig. 3.8; they indicate that 40% of the available energy appears in the blast. In this number there may be information about the state of the initial hot, dense, baryonic matter. If we use the Fermi gas model to estimate the excitation spectrum:

CBB 791-1176

Fig. 3.7

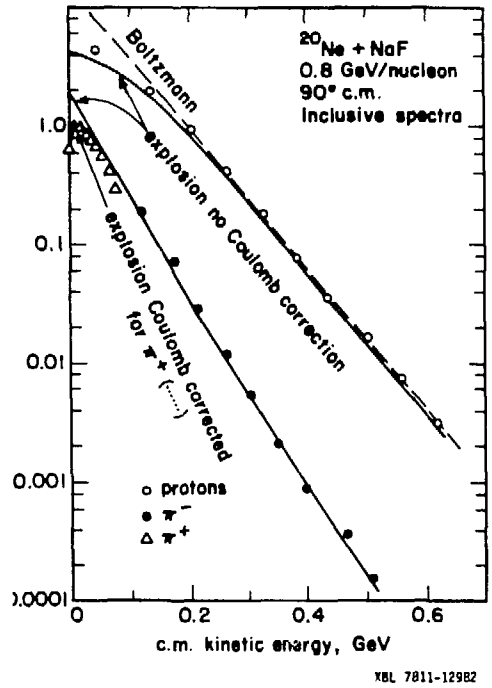

Fig. 3.8

$$E_{THERMAL}/N \approx E_F \approx \rho^{2/3} \tag{3.4}$$

Assume that ρ_1 expands to ρ_2; then,

$$E_{TH}(1) = KE_{CM} - \varepsilon(\rho_1)$$

where $\varepsilon(\rho_1)$ is the potential energy of the initial compressed matter, at a presumed high temperature and pressure. Now,

$$E_{TH}(2) = E_{TH}(1)(\rho_2/\rho_1)^{2/3} \tag{3.5}$$

and therefore the fraction of the energy in the collective flow is easily derived as,

$$Q = \frac{\text{collective E}}{\text{total E}} = 1 - \left(\frac{\rho_2}{\rho_1}\right)^{2/3} + \frac{\varepsilon(\rho_1)}{KE_{CM}}\left(\frac{\rho_2}{\rho_1}\right)^{2/3} \tag{3.6}$$

The final density—at which collisions cease—can be derived from studies of the emission of light composite particles as discussed at the end of lecture 2.

The identification of a blast wave from exploding fireballs is an important step to unravelling the properties of hot, dense baryonic matter. Particles emitted earlier than freeze out might give better clues to the early development of the system. The detection of K^+ mesons may be preferable to pions since they have a mean free path $\lambda \approx 6$ fm at $\rho = \rho_0$ and can escape at all times with only a 50% chance of rescattering. This advantage is illustrated by the total π-p and K-p cross sections in Fig. 3.9, which shows that the K^+-p cross section is by far the lowest. With higher energy accelerators, >4 GeV/A, the K^+ may become our thermometer and barometer (Stock, 1978)!

Shock wave emission, if it exists, would also provide a time marker corresponding to the propagation stages of compression. The early searches were based on the features of Fig. 3.10 (Greiner, 1979; Scheid, 1976) which illustrates the progress of the shock front. In the initial phase a "splashing tidal wave" is expected at a backward angle, where $\sin\phi_1 = v_t/v_i$, with v_t the expansion velocity of the shock compression zone. In the second stage, a strong compression shock is created, accompanied by a Mach cone travelling outwards in the direction ϕ_2, $\cos\phi_2 = v_s/v_i$, where v_s is the shock expansion velocity. In the final stage, matter is emitted in the directions ϕ_1(splashing) and ϕ_2(Mach). However, the source velocity must be reasonably constant for the Mach cone to be observable, and this behavior is not expected at presently available energies. In any case the effects of shock waves have not been observed in single particle inclusive measurements (Baumgart, 1975; Poskanzer, 1975). Recently in the ^{40}Ar + ^{9}Be reaction at 1.8 GeV/nucleon, a test was made of the possible correlations between a particular multiplicity M and the inclusive cross section W, by studying the ratio $R = W_m(\theta_L, y_L)/W(\theta_L, y_L)$ as a function of θ_L and rapidity y_L. This ratio is shown for p, d and t in Fig. 3.11. The multiplicity trigger required that at least seven fragments were detected in an array of

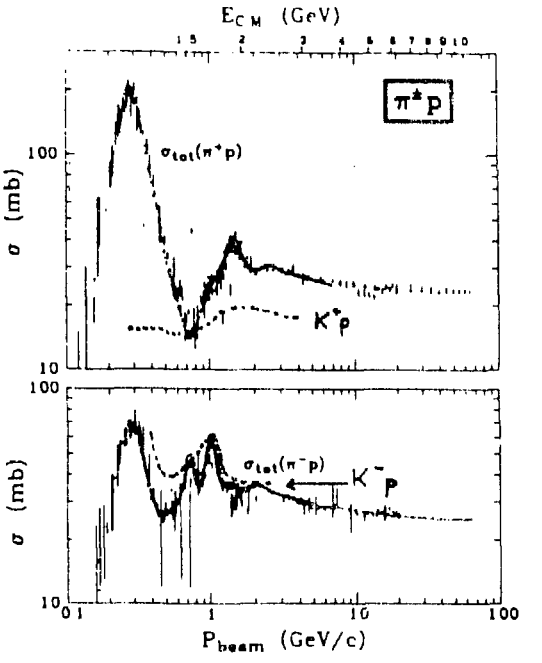

Fig. 3.9

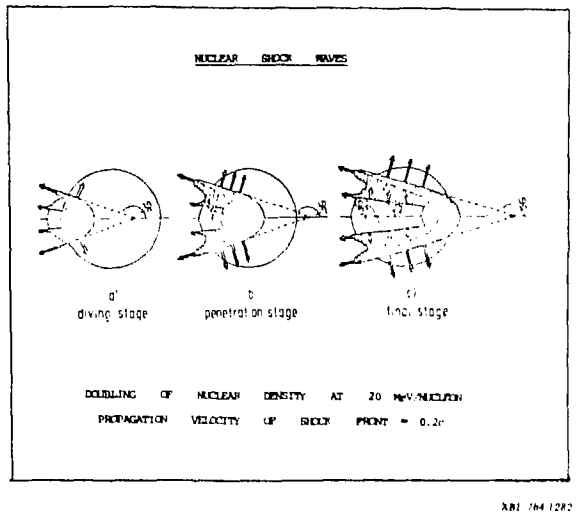

Fig. 3.10

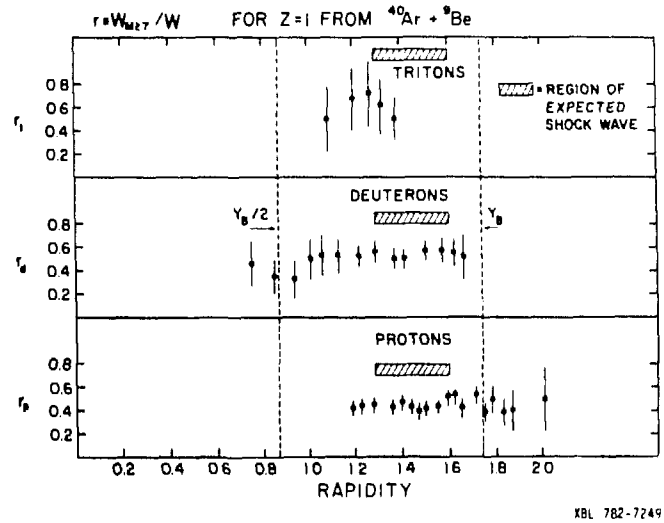

Fig. 3.11

Cerenkov detectors. According to a shock wave model, the fragments from a shock wave in the projectile should peak at rapidities indicated by the shaded regions. The evidence is negative (Gazzaly, 1978). Perhaps the approach outlined in the blast wave studies will be more fruitful, particularly when a high multiplicity selection is imposed (the data in Fig. 3.5 and 3.8 are inclusive).

New evidence has recently come to the fore, which may confirm some of the predictions of hydrodynamics—a model that also deals directly with the equation of state $W(\rho,T)$. In this approach the dynamical evolution of the system follows the continuity equations; it has been applied to the Ne+U reaction at 250 MeV/nucleon (see Fig. 3.12) where the assumptions are better fulfilled than at very high energies. (From the known nucleon-nucleon cross sections of

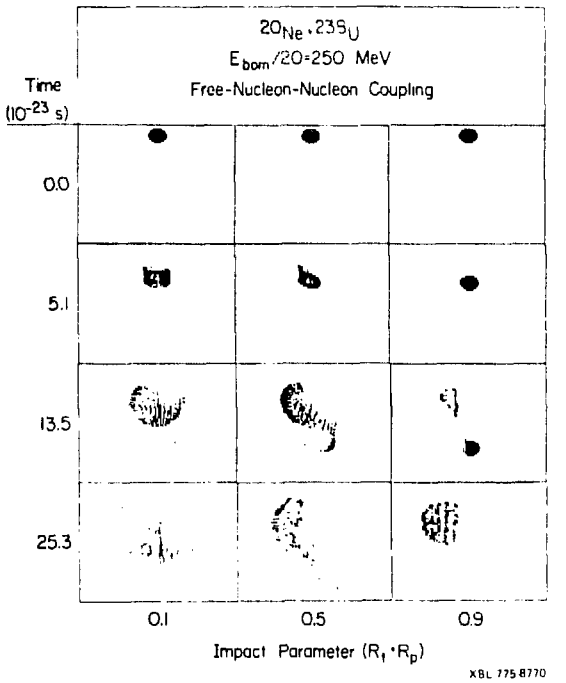

Fig. 3.12

40 mb at 2 GeV, we estimate the mean free path $\lambda \approx 1/\rho\sigma \approx 2$ fm, which is hardly small compared to the macroscopic dimensions). The time evolution of the system is followed for central as well as peripheral collisions. For b = 0.1 R at 5 x 10^{-23} sec, a well-defined shock cone exists but after refraction through the curved surfaces, little trace of it remains. Some indication of a fireball or firestreak is evident for b = 0.5 R. In particular one sees evidence for a strong sideways "splash" (Nix, 1977).

We now turn to the experiment, the apparatus for which is shown in Fig. 2.24 (Gutbrod, 1978). it employs two telescopes, one detecting fission fragments and slow, heavy residues with $A \geq 16$, and the other light intermediate fragments such as π^+, p, d, t. The scintillator array recorded the multiplicity of high energy fragments with E/A > 25. The results for Ne+U at 400 MeV/nucleon are given in Fig. 3.13. Fragments with Z > 26 are associated with multiplicity distributions peaking at M = 0, which probably implies they are associated with peripheral fission and rather small energy transfers. The detection of ^{16}O fragments on the other hand is associated with higher multiplicity of 5 to 10 in rings B and C, which are located intermediate between forward and backward angles (see Fig. 2.24), in which there is roughly a concentration of particles on the opposite side of the detected fragment (Fig. 3.14). It is also noteworthy that no corresponding heavy fragment is found on this side of the beam. Now look back at the hydrodynamical picture of this reaction (Fig. 3.12) for an impact parameter of 0.5 R, and follow the reaction in time. We see that the spectator matter really gets a "kick" and is deflected outwards. Taking the picture seriously one finds this bulk moving out with a velocity of 0.04 c, which for a mass 50 system corresponds to an energy of ≈40 MeV, at least close to the order of magnitude observed in the experiment. Here then one may have the first evidence for the emission of collective chunks of nuclear matter.

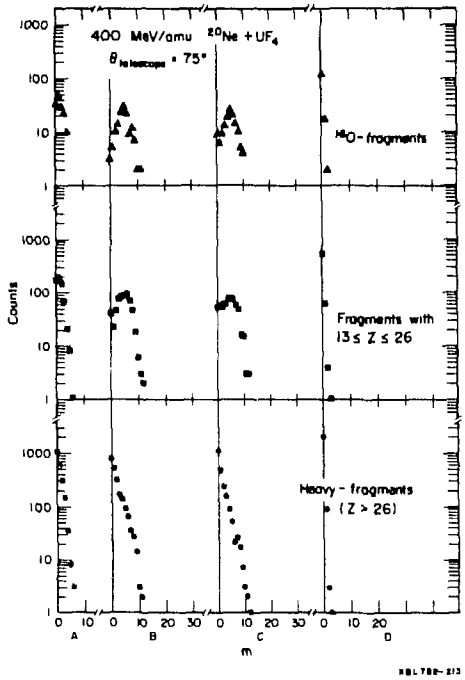

Fig. 3.13

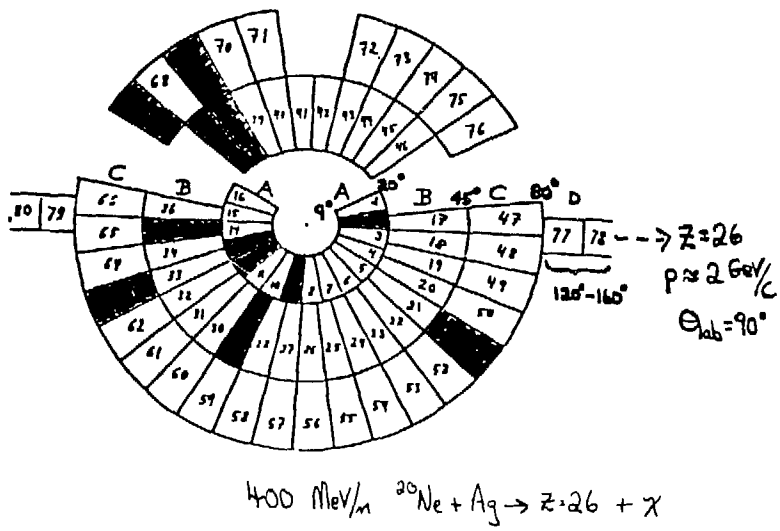

Fig. 3.14

Further evidence for the validity of the hydrodynamical picture may be apparent in Fig. 2.17, which shows a radical departure from the firestreak predictions at forward angles. The same data are shown in Fig. 3.15 as a rapidity plot, with (a) no and (b) high (≥36) multiplicity selection (Sandoval, 1979; Gutbrod, 1978). There is a depletion at forward angles for high multiplicity, which may be a manifestation of the small impact parameter

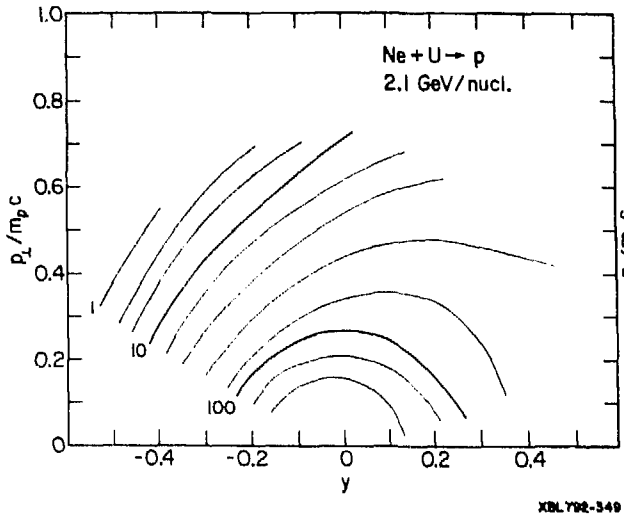

Fig. 3.15a

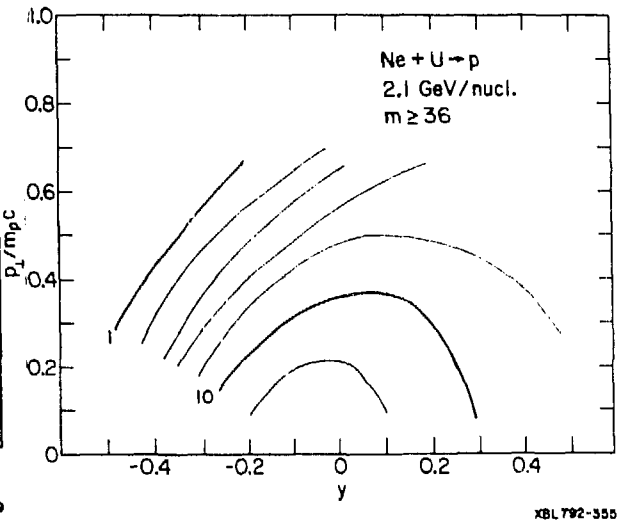

Fig. 3.15b

collision in Fig. 3.12. It is also the effect expected qualitatively from the explosive blast wave model outlined earlier. Whereas it has been established from hydrodynamical calculations that there is virtually no sensitivity to the equation of state, e.g., by changing the compressibility by a factor of two (Nix, 1977), the experiments described here show real hope for greater sensitivity in the exclusive measurements.

Another frightening spectre lurking in the background of relativistic heavy ion collisions, is the possibility that they may be merely superpositions of nucleon-nucleon collisions, conducted at hideous expense. Recent experiments on pion production in the section $^{40}Ar + {}^{40}Ca$ at 1.05 GeV/nucleon give some grounds for optimism. Because of the large energy threshold, pions are produced preferentially in regions of high density and temperature, or from particularly violent nucleon-nucleon collisions. Furthermore, since the pion energies are well below the $\Delta(1232)$ resonance energy, their mean free path is comparable to the dimensions of the mass 40 system, allowing a high chance of escape. The rapidity plot of Fig. 3.16 shows (Wolf, 1979) an enhanced π^+ yield at mid-rapidity, i.e., corresponding to the center of mass of the system, and at a perpendicular momentum of 0.4 m_π ($\approx$55 MeV/c). This feature is quite different from the predictions of a fireball model, which gives semi-circular contours centered at $p_\perp = 0$. The corresponding plot for a proton-proton collision is shown at the bottom, in which the forward and backward peaks are due to the decay of an isobar at rest in the center of mass (Cochran, 1972). There is no indication of enhancement at mid-rapidity. At this stage one can only speculate whether the effect of the "sideways peaking" in the heavy-ion collision is caused by adding compressional energy to the fireball model, or whether it is due to trivial Coulomb effects which push the π^+ out at 90° (like ternary fission) (Koonin, 1979). In the latter case the π^- spectra would show a complementary hole, but these spectra are not yet measured.

One would also like to answer the question: Is the total energy available in the system, viz. $E_{inc} \frac{A_1 A_2}{A_1+A_2}$ GeV, the important quantity or is it just $(\sqrt{2(E_{inc} + 2)} - 2$ GeV, that is available A_1 nucleon-nucleon reactions? The difference between these pictures is important. If we find

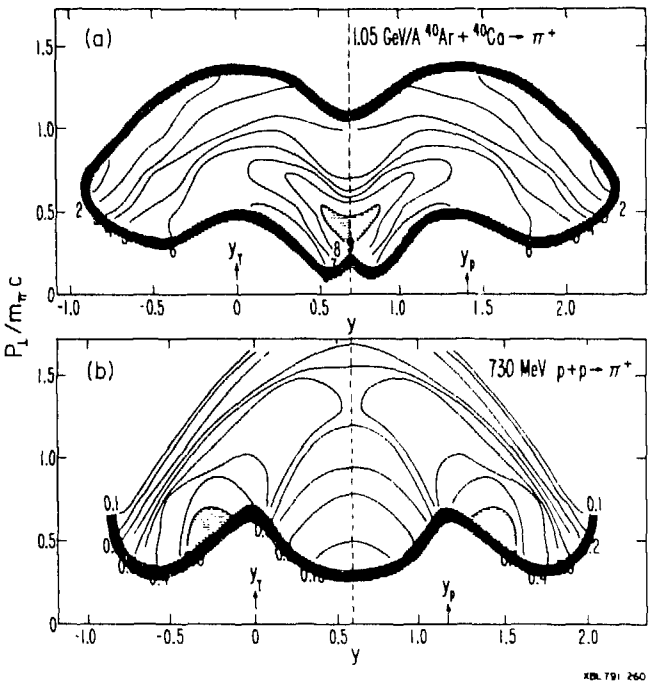

Fig. 3.16

pion production at 0.1 GeV/A, the former expression must be relevant, and collective phenomena are important. A recent experiment sheds some light, by studying pion production in heavy ion collisions below the nucleon nucleon threshold of 280 MeV/nucleon, and also below the nucleon-nucleus threshold of ≈160 MeV (Benenson, 1979; Jacobsson, 1979). It is in this energy region that one could also profitably look for effects of pion condensation, to which the yield of low energy pions might be very sensitive. The measured production cross sections are plotted in Fig. 3.17, and compared with a theoretical "background" calculation from the Fermi momenta of the two nuclei combined to permit pion production by nucleon nucleon collisions. At the lowest energies the theory is correct in magnitude but falls drastically below the data at higher energies. The solid line is the fireball prediction. It is clear that other--not necessarily exotic--mechanisms must be at work to explain the enhanced yield, which nevertheless is well below that claimed in some emulsion experiments (McNulty, 1977). The data in Fig. 3.15 correspond only to 10^{-3} pions per collision, whereas emulsion experiments have claimed, presumably enormously (Lindstrom, 1978; Kullberg, 1978), that the pions were produced in 70% of the central collisions.

A further intriguing aspect of these data is the comparison of π^+ and π^- yields (Fig. 3.18) where an enormous peak appears in the π^- cross section at very low pion energies. This effect may have a trivial Coulomb interpretation, or hopefully some exotic explanation (Benenson, 1979). The point of this figure—and indeed of this whole section—is that new phenomena are appearing and that data are no longer featureless decaying exponentials to be fitted by any of a score of diverse models.

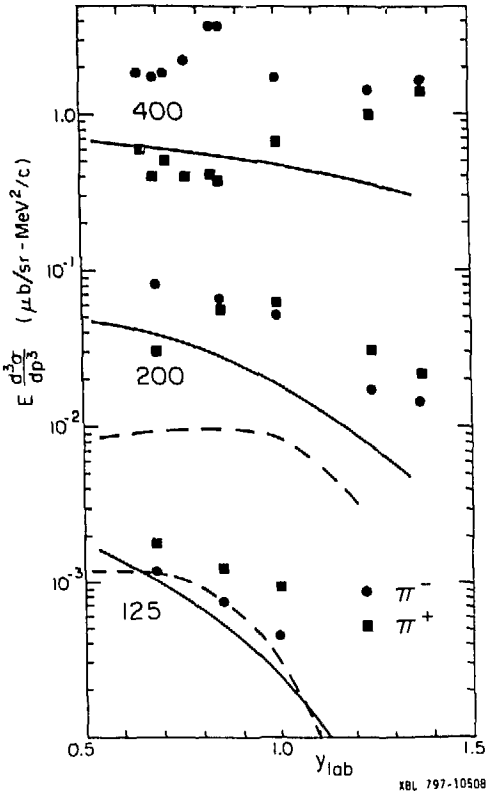

Fig. 3.17

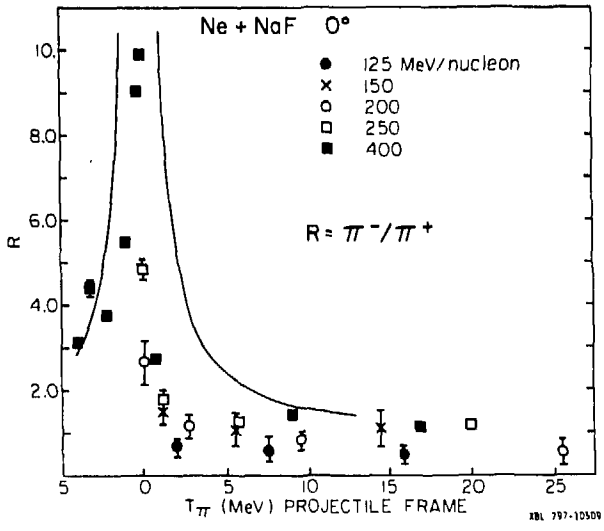

Fig. 3.18

Temporal and Spatial Limits

The measurement of the space-time dimensions of the nuclear interaction regions formed when heavy ions collide at relativistic energies calls for

novel techniques. In lecture 2 we gave indirect evidence from the coalescence model that this dimension was ≈3-4 fm. In this short-lived fireball, nuclear matter may be compressed to high densities (10^{15} gm/cm^3), heated to high temperatures (10^{12} ^oK) and expanding with relativistic speeds on a time scale of 10^{-23} to 10^{-22}sec. For more detailed insight into this interesting region a recent development has been the application of pion interferometry to deduce the space-time geometry (Fung, 1978). The basic idea goes back go Hanbury-Brown and Twiss, who used the technique of second order intensity interferometry to deduce stellar radii (Hanbury-Brown, 1956). For chaotic, incoherent light, although the average photon count measured by two detectors is the same and independent of detector separation, the coincidence rate does depend on the separation.

The principle is illustrated in Fig. 3.19 (Cocconi, 1974; Koonin, 1977; Yano, 1978). Two identical bosons are produced simultaneously (within Δt), and with equal momentum (within Δp) and with random relative phases at α and β separated by R. At a distance r >> R two detectors A and B, separated by D, register coincidences. Define $\theta = D/r$ and $\rho = R/r$. Since there are two indistinguishable ways of creating a coincidence (A hit by particle from α, B by β and vice versa) the total amplitude is for bosons the sum of the partial amplitudes. Call a_1, a_2, b_1, b_2 the lengths of the four possible paths. Then:

$$\text{Coincidence amplitude} \propto e^{ika_1}e^{ikb_1} + e^{ika_2}e^{ikb_2}$$

$$= e^{ik(a_1+b_1)} + e^{ik(a_2+b_2)} \qquad (3.7)$$

$$\text{Rate} \propto |\text{Amplitude}|^2 = 2(1 + \cos kR\theta)$$

where $2\rho D/2 = R\theta$.

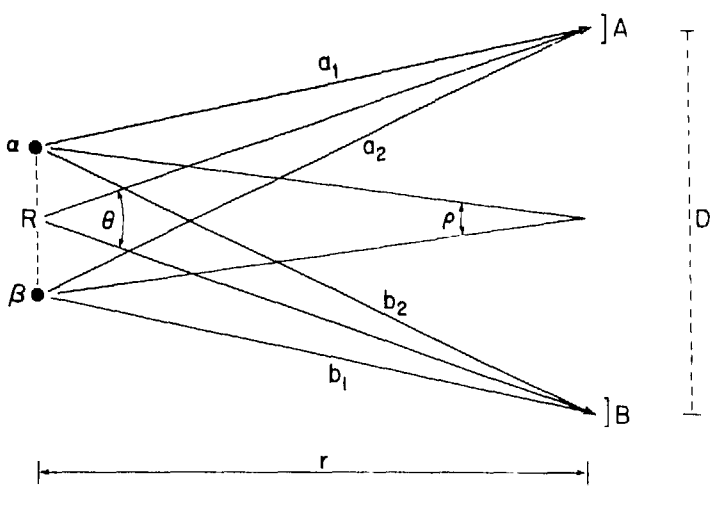

XBL 797-2278

Fig. 3.19

There will be a modulation of the interference pattern as a function of θ, with maxima at $kR\theta/2\pi = 0,1,2 \ldots$, which allows the determination of R. The condition for interference is the existence of a path ambituity, i.e., $(\Delta p)c\Delta t \lesssim \hbar$, for the effect of Bose statistics to operate. From the discussion at the end of lecture 2, we expect the dimensions of the fireball to be $\approx$3 fm and hence we require $\Delta t \lesssim 3$ fm/c, so the phenomena we are discussing should be present provided the momenta of the two pions are equal within,

$$(\Delta p)\ c \lesssim \frac{\hbar}{3\ \text{fm/c}} \approx 60\ \text{MeV} \tag{3.8}$$

In Fig. 3.20, are shown the results of an interferometry experiment (Fung, 1978) for 1.8 GeV/nucleon argon or lead. The pions were detected in a streamer chamber, triggered in the inelastic mode (to bias out peripheral events, i.e., the requirement that there is no leading high energy projectile-like fragment emitted into the forward cone). Plotted is the normalized ratio of the number of negative pion pairs from the same event to the number from different events, $R^{S}_{D}{}^{--}_{--}$ as a function of the relative momentum $q = |p_i - p_k|$ and energy difference $q_0 = |E_i - E_k|$. This function has the form,

$$R^{S}_{D}{}^{--}_{--} \propto \left\{1 + \exp\left[-\left(\frac{\tau^2 q_0^2}{2}\right) - \left(\frac{r_0^2 q^2}{2}\right)\right]\right\} \tag{3.9}$$

where r_0 and τ are characteristic space-time parameters. (The reader will hopefully recognise some semblance to the earlier formulae!) We note that the value of q is indeed $\approx$60 MeV/c, as expected from the above simple arguments. The best fits to the data yield $\tau \approx 3 \times 10^{-24}$ sec and $r_0 \approx 3.5$ fm. One should compare this result with $r_0 \approx 1$ fm in p + p collisions suggesting more extended sources are formed in nuclear collisions (Ezell, 1977).

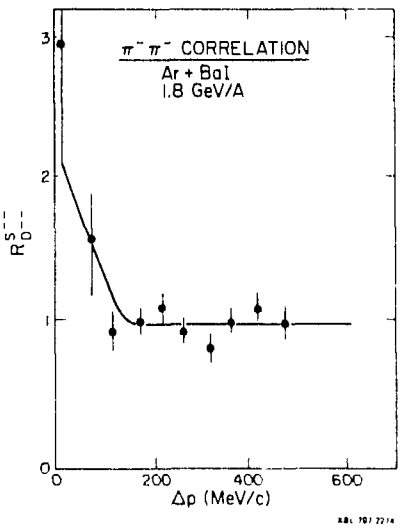

Fig. 3.20

The result agrees surprisingly well with the coalescence model estimate at the end of lecture 2. There is one other approach (Ta-Chung, 1978) used for the space-time structure, which works on the premise that "a pion source is a system of bosons in thermal equilibrium, similar to the case of black-body radiation," Then the volume V, the temperature T, and the total energy E_T are related by the Stefan-Boltzmann law,

$$E_T = \frac{gV(kT)^4}{2\pi^2(hc)^3} \int dx \frac{x^2\sqrt{x^2 - x_0^2}}{(e^x - 1)} \tag{3.10}$$

where $x_0 = mc^2/kT$, $x = E/kT$, and g is a statistical weight.. Using this formula on existing experimental data, again leads to a value of $r \approx 3.7$ fm!

Another area of research possibly addressing itself to the problem of localized emitting sources is the 0° and 180° production of pions and nucleons in hadron or nuclear collisions (Baldin, 1978). There have been several semi-phenomenological approaches to parameterize the data. At one extreme is the notion of the cumulative effect, in which the effective projectile or target is supposed to be a compact object of mass larger than a nucleon. By kinematics alone this permits fast forward or backward emission, which would be forbidden in a quasi-free nucleon nucleon scattering. The hope is that by studying the highest energy fragments, the cluster aspects of nuclei can be deduced. Indeed in such experiments the existence of quark clusters in nuclei may already be revealed (Baldin, 1978).

There exist superficially contradictory interpretations of the data, based on a fragmentation model (Ko, 1979) or on the exponentially falling virtual momentum spectrum of nucleus in nuclei (Landau, 1978). This approach is illustrated in Fig. 3.21 for 180° pion production in collision of protons on copper at 730 MeV, 5.14 GeV and 7.5 GeV. The theoretical curves are calculated with a model employing elementary $p + p \rightarrow \pi^- + x$ collisions with either Gaussian or exponential shapes for the Fermi distribution of the nucleons. In the figure the data are plotted as a function of the scaling parameter $x = k^*/k^*(max)$, with k^* the longitudinal momentum in the center of mass and $k^*(max)$ is the maximum value allowed by energy and momentum conservation. This scaling property has been demonstrated by the fact that at high energies the pion yield depends on x and not on the energy of the projectile. In a relativistic analog of the parton model (Schmidt, 1977) the data for $x \approx 1$ should follow the form $(1 - x)^{6A-5}$ where the exponent for the case illustrated is 350! Values closer to 30 are found in practice for the 180° data, but this may merely reflect that these data do not reside in asymptotia, which calls for $x \approx 1$. Other indications that asymptotic behavior is not reached for the backward pion production spectra are indicated by Fig. 3.22. Here the values of T_0 extracted from the formula

$$E\frac{d\sigma}{dp^3} = Ae^{-T/T_0} \tag{3.11}$$

are plotted as a function of the incident energy, T, in GeV/nucleon. Above 4 GeV, $T_0 \approx 60$ MeV but falls continuously at lower energies. The approach to the asymptotic value of 60 MeV is interpreted with models of cumulative production which involve components in the nuclear wave function based on the quark and parton constituents (Baldin, 1978). The distance at which the

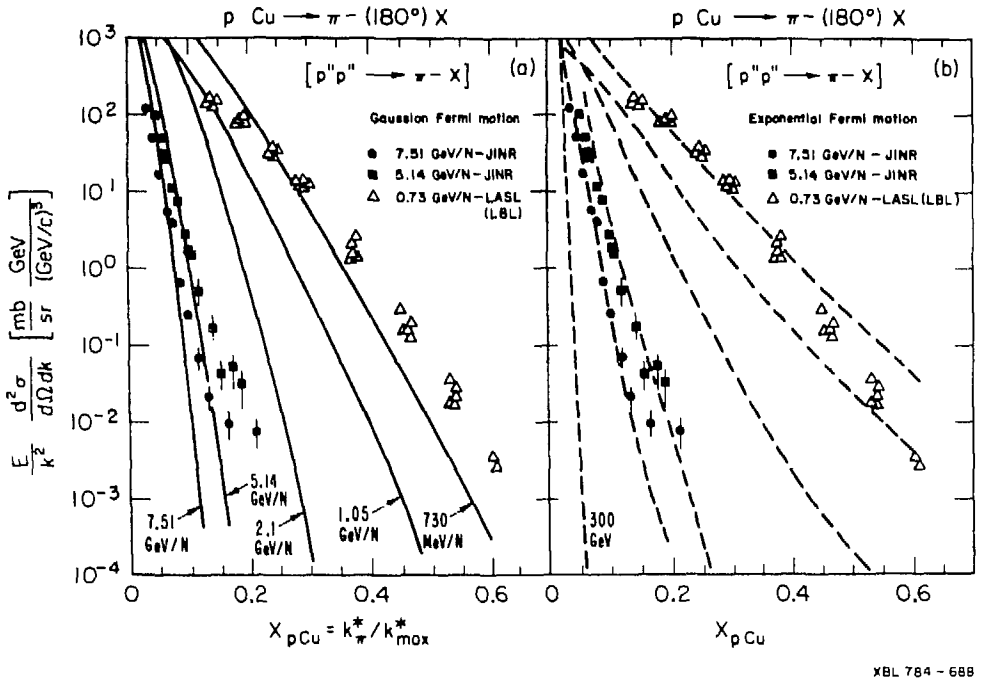

Fig. 3.21

nucleons lose their individuality and which is probed by the experiments, turns out to be ≈0.65 fm. (Note that the data in Fig. 3.22 have been redrawn for purposes of illustration; for precise numbers, reference should be made to the original literature).

The diverse exciting and/or mundane explanations of these experiments in terms of collective effects, Fermi motion, coherent tube..... may actually turn out to be simply different parameterizations of the same underlying phenomenon. The approaches are probably closer conceptually than their presentations would suggest. For example, the addition of an exponential or Gaussian tail to the usual Fermi distribution may be closely linked to clustering aspects of nucleons in nuclei. According to the philosophy we have followed in the first two lectures, one might also gain insight through comparisons with similar studies at lower energies.

Consider the data on backward scattering of 90 MeV protons on several targets in Fig. 3.23 (Wall, 1978), where the spectra are plotted according to the following prescription. It has been shown that if p is the projectile momentum, and q the detected particle momentum, many data can be parameterized by "quasi-two-body-scaling," based on the minimum value of k (k min), the smallest possible momentum for the target nucleon (or nucleons) scattered by the projectile and subsequently detected at a backward angle (Fraenkel, 1977, 1978). In this picture the nucleon is assumed to be moving toward the backward angle when scattered. Then

$$\frac{d^3\sigma}{dq^3} = \frac{CG(k\ min)}{|\bar{p} - \bar{q}|} \qquad (3.12)$$

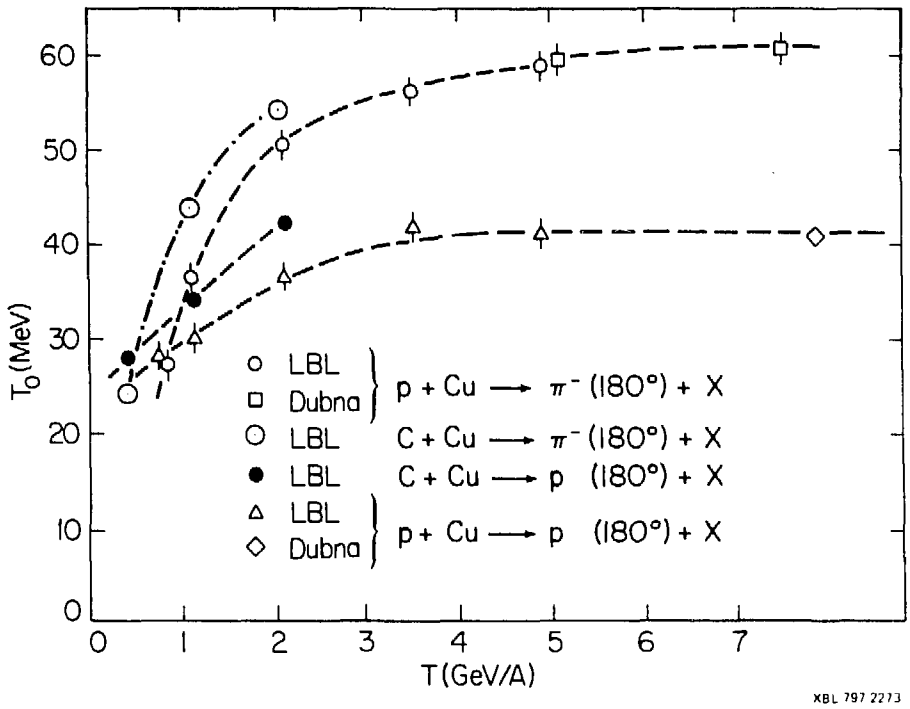

Fig. 3.22

where C is a constant and G(k min) = $\int F(k)\, kdk$ evaluated at k min. F(k) is the internal target nucleon momentum distribution. As Fig. 3.23 shows, the experimental data are described by $G(k) = \exp(-k/k_0)$, with $k_0 \approx 60$ MeV/c. This value of k_0 is shown (Schroeder, 1949) in Fig. 3.24, together with the results of a similar analysis of some of the higher energy data shown in Fig. 3.22, and with results from α + Ag at 720 MeV (Thornton, 1979). From the lowest energy the k_0 values follow a smooth trend up to the saturation at a value of $k_0 \approx 115$ MeV/c (equivalent to the value of $T_0 \approx 60$ MeV in Fig. 3.22).

It has been pointed out, however, that lowest energy data in Fig. 3.24 are also consistent with emission from a localized hot spot on the surface of the nucleus (Wall, 1978, Stelte, 1979), decaying with a temperature of 8 MeV, the relation of which to the higher energy interpretation remains to be worked out. But it is clear that the study of heavy ion collisions over a very broad energy range must surely turn up revealing conceptual links. As we discussed in earlier lectures the production of hot-spots or localized depositions of energy confined in space and time into a region of the nucleus is an active field of study in low energy heavy ion peripheral reactions and fragmentation reactions--as discussed in lecture 2. That the 0° and 180° production is also closely related to fragmentation is suggested by Fig. 3.25, which gives intimations that the 180° data connect nicely onto the target fragmentation region in rapidity space (Gyulassy, 1979). At the other extreme the concepts of hot-spots and fireballs, were first promoted to understand the violent events of p + p collisions. There the concept is used to determine the thermal conductivity of hadronic matter (Weiner, 1976) just as the same concepts are now used to study the relaxation time of nuclear matter in deeply-inelastic scattering (Gottschalk, 1979). A unified description of effects,

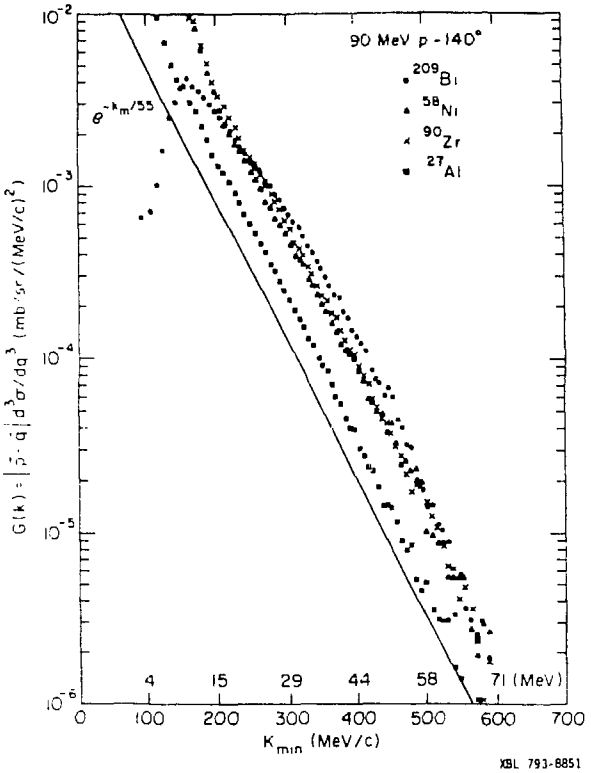

Fig. 3.23

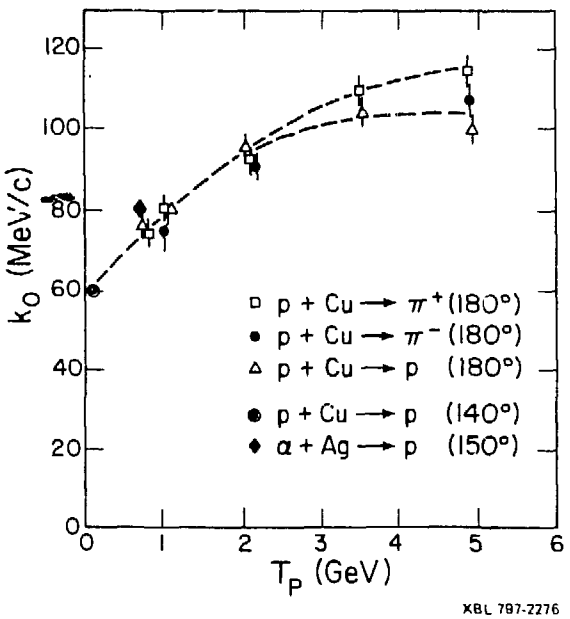

Fig. 3.24

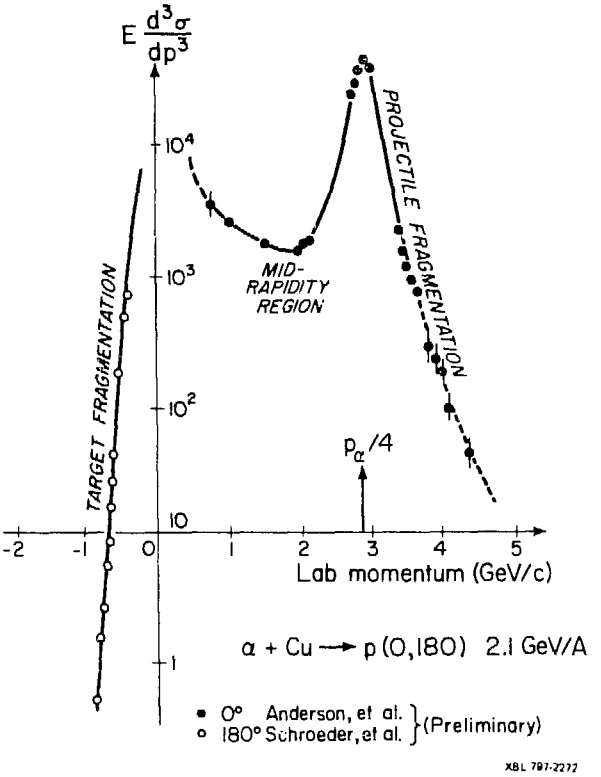

Fig. 3.25

such as those of Fig. 3.24, may tell us much about the Limits of Space and Times. For the moment, however,

> "...chè il tempo che n'è imposto, piu ultimente compartir si vuole."
>
> ...our time which has its limit set, ought to be spent in a more useful way.
>
> Dante, The Divine Comedy

The "more useful way" will be the final topic concerning the Limits of Nuclear Matter and of Nuclei.

The Limits of Nuclear Matter and Nuclei

To address the important question of the investigation of the limits of nuclear matter with relativistic heavy ion collisions, we need more than the plastic ball of Fig. 3.2. Very likely we need a Crystal Ball! And we need a definitive signal to tell us that a new minimum has appeared in the energy-density plot of Fig. 3.3. Let us look at the overall development of the interacting nuclear volume in Fig. 3.26 for the head-on collision of two equal mass nuclei (Stock, 1978). At (a) the initial state of the two separate systems is shown at the minimum for $\rho = \rho_0$. The center of mass kinetic energy per nucleon is given by the horizontal line on which the system must also be found finally. Let us assume that at the stage of highest compression

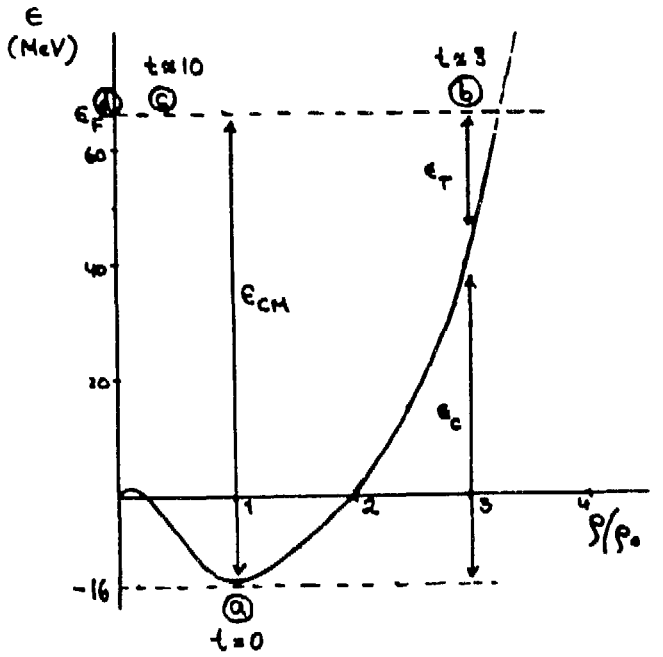

Fig. 3.26

we have reached equilibrium: then it is represented by one system at (b). The internal energy present is compressional, ε_c, and thermal ε_T, with the ratio between them determined by entropy and by the equation of state. The system then expands to $\rho = 0$, passing the fireball freeze-out density at (c). The final product nucleons in the detector correspond to (d). The effect of a possible phase transition to a pion condensate, density isomer or quark matter would show up as a secondary minimum, in which case $\varepsilon_T(t)$ would be changed, and with it the ratio between ε_T and ε_c. These processes depend strongly on the interaction time which is shown in units of 10^{-23} sec. We have seen how this ratio might be extracted from the experimental data earlier in this lecture. These experiments will be difficult but necessary, since the "obvious" signals, like copious pion production in the event of a condensate, are now believed unlikely.

In searching for more sensitive tools to study pion coherence it may be possible to utilize pion interferometry (Fowler, 1977; Guylassy, 1978,1979); Biswas, 1976). Our earlier discussion assumed a completely chaotic source. If there is some particular mode in the pion field which is excited preferentially, the correlation patterns of Fig. 3.20 would be modified, with no interference maximum at zero momentum separation. The experimental problems, however, are formidable, since a fixed impact parameter must be isolated, and the effect of final state interactions allowed for. One other possibility is the measurement of the pion multiplicity distribution (Gyulassy, 1978) As we discussed in lecture 2 (Fig. 2.25) for a particular impact parameter, this distribution has a pure Poisson form for impact parameter b = 0, in the absence of any unusual, coherent pion production processes. Some preliminary measurements with a streamer chamber for the Ar + KCl → $n\pi^-$ reaction at 1.8 GeV/nucleon, operated in a highly inelastic trigger mode to bias in favor of central collisions, are shown in Fig. 3.27 (Schroeder, 1979). This

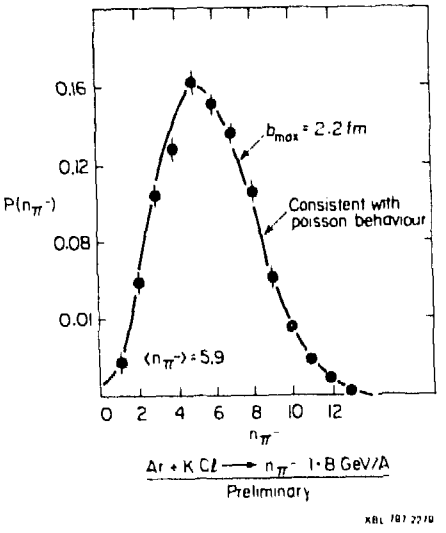

Fig. 3.27

distribution is alarmingly well described in a Poisson, but it is also true that the production of new phases of nuclear matter may require densities ten times in excess of normal, which are unobtainable with the present accelerators.

Another area awaiting the future higher energy accelerator is the study of hadronic matter. As we noted in the introduction to these lectures, the general form of the hadronic mass spectrum may be deduced from the temperatures reflected in the inclusive spectrum of particles (Glendenning, 197[illegible]). It is known experimentally that for each new hadronic threshold, a rich spectrum of resonances ensues for the next interval of a few GeV. According to several models, the hadronic mass spectrum continues indefinitely with an experimental growth in the number of particles (Hagedorn, 1973; Rafelski, 1979). Assuming the feasibility of forming equilibrated, hot hadronic matter of nuclear dimensions, e.g., the fireball, a fundamental question remains whether one can experimentally distinguish between the various possible models of the mass spectrum. The results of a model calculation for nucleus nucleus collisions, designed to answer this question, are shown in Fig. 3.28 (Glendenning, 1978a) indicating the equilibrium temperature attainable in central collisions as a function of energy. Three models are shown: the "bootstrap," which refers to an experimental mass spectrum; the "quark bag," a simple power law, and the "known" which includes only the presently determined resonances. The prediction of these three models of the hadronic spectrum begin to diverge only at energies above 2 GeV/nucleon, well beyond the limit of present accelerators.

The study of nuclei at the limit of stability is, however, a subject ideally suited to present relativistic heavy ion accelerators. The motivation for such a study becomes clear when we take a panoramic view of the stability diagram for nuclear species shown (Bromley, 1973) in Fig. 3.29. There are 300 or so stable nuclei. During the last half century, some 1300 additional radioisotopes have been identified and studied. It is estimated that another 6000 might exist. In our present state of ignorance, an attempt at extrapolating our current knowledge to the description of all these nuclei is analogous to

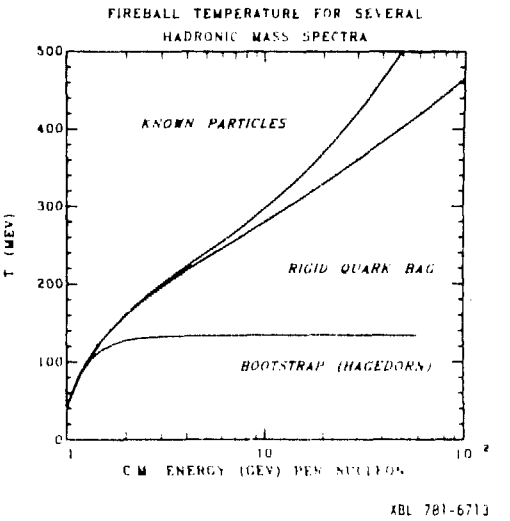

Fig. 3.28

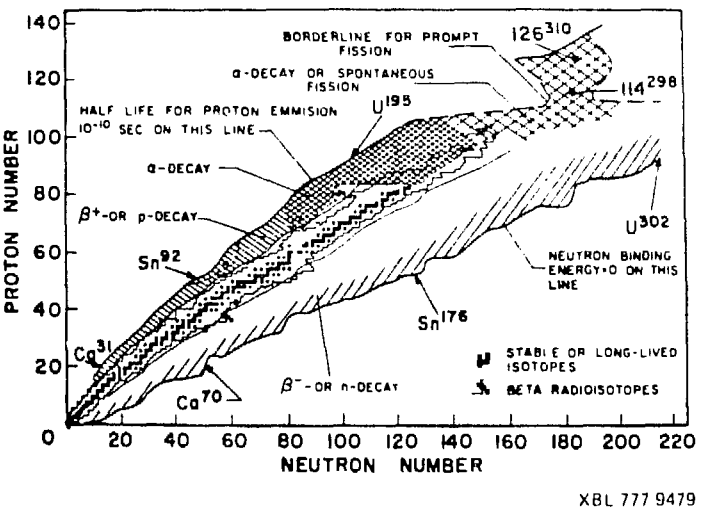

Fig. 3.29

describing the geography of the United States by extrapolation from a detailed study of the deep valley of the Grand Canyon!

How many neutrons a specified number of protons can bind is a well defined query which is proving difficulty to answer experimentally. Clearly the answer is of some importance to nuclear physics. One will attempt to see if nuclear models, such as the shell model applied in the valley of stability will yield comparably good results for more exotic species. In particular, regarding the ground state masses, it is crucial to understand whether the nuclear density alters slightly. If the density were to decrease for large values of N/Z there could be a large change in the total binding energy

(Garvey, 1972). In this context it is amusing to note that in the first calculations on the possible existence of collapsed nuclei, the suggestion was made to look for extremely rare isotopes of known elements (Feenberg, 1966). Referring back to Fig. 3.29, the discovery of a nucleus such as ^{70}Ca, i.e., 20 protons and 50 neutrons, and the study of its properties, could be an event of comparable drama to the detection of shock waves or pion condensates.

In estimating whether a nucleus will be stable against strong interaction decay, there exist a plethora of nuclear models. These range from the semi-empirical droplet model, to ab initio shell models and semiempirical interpolation techniques. To give the spirit of how some of these methods work, consider the original Garvey-Kelson mass formula (Thibault, 1974). On the assumption that the residual interaction is primarily between nucleons in the same shell model level and that the position of the single particle levels vary only slowly with mass number, the following relation holds:

$$M(N+2,Z-2) - M(N,Z) = M(N+1,Z-2) - M(N,Z-1) + M(N+2,Z-1) - M(N+1,Z) \quad .$$

As an example, we know that:

$$M(^{16}C) - M(^{16}O) \approx M(^{15}C) - M(^{15}N) + M(^{17}N) - M(^{17}O)$$

The relation can be generalized to predict the mass difference of nuclei widely separated in Z in terms of the sum of masses of isospin pairs of nuclei close to stability. This approach, with added sophistication, has been followed to predict the boundary of stability of light nuclei shown in Fig. 3.30. Except for the very lightest nuclei, like Be and B, the predicted limit extends well beyond the nuclei observed so far. The different approaches are usually in most marked disagreement out at the limit, since the

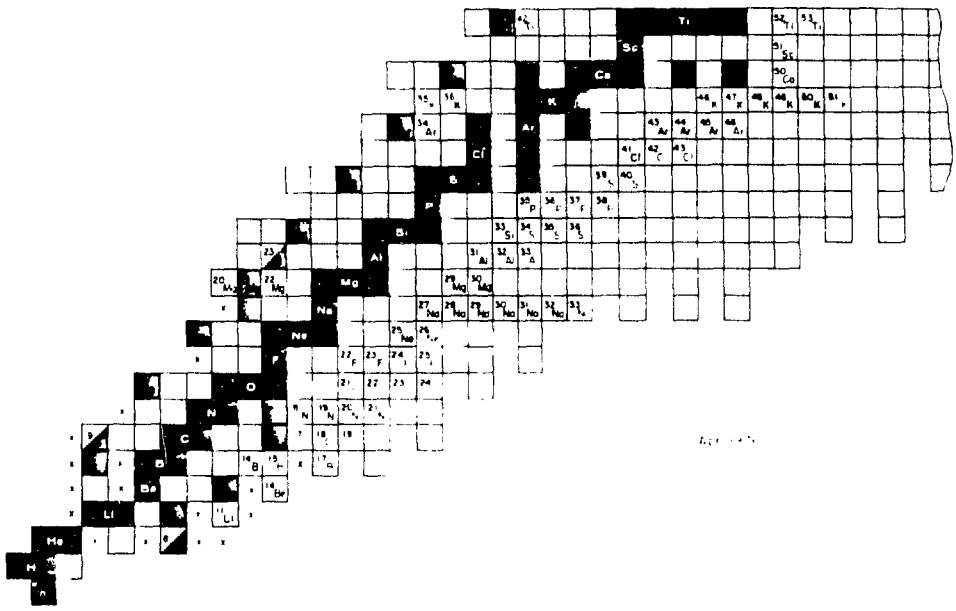

CBB 740-6921A

Fig. 3.30

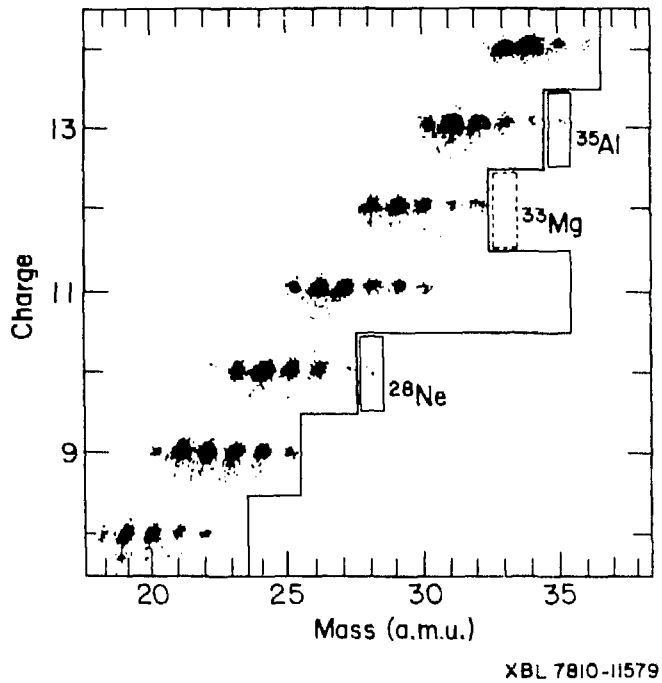

Fig. 3.31

errors of prediction are accumulative (for a review see Nuclear, 1976,1977). The figure shows that many nuclei are predicted unstable, before the final limit is reached, e.g., ^{25}O is unstable and ^{26}O is stable. In these cases the mere observation of a nuclide, and no other information, can make an impact on the development of nuclear models. For example in the case of Na isotopes (Klapisch, 1972), this approach led to the prediction of a new region of deformation around ^{31}Na by means of Hartree-Fock theories (Campi, 1975).

How do we make a global attack on producing all nuclei out to the limit of stability? Relativistic heavy ion beams are ideal, by exploiting the features of abrasion outlined in lecture 1 by Figs. 1.17-1.20. With ^{48}Ca, for example, by suddenly shearing off eight protons it is possible to make ^{40}Mg which is predicted as the last stable isotope. By bringing the beam in at high velocity, this mechanism produces the abraded fragments close to 0^{o}, the transverse velocity corresponding only to the much smaller Fermi nomentum (see the discussion of Figs. 1.12, 1.13, and 1.15). Compared to conventional low energy experiments (Artukh, 1971) the gain in solid angle is $\approx 10^3$. Furthermore the high energies allow the use of thick targets, again boosting the yield by 10^3. The overall gain of 10^6 is a welcome factor in the search for highly exotic isotopes with sub-nanobarn yields. Such an experiment is effectively the kinematic inverse of high energy protons spallation of heavy targets, which is one of the powerful methods used to advance the known limit to the region shown in Fig. 3.29 (Butler, 1977).

In Fig. 3.31 we show (Symons, 1979) how the abrasion of ^{40}Ar at 213 MeV/nucleon already advanced the front by one more nuclide in the cases of Ne, Mg, and Al. With a ^{48}Ca beam, and ultimately a uranium beam of 2 GeV/nucleon, the last frontier should be conquered. While the search for the study of the limits of nuclear matter under the extreme conditions of temperature,

pressure, and density continues hopefully, it is clear that one limit can be overcome, the limits of nuclei themselves. It is possible, however, that much lower deeply inelastic collisions will also be a powerful method of producing new neutron excess nuclei. In this method the statistical fluctuations of neutron diffusion are exploited instead of the ground state quantal fluctuations of relativistic collisions (Remember Fig. 1.21). In concert with the view adopted in these lectures that low and high energy approaches have much to offer each other, let us compare an example of the progress in the study of exotic nuclei by deep in elastic scattering shown in Fig. 3.32 for ^{40}Ar + ^{238}U at 6.5 MeV/nucleon, through which the neutron rich nuclides, ^{37}Si, ^{40}P, $^{41-42}S$ were observed for the first time (Auger, 1979).

In moving the new region of the N-Z diagram, there is a rich field for speculation. It is conjectured that nuclei of very large neutron excess may exist in which the neutrons form an expanded cloud, enveloping a conventional nucleus at the center (Wilkinson, 1976). Such two-component nuclei have not been investigated--nor is it clear if such differentiated nuclei exist, what would be their optimum form. It is possible that bubble and toroidal configurations may be more stable with a central depression of the density (Wong, 1978). Recently the interest in such unusual nuclei has been revived (Grammaticos, 1979) by the possibility of forming exotic configurations in relativistic heavy ion collisions, e.g., nuclei with a cylindrical hole drilled through the center, and then following the subsequent decay of exotic collective modes, by means of TDHF methods. Some examples for three different impact parameters are shown in Fig. 3.33.

ENVOI

In concluding this (incomplete) view of relativistic heavy ion collisions it is appropriate to return to the picture of the Unicorn. Figure 3.34 shows the detail of The Unicorn in Captivity. A fence has been constructed around the wounded creature, but by and large it remains intact! That is pretty much the situation in the relativistic field. The areas of search for novel effects have been narrowed, some preliminary forays are completed, but of the elusive

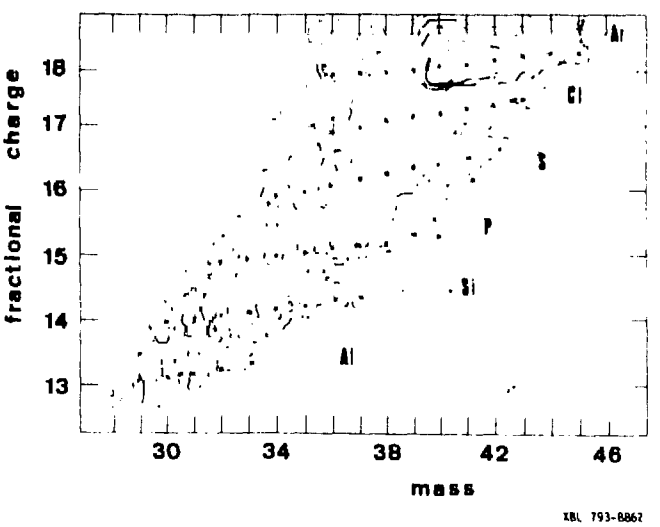

Fig. 3.32

exotic phenomena we have only intimations. There are some who say the phenomena are all myths and we should turn our efforts to other things:

"The Lion and the Unicorn
Were fighting for the Crown,
The Lion beat the Unicorn
All around the Town.
Some gave them white bread
And some gave them brown.
And Some gave them plum cake
And chased them out of Town."

The last lines of this nursery rhyme have not yet come to pass, but the critics have raised the question whether one is being fooled by an implicit ergodic hypothesis--that all particles in one event behave like an average particle in an average event. The inclusive experiments do a gross averaging, which may wash out the dynamics and leave only phase space. So many different models with diverse assumptions fit the exclusive data. I have tried to show examples of new experiments that go beyond the inclusive measurement, proving equilibrium in event by event of the type in Fig. 2.1. One should not forget, however, that whereas in low energy nuclear physics a successful theoretical description of an angular distribution, an interference minimum, is hailed as a triumph, a comparable success by even a sophisticated model in relativistic heavy ion physics is greated as a disaster and an expression of triviality!

In the development of relativistic heavy ion studies, a form of intellectual Ludditism appears to be prevalent. There is a tendency to assume that no significant or valuable progress is being made, when in fact ingriguing and unexplainable phenomena exist, the ultimate understanding of which is likely only to come from sustained research on the whole field of relativistic heavy ion collisions. A well publicized unusual phenomenon mentioned in the introduction to these lectures is the celebrated centauro events found in the Mount Chacaltaya emulsion exposures, which defy all rational explanation (Brazil-Japan Collaboration, 1978). These events have very large hadron multiplicity of 100, without any sign of accompanying neutral pion emission. One suggested explanation (Bjorken, 1978) attributes the shower to a glob of high density (30 to 1000 times normal) nuclear matter in the quark phase, at an energy of 10^6 GeV. Estimates already exist of the residual concentration of quarks in the earth, from the deduced flux of the globs, in the region of $10^{-2}/cm^3$, safely within experimental limits (Jones, 1978). In another context, but one of equal fascination there are theoretical estimates based on the quark bag model of hadrons (Johnson, 1975) that extended massive multiquark states of very large strangeness (strangeness/baryon ≈ 2) may be metastable with lifetimes of 10^{-4} sec (Chin, 1979). Such matter could only be created with measurable cross section in relativistic heavy ion collisions. As a final example of the spectacular, and one closer to direct experimental fact, we show in Fig. 3.35 the collision of a proton in an emulsion at 70 GeV, in which the target nucleus is completely shattered (Asharov, 1976). The mechanism is not understood, but it clearly indicates that for some high energy collisions at least, nuclei are not transparent. However, for the major part of the cross section, it appears that above 4 GeV an asymptotic condition is approached, in which further increases in the proton energy do not result in any changes in the cross sections for the production of a fragment, nor in any change in the average energy of the fragment (Remsberg, 1975). Such observations could argue in favor of transparency (Feshbach, 1979).

Clearly there is much groundwork still required before one can attempt to

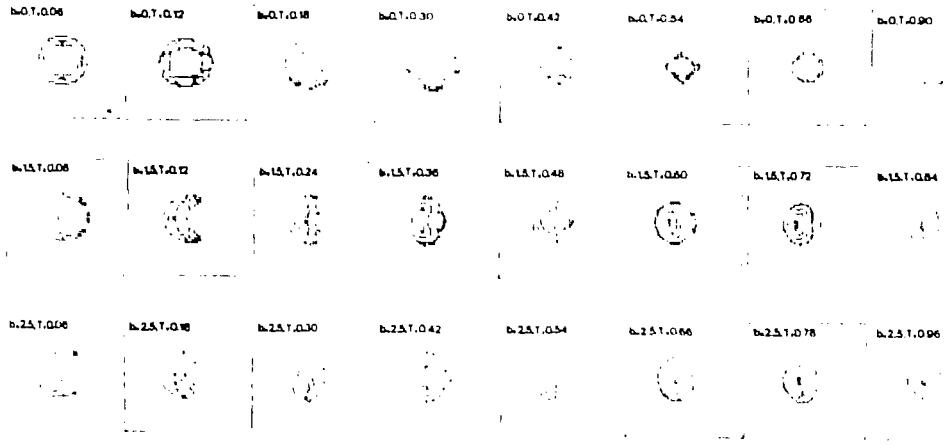

Fig. 3.33

CBB 793-3235

Fig. 3.34

Complete destruction of Ag, Br, Pb nuclei by
70 GeV/c protons and 17 GeV/c alphas
(150 events analyzed)

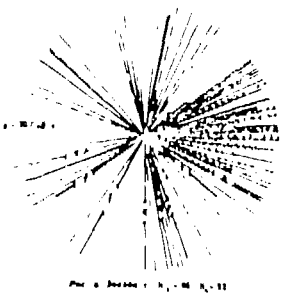

O Akhrorov et al., JINR (Dubna)

Fig. 3.35

understand these remarkable events. In Stock's words, "One should look at the development of elementary particle physics where Hagedorn's fireball model of 1967 is still good enough today to explain the strong interaction background in events that reveal quark structure. The necessary steps in our own field are within reach: two particle correlations, event selection, excitation functions and multiparticle exclusive analysis, new 4π detection schemes; and for crucial searches, like the use of K^+ as a thermometer or shock emission as a barometer, one will need higher energy accelerators" (Stock, 1978).

Nor should be forget the low energy accelerators. One of the aims of these lectures has been to show that there is an interplay of concepts in the different energy regimes. In the framework of the heavy ion reaction phase diagram of Fig. 1.4, one should look on the four sectors as the four cornerstones of a single structure. One is reminded of the words (Wilkinson, 1962) of the chairman of this School, Sir Denys Wilkinson, on the state of nuclear and elementary particle physics in Rutherford's day: "These subjects were simple but not easy. So many zero order questions had to be answered in order to make even remote sense of what was going on. Such questions still exist, but we have to work in two complicated edifices which generate more complicated questions. I have tried to show that we should recognize that these two edifices have common intellectual foundations and that the growth of both will be the quicker and the surer if the builders of each keep an eye on the progress of the other."

REFERENCES

The following bibliography is not meant to be exhaustive, nor attentive to historical development. It comprises a list which was both accessible and illuminating to the author.

Abul-Magd, A. Y., Hufner, J. (1978). Nucl. Phys., A308, 429.
Afek, Y., Berland, G., Dar, A., Eilam, G. (1978). Phys. Rev. Lett., 41, 849.
Alhassed, Y., Levine, R. D., Karp, J. S., Steadman, S. G. (1979). Preprint.
Amsden, A. A., Bertsch, G. F., Harlow, F. H., Nix, J. R. (1977). Phys. Rev., C15, 2059.

Amsden, A. A., Goldhaber, A. S., Harlow, F. H., Nix, J. R. (1978). Phys. Rev. 17, 2080.
Ashkorov, O. (1976). Dubna Preprint P1-9963.
Artukh, A. G., Avdeichikov, V. V., Gridnev, G. F., Mikheev, M. L., Volkov, V. V., Wilczynski, J. (1971). Nucl. Phys. A176, 284.
Auger, P., Chiang, T. H., Galin, J., Gatty, B., Guerreau, D., Nolte, E., Pouthas, J., Tarrago, X., Girard, J. (1979). Z. Phys. A289, 255.
Awes, T. C., Gelbke, C. K., Back, B., Mignerey, A., Wolf, K., Dyer, P., Breuer, H., Viola, V. E. (1979). Preprint, submitted to Phys. Lett. B.
Baldin, A. M., Giodensch, N., Zubarav, V. N., Ivanova, L. K., Moroz, N. S., Povtorecko, A. A., Radomanov, V. B., Stanvinskii, V. S. (1974). Yad. Fiz. 20, 1201.
Baldin, A. M. (1978), XIX International Conference on High Energy Physics, (Tokyo).
Ball, J. B., Fulmer, C. B., Mallory, M. L., Robinson, R. L. (1978). Phys Rev. Lett. 40, 1698.
Bannik, B. P., El-Naghy, A., Ibatov, R., Salomev, J. A., Shabratova, G. S., Sherif, M., Tolstov, K. D. (1978). Z. Phys. A 284, 283.
Baumgart, H. G., Schott, J. U., Sakamoto, Y., Schopper, E., Stocker, H., Hofmann, J., Scheid, W., Greiner, W. (1975). Z. Phys. A 273, 359.
Baym, G., Pethick, C. (1975). Ann. Rev. Nucl. Sci. 25, 27.
Beiser, F., Crawford H., Doll, P., Greiner, D. E., Gelbke, C. K., Heckman, H. H., Hendrie, D. L., Lindstrom, P. J., Mahoney, J., Scott, D. K., Symons, T. J. M., Van Bibber, K., Viyogi, Y. P., Westfall, G. D., Weiman, H. (1979). To be published.
Benecke, J., Chou, T. T., Yang, C. N., Yen. E. (1969). Phys. Rev. 188, 2159.
Benenson, W., Bertsch, G., Crawley, G. M., Kashy, E., Nolen, J. R., Bowman, H., Ingersoll, J. G., Rasmussen, J. O., Sullivan, J., Korke, M., Sasao, M., Peter, J., Ward, T. E. (1979). Preprint.
Berlanger, M., Gobbi, A., Hanappe, F., Lynen, U., Ngo, C., Olmi, A., Sann, H., Stelzer, H., Richel, H., Rivet, M. F. (1979). Preprint. See also Proc. of Gross Properties of Nuclei and Nuclear Excitations, Hirschegg, 1979.
Bertrand, F. (1978). Lectures presented at NATO Advanced Study Institute or Theoretical Methods in Medium Energy Physics (Banff, Canada).
Bertsch, G., Mundinger, D., (1978). Phys. Rev. C17, 1646.
Bertsch, G., Amsden, A. A. (1978a). Phys. Rev. C18, 1293.
Bertsch, G., Borysowicz, J. (1979). Preprint.
Bethe, H. A., Brown, G. E., Applegate, J., Lattimer, J. M., (1978). Preprint on Equation of State in Gravitational Collapse of Stars.
Bhalla, K. B., Hertzman, S., Oskarsson, A., Otterlund, I. (1979). Phys. Lett. 82B, 216.
Bjorken, J. D., McLerran, L. D. (1978). Proc. Conf. on Cosmic Rays and Particle Physics (Bartol Conference), T. K. Garsser, ed., p. 317.
Biswas, N. N., Bishop, J. H. Cason, N. M., Kenney, V. P., Shephard, W. D., Fortney, L. R. Goshaw, A. T., Lamsa, J. W., Loos, J. S., Robertson, W. J., Walker, W. D., Levman, G., Sreadhar, V. A., Yoon, T. S., Hartner, G., Patet, P. M. (1976). Phys. Rev. Lett. 37, 175.
Birkelund, J. R., Huizenga, J. R. (1978). Phys. Rev. C17, 126.
Birkelund, J. R., Tubbs, L. E., Huizenga, J. R., De, J. N., Sperber, D. (1979). Rochester preprint UR-NSRL-193, to be published in Phys. Reports.
Blann, M. (1975). Ann. Rev. Nucl. Sci., 25, 123.
Blann, M., Mignerey, A., Scobel, W. (1976). Nukleonika 21, 335.
Blocki, J., Boneh, Y., Nix, J. F., Randrup, J., Robel, M., Sierk, A. J., Swiatecki, W. J. (1978). Ann. of Phys. 113, 330.
Bock, R., Stock, R. (1978). Proc. Symp. on Relatiistic Heavy Ion Research, GSI, Darmstadt.
Bodmer, A. R., Panos, C. N. (1977). Phys. Rev. C15, 1342.

Boelmer, A. R. (1977a). Proc. of Conf. on Theoretical Aspects of Heavy Ion Collisions (Fall Creek, TN), ORNL Report 770602.
Boggild, H., Ferbel, T., (1974), Ann. Rev. Nucl. Sci. 24, 451.
Bohning, H. (1970). Proc. Intern. Conf. on Nucl. React. Induced by Heavy Ions (R. Bock and W. R. Heriog), North-Holland, Amsterdam, p. 633.
Bonche, P., Koonin, S., Negele, J. W. (1976). Phys. Rev. C13, 1226.
Bonche, P., Davies, K. T. R., Flanders, B., Flocard, H., Garammatices, B. Koonin, S. E., Krieger, S. J., Weiss, M. S. (1979). Preprint.
Bondorf, J., Norenberg, W. (1973). Phys. Lett. 44B, 487.
Bondorf, J. (1974). Lectures at International School of Physics (Eorio Fermi).
Bondorf, J. (1976), J. de Phys. (supplement) FASC 11 C5, 195.
Bondorf, J. P., Feldmeier, H. T., Garpman, S., Halbert, E. C. (1976a). Phys. Lett. 65B, 217.
Bondorf, J. (1978). Workshop on High Resolution Heavy Ion Physics at 20-100 MeV/A, Saclay, 1978, p. 37.
Bondorf, J., Fai, G., Neilsen, O. B. (1978a). Phys. Rev. Lett. 41, 391.
Bondorf, J. P., Fai, G., Nielsen, O. B. (1978b). Nucl. Phys. A312, 149.
Bondorf, J. P., De, J. N., Karvinen, A. O. T., Fai, G., Jackbsson, B. (1979) Niels Bohr Institute Preprint NBI 78-40.
Brazil-Japan Collaboration (1978). Proc. of Conference on Cosmic Rays and Particle Physics (Bartol Conference), T. K. Gaisser, ed., p. 317.
Broglia, R. A. Civitarese, O., Dasso, C. H., Winther, A. (1978), Phys. Lett. 73B, 405 and refs. therein.
Bromley, D. A. (1973). Proc. Intern. Conf. on Nucl. Phys. (Munich, 1973), J. de Boer and H. J. Mang, ed. (North Holland, 1973), p. 21.
Brosa, U., Krappe, H. J. (1978). Z. Physik A284, 65.
Butler, G. W., Perry, D. G., Remsberg, L. P., Poskanzer, A. M., Natowitz, J. B., Plasil, F (1977). Phys. Rev. Lett. 38, 1380.
Campi, X., Flocard, H., Kerman, A. K., Koonin, S. (1975). Nucl. Phys. A251, 193.
Chapline, G. F., Nauenberg, M. (1977). Phys. Rev. D 16, 450.
Chemtob, M., Schurmann, B. (1979). Saclay preprint, DPh-T/79-74.
Chin, S. A., Kerman, A. K. (1979), MIT preprint 785.
Cocconi, G. (1974). Phys. Lett. 49B, 459.
Cochran, D. R. F. Dean, P. N., Gram, P. A. M., Krapp, E. A., Martin, E. R., Nagle, D. E., Perkins, P. B., Schlaer, W. J., Thiessen, H. A., Theriot, E. O. (1972). Phys. Rev. D 6, 3085.
Cohen, S., Plasil, F., Swiatecki, W. J. (1974). Ann. of Phys. 82, 557.
Cugnon, J., Mizutani, T., Vandermeulen, J. (1979). University of Liege Preprint.
Cumming, J. B., Haustein, P. E., Stoenner, R. W., Mausner, L., Naumann, R. A. (1974). Phys. Rev. C10, 739.
DeVries, R. M., Peng, J. C. (1979). Los Alamos preprint LA-UR-79-730.
Dhar, A. K., Nilsson, S. B., Jaqaman, H. (1979), Niels Bohr Institute Preprint, NBI-78-31.
Doll, P., Hendrie, D. L., Mahoney, J., Menchaca-Rocha, A., Scott, D. K., Symons, T. J. M., Van Bibber, K., Viyogi, Y. P., Weiman, H. (1979). Phys. Rev. Lett. 42, 366.
Dyer, P., Awes, T. C., Gelbke, C. K., Back, B. B., Mignerey, A., Wolf, K. L., Brever, H., Viola, V. E., Meyer, W. G. (1979). Phys. Rev. Lett. 42, 560.
Ezell, C., Gutay, L. J., Laasanen, A. T., Dao, F. T., Schubelin, P., Turkot, F. (1977). Phys. Rev. Lett. 38, 873.
Feenberg, E., Primakoff, H. (1946). Phys. Rev. 70, 980.
Fermi, E. (1950). Prog. Th. Phys. 5, 570.
Feshbach, H., Huang, K. (1973). Phys. Lett. 47B, 300.
Feshbach, H. (1977). Lectures at Les Houches Summer School.
Feshbach, H. (1979). Proc. of 2nd Symposium on Nuclear Physics (Oaxteper, Mexico), p. 80.

Feynman, R. P. (1969). Phys. Rev. Lett. 23, 1415.
Fowler, G. N., Werner, R. H. (1977). Phys.Rev. Lett. 70B, 201.
Fraenkel, S. (1977). Phys. Rev. Lett. 38, 1338.
Fraenkel, S. (1978). Phys. Rev. C17, 694.
Frazer, W. R., Ingber, I., Mehta, C. H., Poon, C. H., Silverman, D., Stowe, K., Ting, P. D., Yesian, H. Y. (1972). Rev. Mod. Phys. 44, 284.
Freier, P., Lofgren, E. J., Ney, E. P., Oppenheimer, F. (1948). Phys. Rev. 74, 1818.
Fung, S. Y., Gorn, W., Kiernan, G. P., Lu, J. J., Oh, Y. T., Poe, R. T. (1978). Phys. Rev. Lett. 41, 1592.
Fung, S. Y., Gorn, W., Kiernan, G. P., Liu, F. F., Lu, J. J., Oh Y. T., Ozawa, J., Poe, R. T., Van Dalan, C., Schroeder, L., Steiner, H. (1978a). Phys. Rev. Lett. 40, 292.
Gaidos, J. A., Gutay, L. J., Hirsch, A. S., Mitchell, R., Ragland, T. V., Scharenberg, R. P., Turkot, F., Willmann, R. B., Wilson, C. L. (1979). Phys. Rev. Lett. 42, 82.
Gaisser, T. K., Protheroe, R. J., Turner, K. E., McComb, T. J. L. (1978). Rev. Mod. Phys. 4, 859.
Garpman, S. I. A., Sperber, D., Zielinska-Pfabe, M. (1979). Preprint.
Garvey, G. T. (1973). Comments on Nucl. and Part. Physics V, 65.
Gazzaly, M. M., Carroll, J. B., Geaga, J. V., Igo, G., McClelland, J. B., Nasser, M. A., Spinka, H., Sagle, A. L. Perez-Mendez, V., Talaga, R., Whipple, E. T. B., Zarbakash, F. (1978). Phys. Lett. 79B, 325.
Gelbke, C. K., Olmer, C., Buenerd, M., Hendrie, D. L., Mahoney, J., Mermaz, M. C., Scott. D. K. (1978). Phys. Rep. 42, 312.
Glendenning, N. K., Karant, Y. (1978). Phys. Rev. Lett. 40, 374.
Glendenning, N. K. (1978a). Theoretical Methods in Medium Energy and Heavy Ion Physics, ed. by K. W. McVoy, W. A. Friedman, (Plenum), p. 451.
Goldhaber, A. S. (1974). Phys. Lett. 53B, 306.
Goldhaber, A. S. (1978). Nature 27, 114.
Goldhaber, A. S., Heckman, H. H. (1978a). Ann. Rev. Nucl. Part. Sci. 28, 161.
Gosset, J., Gutbrod, H. H., Meyer, W. G., Poskanzer, A. M., Sandoval, A., Stork, R., Westfall, G. D. (1977). Phys. Rev. C16, 629.
Gosset, J., Kapusta, J. I., Westfall, G. D. (1978). Phys. Rev. C18, 844.
Gottschalk, P. A., Westrom, H. (1979). Nucl. Phys. A314, 232.
Grammaticos, B., Lumbroso, A. (1979). Saclay preprint DPh-T/79/36.
Greiner, D. E., Lindstrom, P. E., Heckman, H. H., Cork, B., Bieser, F. (1975). Phys. Rev. Lett. 35, 152.
Greiner, W. (1979). Lectures at this school.
Griffin, J. J. (1967). Phys. Lett. 24B, 5.
Gutbrod, H. H. (1978). Proc. of the 4th High Energy Heavy Ion Summer Study (Berkeley). LBL-7766, CONF 780766, p. 1.
Gutbrod, H. (1979). Bevalac Proposal on Plastic Ball.
Gyulassy, M. (1977). Fizika, Vol. 9, Supplement 3, 523.
Gyulassy, M. (1978). Proc. of Symp. on Relativistic heavy Ion Research (GSI, Darmstadt) GSI-9-5-78, p. 273.
Gyulassy, M., Kauffman, S. K. (1978a). Phys. Rev. Lett. 40, 298.
Gyulassy, M., Schroeder, L. S., (1979). Private communication.
Gyulassy, M., Kaufmann, S. K., Wilson, L. W. (1979a). Preprint LBL-8759.
Hagedorn, R. (1973). Cargese Lectures in Physics, Vol. 6, E. Schatzman, ed. (Gordon Breach, 1973).
Hanbury-Brown, R., Twiss, R. Q. (1956). Nature 10, 1046.
Harp, G. D., Chen, K., Friedlander, G., Fraenkel, Z., Miller, J. M. (1973). Phys. Rev. C8, 851.
Hatch, R. L., Koonin, S. E. (1979). Phys. Lett. 81B, 1.
Heckman, H. H., Lindstrom, P. J. (1976). Phys. Rev. Lett. 37, 56.
Ho, H., Ablrecht, R., Dunnweber, W., Graw, G., Steadman, S. G., Wurm, J. P., Disdier, D., Rauch, V., Schiebling, F. (1977). Z. Phys. A283, 235.

Hofmann, J., Muller, B., Greiner, W. (1979). Phys. Lett. 82B, 195.
Hufner, J., Sander, C., Wilschin, G. (1978). Phys. Lett. 73B, 289.
Hufner, J., Schafer, K., Schurmann, B. (1975). Phys. Rev. C12, 1888.
Hufner, J. (1978). Proc. of 4th High Energy Heavy Ion Summer Study (Berkeley), LBL-7756, CONF 7807[illegible], p. [illegible].
Irvine, J. M. (1978). Rep. on Prog. in Phys.
Iwe, H. (1978). JINR Preprint, E2-11964.
Jackson, D. F. (1977). Phys. Lett. 71B, 57.
Jacobsson, B., Bondorf, J. P., Fai, G. (1979). Phys. Rev. Lett. 82B, 35.
Johansen, P. J., Sie[illegible], F. A., Jensen, A. S., Hofmann, H. (1977). Nucl. Phys. A288, [illegible].
Johnson, K. [illegible]. Acta Phys. Polonica B6, 865.
Jones, L. (1978). Phys. Rev. D17, 1462.
Kitazoe, Y., Sano, M. (1976). Prog. Th. Phys. 56, 860.
Kit[illegible], Y., Sa[illegible], M. [illegible]. Preprint.
Kind[illegible], F., Lattanzi, G. (1964). Nuovo Cimento 10, 1375.
Kittel, C. (1958). Elementary Statistical Physics (Wiley and Sors, NY), p. 219.
Klapisch, R., Thibault, C., Postanzer, A. M., Preels, R., Rigaud, C., Roeckl, E. (1972). Phys. Rev. Lett. 29, 1254.
Knoll, J., Hufner, J., Bouyssy, A. (1978). Nucl. Phys. A308, 500.
Ko, C. M., Ta-Chung, M. (1979). LBL preprint 8933.
Koonin, S. E. (1977). Phys. Lett. 70B, 43.
Koonin, S. (1979). Private communications.
Kullberg, R., Oskarsson, A., Otterlund, I. (1978). Phys. Rev. Lett. 40, 289.
Kullberg, R., Oskarsson, A. (1978a). Z. Phys. A288, 283.
Laasanen, A. T., Ezell, C., Gutay, L. J., Schreiner, N. W., Schubelin, P., von Linder, L., Turkot, F. (1977). Phys. Rev. Lett. 38, 1.
Landau, R. H., Gyulassy, M. (1978). LBL preprint 7719, to be published in Phys. Rev. C.
Lee, T. D. (1975). Rev. Mod. Phys. 47, 267.
Lefort, M. (1974). J. Phys. A7, 107.
Lefort, M. (1976). European Conf. on Nucl. Phys. with Heavy Ions (Caen), Coll. du J. de Phys. 37, C5-57.
Lefort, M., Ngo, Ch. (1978). Ann. Phys. V3, 5.
Lemaire, M. C., Nagamiya, S., Schnetzer, S., Steiner, H., Tanihata, I. (1979). LBL preprint 8978, to be published in Phys. Lett. B.
Levine, R. D., Steadman, S. G., Karp, J. S. Alhassid, Y. (1978). Phys. Rev. Lett. 41, 1537.
Lindstrom, P. J., Crawford, H. J., Greiner, D. E., Hagstrom, R., Heckman, H. H. (1978). Phys. Rev. Lett. 40, 93.
Lukyanov, V. K., Titov, A. I. (1975). Phys. Lett 57B, 10.
Mantzouranis, G., Weidenmuller, H. A., Agassi, D. (1976). Z. Phys. A276, 145.
McNuty, P. J., Farrell, G. E., Filz, R. C., Schimmerling, W., Vosburgh, K. (1977). Phys. Rev. Lett. 40, 289.
Mekjian, A. (1978). Phys. Rev. C17, 1051.
Mekjian, A. (1978a). Nucl. Phys. A312, 491.
Moretto, L. G., R. P. Schmitt (1978). Intern. Conf. Nucl. Interaction, Canberra 1978.
Morrissey, D. J., Loveland, W., Marsh, W. R., Seaborg, G. T. (1978). Z. Phys. A289, 123.
Morrissey, D. J., Marsh, W. R., Otto, R., Loveland, W., Seaborg, G. T. (1978a). Preprint LBL-6579.
Morrissey, D. J., Olivera, L. F., Rasmussen, J. O., Seaborg, G. T., Yario, Y., Fraenkel, Z. (1979). Phys. Rev. C18, 1267.
Myers, W. D. (1978). Nucl. Phys. A296, 177.

Nagamiya, S. (1978). Proc. 4th High Energy Heavy Ion Summer Study (Berkeley), LBL-7766, p 71.
Nagamiya, S., Anderson, K., Bruckner, W., Chamberlain, O., Lemaire, M. C., Schnitzer, S., Schapiro, G., Steiner, H., Tanihata, I. (1979). Phys. Lett. 81B, 147.
Nagamiya, S. (1979a). Private communication.
Negele, J. (1978).Theoretical Methods in Medium Energy and Heavy Ion Physics ed. by K. McVoy and W. A. Friedman (Plenum), p. 325.
Nemes, M. C., Seligman, T. H. (1979). Memorias del Segundo Simposio de Fisica Nuclear en Oaxtepec, Institute de Fisica, Vol. 2, 298.
Nix, J. R. (1978). Los Alamos preprint LA-UR-77-2952 to be published in Prog. Part. Nucl. Phys.
Norenberg, W. (1976). J. de Phys. (Suppl.) C5, 141.
Nuclear Data Tables (1976), Nos. 5-6.
Nuclear Data Tables) (1977), 19, No. 3.
Oliveira, L. F. Donangelo, R., Rasmussen, J. O. (1979). Phys. Rev. C19, 826.
Pandharpande, V. R. (1970). Phys. Lett. 31B, 635.
Poskanzer, A. M. Sextro, R. G., Zebelman, A. M., Gutbrod, H. H., Sandoval, A., Stock, R. (1975). Phys. Rev. Lett. 35, 1701.
Poskanzer, A. M. (1978). Proc. Intern. Conf. on Dynamical Properties of Heavy Ion Reaction (Johannesburg, S. Africa).
Preston, M. A., Bhaduri, R. K. (1975). Structure of the Nucleus (Addison Wesley), p. 202.
Price, B. (1977). Phys. Rev. Lett. 39, 177.
Price, B., Stevenson, J. (1978). Phys. Lett. 78B, 197.
Rafelski, J., Hagedorn, R. (1979). Lecture at 11th Intern. Winter Meeting on Nuclear Physics (Bermio, Italy).
Randrup, J. (1979). Nucl. Phys. A314, 429.
Remsberg, L. M., Perry, D. G. (1975). Phys. Rev. Lett. 35, 361.
Robel, M. C. (1979). University of California Thesis, LBL preprint 8181.
Rybicki, K. (1963). Nuovo Cimento 28 [illegible]57.
Sandoval, A. (1979). Private communication.
[illegible]neid, W., Muller, H., Greiner, W. (1976). Phys. Rev. Lett. 36, 88.
[illegible]nibata, T., Ejiri, H., Chiba, J., Nagamiya, S., Nakai, K., Anholt, R., Bowman, H., Ingersoll, J. G., Rauscher, E. A., Rasmussen, J. O. (1978) Nucl. Phys. A308, 513.
Schmidt, I. A., Blankenbecler, R. (1977). Phys. Rev. D 15, 3321.
Schroeder, L. S. (1976). Proc. of Topical Meeting on Multiparticle Production of Nuclei at Very High Energy, ICTP (Trieste).
Schroeder, L. S. (1979). Private communication.
Schroeder, L. S., Chessin, S. A., Geaga, J. V., Grossiard, J. Y., Harris, J. W., Hendrie, D. L., Treuhaft, R., Van Bibber, K. (1979a). To be published.
Schroder, W. U., Huizenga, J. R. (1977). Ann. Rev. Nucl. Sci. 27, 465.
Scott, D. K. (1978). Memorias del Primer Simposia de Fisica Nuclear en Oaxtepec. Instituto de Fisica, Vol.1, 221.
Scott, D. K. (1978a). Theoretical Methods in Medium Energy and Heavy Ion Physics, ed. by K. McVoy and W. A. Friedman (Plenum), p. 3.
Scott, D. K., Bini, M., Doll, P., Gelbke, C. K., Hendrie, D. L., Laville, J. L., Mahoney, J., Menchaca-Rocha, A., Mermaz, M. C., Olmer, C., Symons, T. J. M., Viyogi, X. P., Van Bibber, K., Weiman, H., Seimens, P. J. (1979). LBL preprint 7729.
Siemens, P. J., Rasmussen, J. O. (1979). Phys. Rev. Lett. 42, 880.
Smith, R. K., Danos, M. (1977). Proc. Meet. Heavy Ion Collisions (Fall Creek, TN), ORNL Report CONF-770602, p. 363.
Smith, R. K., Danos, M. (1979). Private communication to M. Gyulassy. Cover Illustration of Proc. of 4th High Energy Heavy Ion Summer Study (Berkeley), LBL-7766, CONF 780766.

Sobel, M. I., Siemens, P. J., Bondorf, J. P., Bethe, H. A. (1975). Nucl. Phys. A251, 502.
Stelte, N., Westrom, M., Weiner, R. M. (1979). Univ. of Marburg preprint.
Stevenson, J., Price, P. B., Frankel, K. (1977). Phys. Rev. Lett. 38, 1125.
Stock, R. (1978). Proc. Sym. on Relativistic Heavy Ion Research (GST, Darmstadt). GSI-P-5-78, p. 66.
Stocker, H., Maruhn, J., Greiner, W. (1979). Phys. Lett. 81B, 303.
Stokstad, R. G. (1977). Theoretical Aspects of Heavy Ion Collisions (Fall Creek, TN), ORNL Report 770602.
Stokstad, R. G., Dayras, R. A., Gomez del Campo, J., Stelson, P. H., Olmer, C., Zisman, M. S. (1977a). Phys. Lett. 70B, 289.
Symons, T. J. M., Viyogi, Y. P., Westfall, G. D., Doll, P., Greiner, D. E., Faraggi, H., Lindstrom, P. J., Scott, D. K., Crawford, H. J., McParland, C., (1979). Phys. Rev. Lett. 42, 40.
Symons, T. J. L., Doll, P., Bini, M., Hendrie, D. L., Mahoney, J., Mantzouranis, G., Scott, D. K., Van Bibber, K., Viyogi, Y. P., Weiman, H. H., Gelbke, C. K. (1979a). Submitted to Phys. Lett. B, LBL Report 8379.
Ta-Chung, M. (1978). LBL preprint 8358.
Ta-Chung, M., Moeller, E. (1978a). Phys. Rev. Lett. 41, 1352.
Thibault, C., Klapisch, R. (1974). Phys. Rev. C 9, 793 and refs. therein.
Thornton, S. T., Cordell, K. R., Dennis, L. C., Doering, R. R., Schweizer, T. C. (1979). Preprint.
Toki, H., Futami, Y., Weise, W. (1978). Phys. Lett. 78B, 547.
Tomonaga, S. (1938). Z. Phys. 110, 573.
Van Bibber, K., Hendrie, D. L., Scott, D. K., Wieman, H. H., Schroeder, L. S., Geaga, J. V., Chessin, S. A., Treuhaft, R., Grossiard, J. Y., Rasmussen, J. O., Wong, C. W. (1979). Preprint LBL-8939.
Vary, J. (1978). Phys. Rev. Lett. 40, 295.
Vigdor, S. E., Kovar, D. G., Sperr, P., Mahoney, J., Menchaca-Rocha, A., Olmer, C., Zisman, M. S. (1979). Preprint.
Viola, V. E., Clark, R. J., Meyer, W. G., Zebelman, A. M., Sextro, R. G. (1976). Nucl. Phys. A261, 174.
Viyogi, Y. P., Symons, T. J. M., Doll, P., Greiner, D. E., Heckman, H. H., Hendrie, D. L., Lindstrom, P. J., Mahoney, J., Scott, D. K., Van Bibber, K., Westfall, G. D. Weiman, H., Crawford, A. J., McParland, C., Gelbke, C. K. (1979). Phys. Rev. Lett. 42, 33.
Volkov, V. V., (1978). Phys. Reports 44, 93.
Wall, N. S., Wu, J. R., Chang, C. C., Holmgren, H. D. (1978). U. of Maryland Preprint NSF-6-78.
Webb, C., Kingston, J., Mahoney, J. (eds) (1978). Proc. 4th High Energy Heavy Ion Summer Study (Berkeley 1978), LBL-7766.
Weidenmuller, H. A. (1978), to be published in Prog. Part. Nucl. Phys. (Pergamon Press), Heidelberg Preprint MPI H-1978-V29.
Weinberg, S., (1977). The First Three Minutes (Basic Books, NY, 1977).
Weiner, R. (1974). Phys. Rev. Lett. 32, 630.
Weiner, R. (1976). Phys. Rev. D 13, 1363.
Weiner, R., Westrom, M. (1977). Nucl. Phys. A286, 282.
Weiner, R. (1979). University of Marburg Preprint: "Hot Spots"--A Common Market of Nuclear and Elementary Particle Physics.
Westerberg, L., Sarantites, D. G., Hensley, D. C., Dayras, R. A., Halbert, M. L., Barker, J. H. (1978). Phys.Rev. C 18, 797.
Westfall, G. D., Posset, J., Johansen, P. J., Poskanzer, A. M., Meyer, W. G., Gutbrod, H. H., Sandoval, A., Stock, R. (1977). Phys. Rev. Lett. 37, 1202.
Westfall, G. D., Sextro, R. G., Poskanzer, A. M., Zebelman, A. M., Butler, G. W., Hyde, E. K. (1978). Phys. Rev. C 17, 1368.
Westfall, G. D., Wilson, L. W., Lindstrom, P. J., Crawford, H. J., Greiner, D. G., Heckman, H. H. (1979). Phys. Rev. C 19, 1309.
Wilkinson, D. H. (1962). Proc. Phys. Soc. 80, 997.

Wilkinson, D. H. (1975). The quotations from Dante were used by D. H. Wilkinson in a forerunner of this School, Proc. of Intern. School of Nucl. Phys. (Erice, Sicily, 1974), H. Schopper, ed. (North Holland-Elsevier, 1975), p. 2. (The translations are from the Dorothy Sayers edition of the Divine Comedy, published by Pergamon.

Wilkinson, D. H. (1976). Proc. of 3rd Intern. Conf. on Nuclei Far from Stability (Cargese) CERN Report 76-13, p. 71.

Wolf, K., Gutbrod, H. H., Meyer, W. G., Poskanzer, A. M., Sandoval, A., Stock, R., Gosset, J., King, C. H., King, G., Nguyen Van Sen, Westfall, G. D. (1979). Phys. Rev. Lett. 42, 1448.

Wong, C. Y., Maruhn, J. A., Welton, T. A. (1977). Phys. Lett. 66B, 19.

Wong, C. Y. (1978). Proc. of Intern. Symp. on Superheavy Elements (Lubbock, TX), M. A. K. Lodhi, ed. (Pergamon), p. 524.

Wu, J. R., Chang, C. C., Holmgren, H. D. (1979). Phys. Rev. C 19, 370, 659, 698.

Yano, F. B., Koonin, S. E. (1978). Phys. Lett. 78B, 556.

Youngblood, D. H., Rosza, C. M., Moss, J. M. Brown, D. R., Bronson, J. D. (1977). Phys. Rev. Lett. 39, 1188.

ACKNOWLEDGEMENTS

I wish to thank the many workers in the field of heavy ion physics who have written excellent reviews which helped me to prepare these lectures. Also I owe an enormous debt to my colleagues in Berkeley on this and many other occasions, for freely explaining their ideas and interpretation of data, often long before publication. As always, this manuscript would not have seen the light of day without the superb cooperation and organization of the Word Processing Department, the Illustration Department and the Photographic Department. On this occasion, I am particularly indebted to Jean Wolslegel, wo typed the final version.

This work was done under the auspices of the U. S. Department of Energy, Contract Number W-7405-ENG-48.